

Fabrication of Single-Walled Carbon Nanotube Electrodes for Ultracapacitors

by

Joshua John Edward Moore

A thesis
presented to the University of Waterloo
in fulfillment of the
thesis requirement for the degree of
Master of Applied Science
in
Mechanical Engineering

Waterloo, Ontario, Canada, 2011

©Joshua John Edward Moore 2011

Author's Declaration

I hereby declare that I am the sole author of this thesis. This is a true copy of the thesis, including any required final revisions, as accepted by my examiners.

I understand that my thesis may be made electronically available to the public.

Abstract

Well dispersed aqueous suspensions containing single-walled carbon nanotubes (SWCNTs) from bulk powders were prepared with surfactant and without surfactant by acid functionalization. SWCNT coated electrodes were then prepared from the SWCNT aqueous suspensions using various methods to create uniform nanoporous networks of SWCNTs on various substrates and stainless steel (SST) current collectors for use as ultracapacitor electrodes. Drop coating, high voltage electro-spraying (HVES), inkjet printing, and electrophoretic deposition (EPD) methods were evaluated. Optical and scanning electron microscope images were used to evaluate the SWCNT dispersion quality of the various electrodes. Ultimately an EPD process was established which reliably produced uniform SWCNT nanoporous networks on SST substrates.

The prepared SWCNT coated electrodes were characterized using cyclic voltammetry and their capacitance was determined. A correlation between extended EPD processing times, EPD processing temperatures, and electrode capacitance was quantified. Optimum EPD processing occurs where linear capacitance gains were observed for processing times less than 10 minutes. At processing times between 10 – 60 minutes a non-linear relationship demonstrated diminishing capacitance gains with extended EPD processing times. Likewise, optimum EPD processing occurs when the processing temperature of the SWCNT suspension is raised above room temperature. At processing temperatures from 45°C to 60°C an increase in capacitance was observed over the room temperature (22°C) electrodes processed for the same durations. Conversely, for processing temperatures less than room temperature, at 5°C, a decrease in capacitance was observed. It was also observed that SWCNT electrodes processed at 60°C processing temperatures resulted in 4 times the capacitance of 5°C electrodes for the same processing times, when the durations were 8 minutes or less. For samples with raised processing temperatures the time dependent capacitance gains were observed to be

significantly diminished beyond 10 minute processing times. The SWCNT network thickness was also correlated to EPD processing temperature and capacitance. A linear relationship was identified between the SWCNT network thickness and the capacitance of the electrode. It was also observed that elevated processing temperatures increase the EPD deposition rate of SWCNTs, produce thicker SWCNT networks, and thus create electrodes with higher capacitance than electrodes processed at lower EPD processing temperatures.

EPD of SWCNTs was demonstrated in this work to be an effective method for the fabrication of SWCNT ultracapacitor electrodes. Characterization of the process determined that optimal EPD processing occurs within the first 10 minutes of processing time and that elevated processing temperatures yield higher SWCNT deposition rates and higher capacitance values. In this work the addition of SWCNT nanoporous networks to SST electrodes resulted in increases in capacitance of up to 398 times the capacitance of the uncoated SST electrodes yielding a single 1cm^2 electrode with a capacitance of 91mF and representing an estimated specific capacitance for the processed SWCNT material of 45.78F/g.

Acknowledgements

First I would like to express my appreciation to my supervisor Dr. John Wen for providing me with this exciting and innovative topic. I would also like to thank Dr. Wen for giving me the flexibility to experiment with various processes and techniques. I would most like to thank Dr. Wen for giving me the opportunity to join his group and enter the world of nanotechnology.

I would like to thank the entire group at the Center for Advanced Materials Joining for allowing me to work in their microjoining lab during the early stages of our project. Without their early help and consideration we could not have made all the progress that we have to date.

I would also like to express my gratitude to Dr. Keryn Lian at the University of Toronto for opening her lab to us and sharing her equipment, her knowledge, and her students. Dr. Lian introduced me to my first potentiostat and without her I am certain that the path to results would have been much longer.

Finally I would like to thank my friends and colleagues in the Lab for Emerging Energy Research and around the UW campus for engaging in meaningful conversations, providing useful insights, and generally making the time here a great one.

Thank you.

Dedication

This thesis is dedicated to my loving wife who has provided patience, love, and support throughout this journey, and to our amazing daughter who sleeps through the night and provides endless smiles at the end of long days.

Table of Contents

Author's Declaration	ii
Abstract	iii
Acknowledgements	v
Dedication	vi
Table of Contents	vii
List of Figures	ix
List of Tables	xii
Chapter 1 Introduction.....	1
1.1 Motivation	1
1.1.1 Energy Storage Devices	1
1.1.2 Nanostructures in Energy Storage Devices	4
1.1.3 Single-Walled Carbon Nanotubes	6
1.2 Objectives	9
Chapter 2 Literature Review	11
2.1 Single-Walled Carbon Nanotube Suspensions	11
2.1.1 Sonication Mixed Suspensions.....	11
2.1.2 Surfactant and Polymer Based Suspensions	12
2.1.3 Functionalized Suspensions.....	13
2.2 Single-Walled Carbon Nanotube Suspension Deposition Methods	15
2.2.1 Vacuum Filtration Method	15
2.2.2 Spin Coating	16
2.2.3 Wire Wound Rod Coating	17
2.2.4 Electrophoretic Deposition.....	18
2.3 Published Results and Commercial Benchmarks	20
2.3.1 Carbon Nanotube Ultracapacitor Properties.....	20
2.3.2 Commercially Available Ultracapacitor Properties.....	21
Chapter 3 Experimental Procedures	23
3.1 Single-Walled Carbon Nanotube Suspensions	23
3.1.1 Single-Walled Carbon Nanotubes in H ₂ O Using Surfactants.....	23
3.1.2 Acid Functionalized Single-Walled Carbon Nanotubes in H ₂ O.....	25
3.2 Single-Walled Carbon Nanotube Suspension Processing	27

3.2.1 Drop Coating	27
3.2.2 High Voltage Electro Spraying	28
3.2.3 Inkjet Printing.....	29
3.2.4 Electrophoretic Deposition.....	31
Chapter 4 Results.....	37
4.1 Structural and Morphological Characterization	37
4.1.1 Drop Coating Optical and Scanning Electron Microscope Results.....	38
4.1.2 High Voltage Electro Spraying Scanning Electron Microscope Results.....	43
4.1.3 Inkjet Printing Scanning Electron Microscope and Raman Results.....	44
4.1.4 Electrophoretic Deposition Scanning Electron Results.....	50
4.2 Brunauer-Emmett-Teller (BET) Pore Size Analysis	61
4.3 Electrical Resistance.....	62
4.4 Electrochemical Characterization – Cyclic Voltammetry	63
4.4.1 Cyclic Voltammetry – Electrophoretic Deposition Time Dependence	63
4.4.2 Cyclic Voltammetry – Electrophoretic Deposition Temperature Dependence	68
Chapter 5 Conclusions.....	76
Chapter 6 Recommendations.....	78
Appendix A BET Surface Analyzer Data.....	80
References	87

List of Figures

Figure 1.1 - Visual representation of attributes of different energy storage technologies.....	2
Figure 1.2 - Energy density vs power density for select portable energy devices.....	3
Figure 1.3 - Representation of electrochemical double layer ultracapacitor in the charged state	5
Figure 1.4 – Conceptual representations of CNTs from a monolayer graphene sheet	6
Figure 1.5 – Carbon nanotube powder	7
Figure 1.6 – Representation of single-walled (left) and multi-walled (right) CNT structures	8
Figure 2.1 - Schematic representation of surfactant adsorption on CNT walls	13
Figure 2.2 - Acid-cut nanotubes with carboxyl groups on ends and sidewalls	14
Figure 2.3 - Optical images of water droplet contact angle vs acid functionalization duration	14
Figure 2.4 - Vacuum filtration setup for production of SWCNT films	16
Figure 2.5 - Schematic image of spin coating process	17
Figure 2.6 – Illustration of wire wound rod coating technique	18
Figure 2.7 – Schematic of electrophoretic deposition cell used to create CNT thin films	19
Figure 2.8 – Surface roughness for CNT films produced by various methods compared to ITO	19
Figure 3.1 – SWCNTs dispersed in H ₂ O using decreasing concentrations of SDS	24
Figure 3.2 - Images showing acid removal and filtering of SWCNTs	26
Figure 3.3 - Optical image of functionalized SWCNT suspension two months after preparation	26
Figure 3.4 - Schematic diagram of SWCNT drop coating process	28
Figure 3.5 - Schematic diagram of HVES SWCNT coating process	29
Figure 3.6 - 1) Epson Stylus NX510 and 2) HP Deskjet F4480 printers	30
Figure 3.7 - Schematic diagram of EPD cell 1 SWCNT coating process	33
Figure 3.8 - Schematic diagram of EPD cell 2 with temperature controlled process	35
Figure 3.9 - Photos of temperature controlled EPD cell 2 with plastic and glass vessels	36
Figure 4.1 - Optical image of SWCNT SDS drop coated sample	38
Figure 4.2 - SEM images of SWCNT 0.1M SDS drop coating samples.....	39
Figure 4.3 - SWCNT and pure H ₂ O drop coating samples	40
Figure 4.4 - SWCNT SDS drop coating samples	41
Figure 4.5 - Substrate treated 0.1M SDS drop coated sample	41
Figure 4.6 - Acid functionalized SWCNT drop coated sample	42
Figure 4.7 - H ₂ O based SWCNT HVES coating method	43
Figure 4.8 - Ethanol based SWCNT HVES coating method	44

Figure 4.9 - Electrically conductive SWCNT network on copy paper using drop coating method	45
Figure 4.10 - Reference Raman plot for SWCNTs	46
Figure 4.11 - Raman plot of SWCNTs printed using HP inkjet printer	46
Figure 4.12 - Inkjet printed SWCNTs on copy paper A) 150 prints using HP printer, B) 50 prints using HP printer, C) 45 prints using HP printer, D) 80 prints using Epson printer	47
Figure 4.13 – SEM images of electrically conductive SWCNT network on copy paper using drop coating method	48
Figure 4.14 - SEM images of insufficient SWCNT coverage on copy paper using inkjet printing	48
Figure 4.15 - Printed pattern (left) and actual SWCNTs printed pattern on ITO PET	49
Figure 4.16 - SEM image of SWCNT network created using EPD at 30V for 3 minutes	51
Figure 4.17 - SEM image of SWCNTs coated on substrate using EPD at 20V for 1min	51
Figure 4.18 - Formation of SWCNT network across a hole using EPD at 30V for 3min	52
Figure 4.19 - Large area SEM images of A) Uniform 0.5mm EPD SWCNT network, B) Bare SST substrate in uncoated region, C) Boundary between EPD SWCNT coated and uncoated areas	53
Figure 4.20 - Optical images of SWCNT electrodes coated using EPD at various processing times 3, 8, 15, 30, and 60 minutes at 5°C and 60°C	54
Figure 4.21- SWCNT network using EPD at 40V for 8 minutes at 5°C	55
Figure 4.22- SWCNT network using EPD at 40V for 8 minutes at 22°C	55
Figure 4.23- SWCNT network using EPD at 40V for 8 minutes at 45°C	56
Figure 4.24- SWCNT network using EPD at 40V for 8 minutes at 60°C	56
Figure 4.25 - Cross sections of SWCNT coated SST electrode using 40V EPD for 8min at 5°C	58
Figure 4.26 - Cross sections of SWCNT coated SST electrode using 40V EPD for 8min at 22°C	58
Figure 4.27 - Cross section of SWCNT coated SST electrode using 40V EPD for 8min at 45°C	59
Figure 4.28 - Cross section of SWCNT coated SST electrode using 40V EPD for 8min at 60°C	59
Figure 4.29 - Plot of SWCNT network thickness against EPD processing temperature	60
Figure 4.30 - CV curves of SWCNT coated SST electrodes at 20mV/s showing the effect of EPD processing time on capacitance for 0-8 minutes	64
Figure 4.31 - CV curves of SWCNT coated SST electrodes at 50mV/s showing the effect of EPD processing time on capacitance for 0-8 minutes	65
Figure 4.32 - CV curves of SWCNT coated SST electrodes at 100mV/s showing the effect of EPD processing time on capacitance for 0-8 minutes	65

Figure 4.33 - CV curves of SWCNT coated SST electrodes at scan rate of 20mV/s for EPD processing times 0-60min.....	66
Figure 4.34 - Relationship between SWCNT EPD processing time and capacitance 0-60min, inset extrapolated slope curve showing trail off of capacitance to processing time ratio.....	67
Figure 4.35 - CV curves for SWCNT EPD processed electrodes at scan rate of 20mV/s for 3-60 mins at various EPD processing temperatures: A) 5°C, B) 22°C, C) 45°C, D) 60°C.....	69
Figure 4.36 - CV curves of SWCNT coated electrodes using EPD for 60min at 5°C, 22°C, 45°C, 60°C: A) Scan rate of 100mV/s, B) Scan rate of 500mV/s.....	70
Figure 4.37 - Plot showing small decrease in capacitance with increasing scan rates 20-500mV/s for SWCNT electrodes.....	71
Figure 4.38 - Capacitance values and trend lines of SWCNT coated electrodes EPD processed for 0-60 minutes at 5°C, 22°C, 45°C, and 60°C.....	73
Figure 4.39 - Capacitance curves of SWCNT coated electrodes EPD processed for 0-8 minutes at 5°C, 22°C, 45°C, and 60°C.....	74
Figure 4.40 - Linear relationship between SWCNT network thickness and electrode capacitance.....	75
Figure 6.1 - Schematic diagram of reel to reel EPD cell for continuous SWCNT deposition.....	79

List of Tables

Table 2.1 - Summary of published capacitance values for various carbon ultracapacitor electrodes ..	21
Table 2.3 - Commercially available carbon EDLCs	22
Table 3.1 - Summary of EPD parameters used in EPD of CNTs	31
Table 3.2 - Summary of CNT type and suspension preparation for CNT EPD	32
Table 4.1 - Internal resistance of SWCNT electrodes	62

Chapter 1

Introduction

As portable energy dependence moves away from fossil fuels and other consumable energy sources, the need for portable energy storage devices with larger electrical storage capacities and faster charge rates becomes more critical to the success of products and technologies that rely on these portable energy sources [1-3].

1.1 Motivation

The work presented in this thesis is motivated by the need to create an energy storage device that can obtain the high energy density, or charge capacity, of batteries yet also obtain the high power density, or charge and discharge rates, of capacitors. From the fundamental equation for electrode capacitance nanomaterials, specifically single-walled carbon nanotubes (SWCNTs), were selected as the building blocks for the fabrication of electrically conductive nanoporous electrodes.

1.1.1 Energy Storage Devices

Traditional portable energy storage devices include various types of batteries, capacitors, supercapacitors or ultracapacitors, and fuel cells. Each has inherent advantages and disadvantages, including performance cost, reliability, and lifetime performance [2]. Figure 1.1 shows a visual representation of these attributes to compare batteries, ultracapacitors (UC), fuel cells (FC), and flywheels (FW). From the figure it can be generalized that ultracapacitors have the best durability, lifespan, specific power, and fastest operating dynamics, but that the batteries have the highest specific energy, and are the most affordable [3].

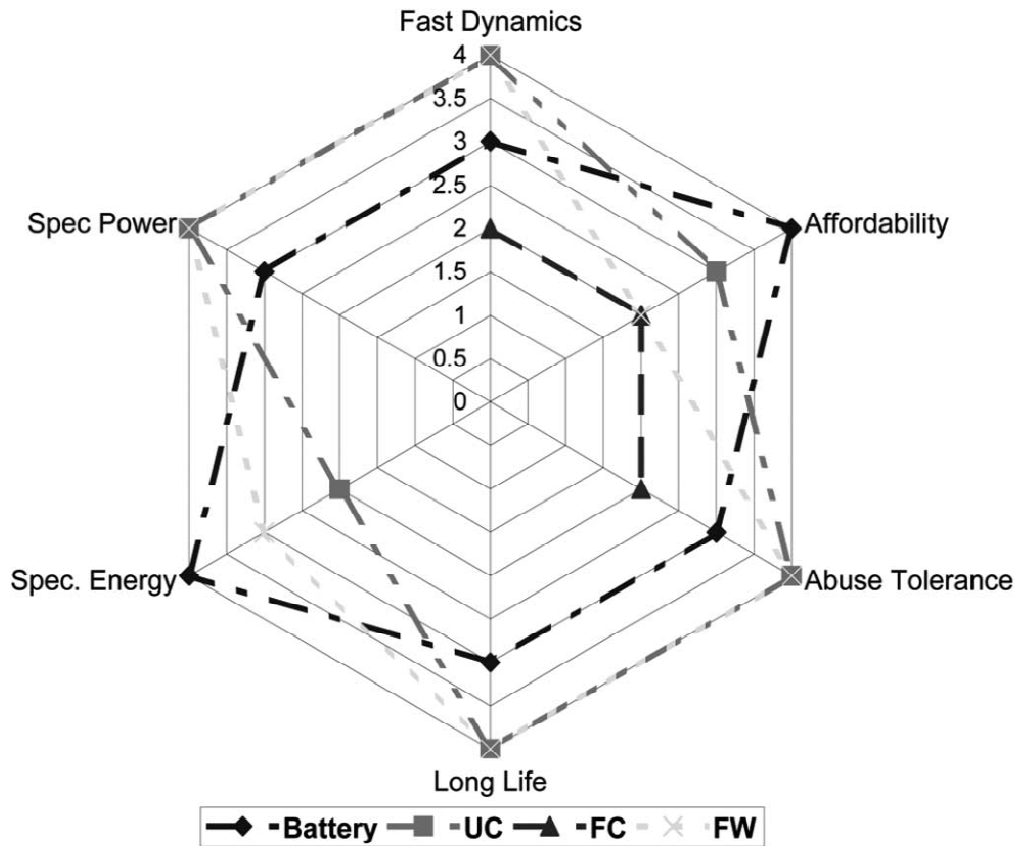


Figure 1.1 - Visual representation of attributes of different energy storage technologies [3]

For the purpose of this work on ultracapacitor electrodes the primary comparison for energy storage devices will focus on the differences in specific energy and specific power and how to increase the energy density of ultracapacitors. Energy density refers to the amount of energy stored per unit volume and when used to describe energy storage systems is often used in synonym with the term specific energy which alternatively refers to the energy stored per unit mass. Power density refers to the rate at which energy can be charged or discharged per unit volume and again when used to describe energy storage systems is often used interchangeably with the term specific power referring to the energy charge-discharge rate per unit mass [3]. The Ragone chart in Figure 1.2 below shows a comparison between specific energy and specific power for various energy storage devices. It is a way to compare the energy characteristics of

different batteries, capacitors, ultracapacitors and fuel cells in terms of their energy carrying and transfer limitations.

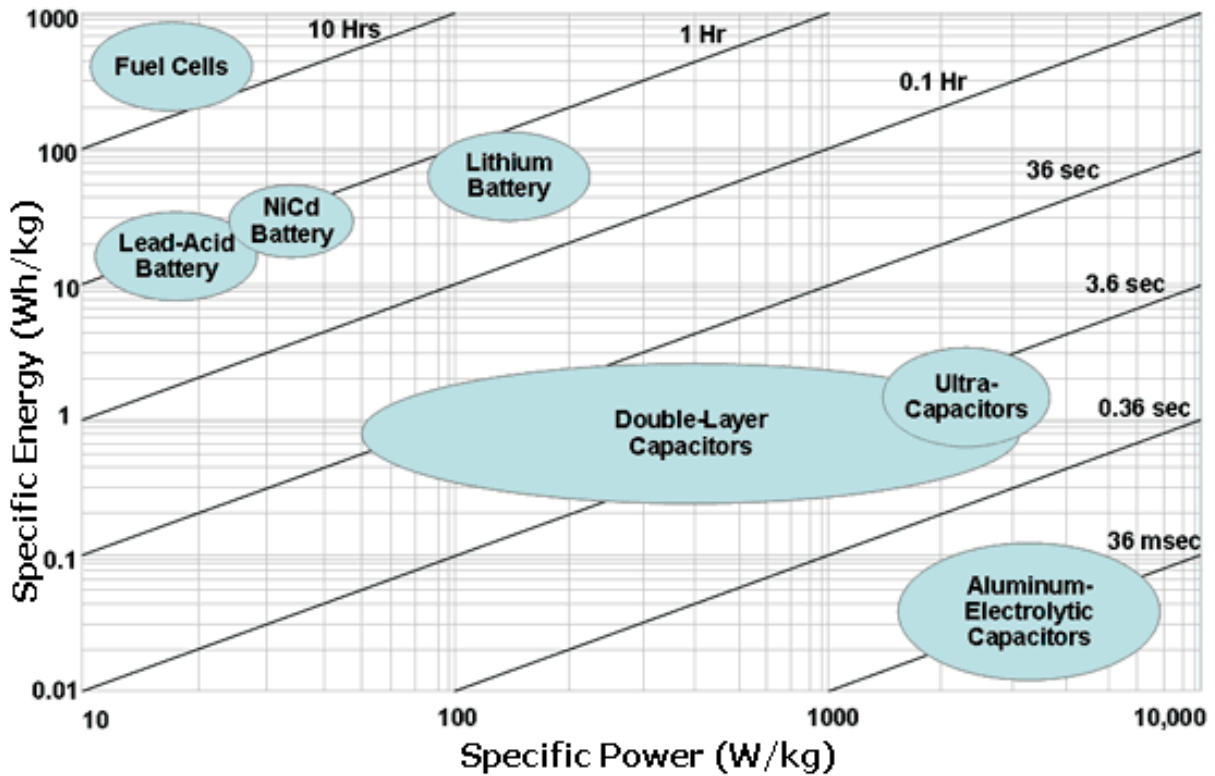


Figure 1.2 - Energy density vs power density for select portable energy devices [4]

As can be seen from the plot, fuel cells have the highest specific energy between 200-900Wh/kg. However, their specific power remains low between 10-20W/kg. On the other hand traditional capacitors have a very high specific power 1000-7000W/kg, but have a very low storage capacity or specific energy at 0.01-0.11Wh/kg. The diagonal lines demonstrate the energy charge/discharge times. For capacitors the stored energy can be discharged in a few milliseconds (36ms). For batteries the discharge times are closer to 1hr. As can be seen from the chart the progression of battery technology from lead acid to nickel cadmium to lithium ion has allowed batteries to improve in both specific energy and specific power properties. The goal of many researchers is to continue improving battery and ultracapacitor technologies

to develop devices that will bridge the gap between batteries and ultracapacitors to edge further into the upper right corner of the Ragone plot, thus having both large specific energy and large specific power properties. The use of nanotechnology is one of the tools that researchers are focusing on to achieve these goals.

1.1.2 Nanostructures in Energy Storage Devices

Nanotechnology, the creation and use of sub micron ($0.1\mu\text{m}=100\text{nm}$) structures, is not a new field of study but recently has become an important topic for high level research in the areas of energy storage and electronic devices. Since many of the phenomena that enable energy transfer occur at the atomic or molecular level the use of nanostructures to better control and enable these phenomena has great potential for improved energy transfer efficiency, higher energy densities, and better material utilization. Energy transfer devices such as batteries, capacitors, ultracapacitors, fuel cells, solar cells, and consumer electronics can all benefit from the use of nanotechnology [5]. Lithium Ion batteries for example have been shown to benefit from the use of Si-C nanocomposites or nanostructured Fe-O in the chemical diffusion of Li showing improved reversibility and charge capacity [5]. Likewise, fuel cells are benefiting from the use of Pt coated nano-whiskers and Pt-Ru nano particles to improve catalytic reactions and obtain better utilization of expensive precious metals [5]. In ultracapacitors, where the charge transfer does not rely on chemical reactions for charge transfer and thus are not limited in speed or lifetime by the chemical kinetics, nanostructures play a critical role [6,7]. The charge from an ultracapacitor is created by the charge separation in the electrolyte immediately surrounding the porous electrodes, this phenomenon is also where the term double-layer capacitor comes from [1,6]. Figure 1.3 shows a representation of an electrochemical double layer ultracapacitor in the charged state.

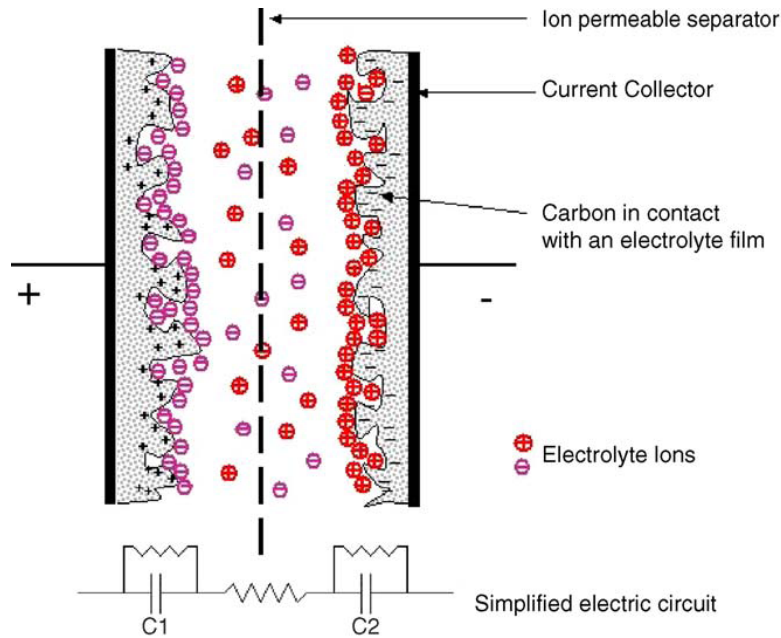


Figure 1.3 - Representation of electrochemical double layer ultracapacitor in the charged state [1]

From an ultracapacitor device standpoint the amount of charge is primarily dependent on the effective surface area sites available for ion attraction on each electrode pair and the separation distance between the electrodes as shown in the following equation [7]:

$$C = \epsilon A/d \quad (1.1)$$

where C is the capacitance, A is the surface area of an electrode pair, d is the distance between them, and ϵ is the permittivity relating to the electrolyte.

Another useful equation for the characterization of ultracapacitors is the specific energy equation:

$$E = \frac{1}{2}CV^2 \quad (1.2)$$

where E is the energy stored for the ultracapacitor, C is the capacitance per kg, and V is the applied voltage [7]. However, research has shown that the pore size of porous materials can play an important role in the amount of charge an electrode can store [8,9]. The literature shows that there is a critical pore size less than 1nm in diameter which can provide the largest charge storage capability. Typical porous

materials for use in ultracapacitors such as carbon foams and fabrics have pore sizes much larger than this critical nanopore size which can be in the order of micrometers [10]. Control of pore size is critical to optimize the ion transport channels and increase the stored charge on ultracapacitor electrodes. For this control an interesting nanostructure which is being investigated for use in many engineering applications including the fabrication of ultracapacitor electrodes is the use of electrically conductive carbon nanotubes.

1.1.3 Single-Walled Carbon Nanotubes

One of the most promising nanostructures being investigated currently for use in ultracapacitor electrodes are carbon nanotubes (CNTs). Essentially, CNTs consist of monolayer atomic sheets of sp^2 bonded carbon atoms which are rolled up and joined to form a seamless hollow tube as shown in Figure 1.4.

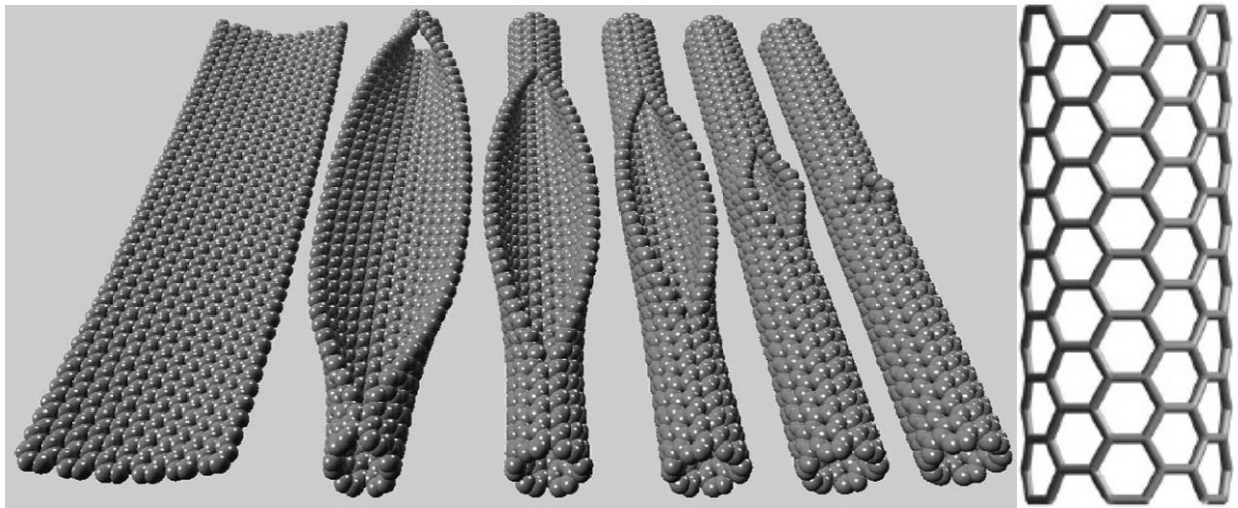


Figure 1.4 – Conceptual representations of CNTs from a monolayer graphene sheet [11,12]

CNTs can be produced by a number of methods and are generally categorized into two fabrication types: powders and arrays. Powder processes such as arc discharge, laser ablation, and combustion are cheap high output processes that can produce large volumes of carbon powder that contain millions of individual CNTs. The process is quick and relatively inexpensive with high volumes of material

produced. Further purification steps remove impurities and catalyst particles to leave upwards of 97% pure CNT powders (Figure 1.5).



Figure 1.5 – Carbon nanotube powder

Vapor deposition processes are used to grow vertically aligned arrays of CNTs on substrates which can have high precision but are slower, more expensive to produce, have lower output volumes and are process intensive.

Learning about the unique combination of properties displayed by individual CNTs helps to understand why CNTs show so much promise for the advancement of the properties of the bulk products. CNTs can have length to diameter ratios of up to 132,000,000:1 with lengths that can range from a few nanometers to a few centimeters [13]. CNT diameters vary depending on the type of CNT but remain within the nanoscale at 0.4 to 100nm [14]. There are two primary types of CNTs, single-walled carbon nanotubes (SWCNTs) and multi-walled carbon nanotubes (MWCNT). The diameters of SWCNTs are smaller and range from 0.4 to 2nm consisting of a single hollow carbon nanotube. MWCNTs on the other hand have larger diameters from 2 to 100nm and consist of multiple concentric carbon nanotubes with the largest tube representing the overall MWCNT diameter [14].

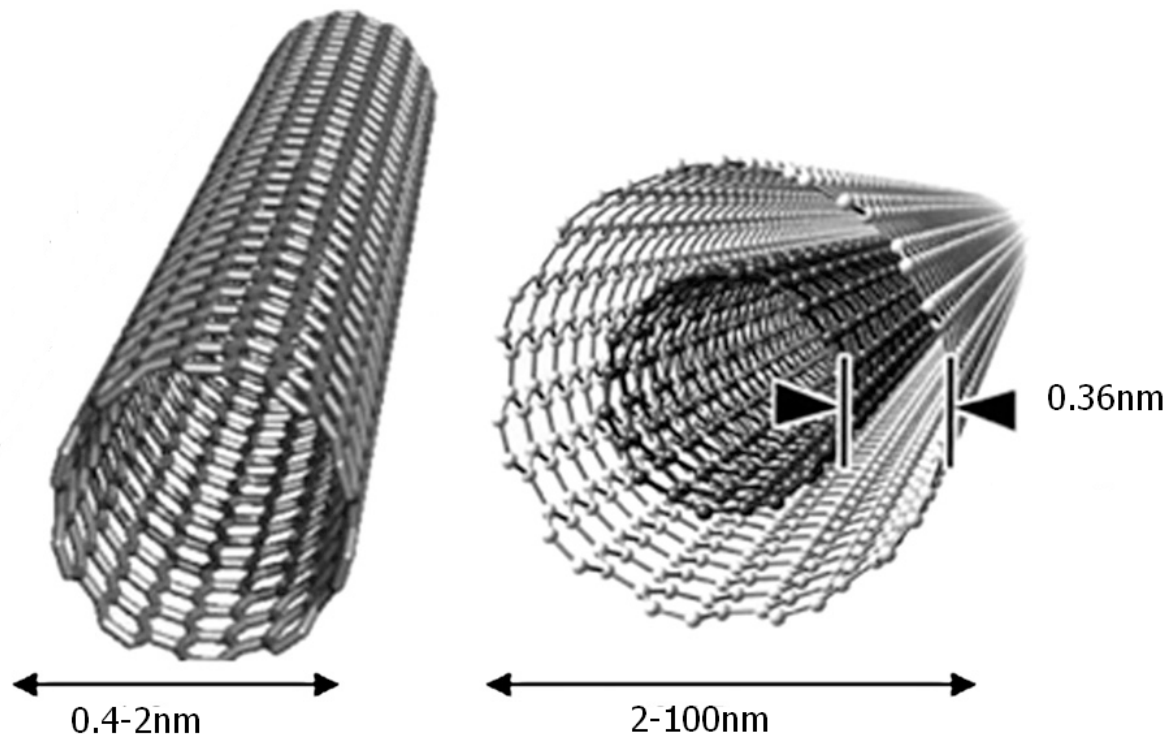


Figure 1.6 – Representation of single-walled (left) and multi-walled (right) CNT structures [15]

These nanoscale diameters and strong sp^2 carbon bonds create very high strength to weight ratios.

Individual CNTs are currently the strongest material discovered with reported tensile strength of upwards of 63 GPa, twenty times stronger than steel at approximately 3GPa [16]. At $1.3\text{-}1.4\text{g/cm}^3$ they are also very low in density and thus their specific strength is the highest currently known, $48,000\text{ kN}\cdot\text{m/kg}$ compared to high-carbon steel at only $154\text{ kN}\cdot\text{m/kg}$ [17]. In addition to their impressive mechanical properties one of the most useful properties of CNTs for energy systems is their ability to act as metallic conductors. This property results in strong interest for their use in electronic devices. The carbon bonds within CNT structures can transfer electrons easily such that they can act as metals and in theory are reported to have current densities of up to $4 \times 10^9\text{ A/cm}^2$ which compared to copper $1\text{ to }4 \times 10^6\text{ A/cm}^2$ is almost one thousand times greater [18,19]. Likewise their aspect ratios and low densities provide CNTs with a very high surface area to weight ratio. This is important for increasing the active surface sites for

energy transfer while keeping the overall size and weight of the energy systems low. Another desirable property of CNTs is their excellent chemical stability and high corrosion and temperature resistance.

These desirable electrical and mechanical properties make CNTs ideal building blocks for the advancement of energy systems and electronic devices in general. In particular, for this work on ultracapacitor devices, SWCNTs were selected since they generally have fewer defects and better electrical properties than MWCNTs and the well controlled 0.4-2nm diameter SWCNTs make ideal structures for the creation of thin three dimensional nanoporous networks for use in ultracapacitor electrodes [19,20]. By controlling SWCNTs to form nanopores for electrolyte ion transporting and adsorption in ultracapacitors the SWCNT electrode nanostructures can be optimized for maximum energy storage capacity [21,22].

1.2 Objectives

For the production of energy storage devices, such as ultracapacitors, bulk produced CNT powders are better suited for high volume manufacturing products than CNT arrays or forests. Unfortunately, one of the difficulties that have been reported with the use of CNT powders in the production of thin films is the agglomeration of CNTs during suspension processing [23]. The strong van der Waals forces and hydrophobicity of the SWCNTs result in the formation of ropes and tangled networks within aqueous suspensions and can result in non-uniform or uneven SWCNT coatings [23]. A process is therefore needed which is repeatable and can uniformly deposit purified SWCNT powders over large areas for high volume production of SWCNT electrodes while producing uniform nanopores to create maximum charge capacity.

Using purified SWCNT powders prepared into suspensions, various SWCNT deposition processes and their effect on the energy density of ultracapacitors can be evaluated. SWCNT dispersion techniques such as drop coating, high voltage electro-spraying (HVES), inkjet printing, and electrophoretic deposition

(EPD) [24,25,66] are investigated here for their ability to form uniform nano-structures from SWCNT suspensions. Once a suitable deposition method is identified the specific processing parameters of that method are characterized. More specifically this work shows that EPD is an effective method for the production of SWCNT ultracapacitor electrodes and identifies the relationships between SWCNT electrode capacitance and EPD processing parameters such as processing time and processing temperature. The characterization of these process parameters and the methods defined in this work allow for the optimization of EPD processed SWCNT ultracapacitor electrodes to create high capacitance electrodes.

Understanding and optimizing the methods for SWCNT electrode fabrication and defining the process parameters to create large areas of uniform nanoporous networks will help increase the energy density of ultracapacitors and bridge the gap between high energy density and high power density storage devices.

Chapter 2

Literature Review

A review of various techniques and processes for manipulating carbon nanotubes and other nano materials for the purposes of creating structures, coatings, and devices is necessary for the experimental fabrication of SWCNT electrodes. A preliminary need which has also been identified is the need to produce a stable and well dispersed SWCNT suspension for handling and processing of purified SWCNT powders. Methods for dispersing SWCNT suspensions onto substrates were also reviewed to determine which methods were suitable for or could be adapted for use in the fabrication SWCNT ultracapacitor electrodes. A review of current devices, including ultracapacitors, created using SWCNT suspensions and the tools used to produce them were also identified throughout the literature review. Finally a review of the benchmark research results as well as the best in class commercially available carbon ultracapacitors were investigated and summarized for reference.

2.1 Single-Walled Carbon Nanotube Suspensions

Purified as received SWCNTs are typically in the form of a fine powder as shown previously in Figure 1.5. The nanotubes are extremely lightweight, mimicking dust particles, and are difficult to work with in a powder form. To facilitate the uniform coating of SWCNTs onto substrates the SWCNTs need to be well dispersed into liquid suspensions. Through the course of the literature review 3 methods for the dispersion of SWCNTs into liquids were identified and are discussed in more detail below.

2.1.1 Sonication Mixed Suspensions

SWCNTs are extremely hydrophobic and due to the strong Van der Waals forces along the lengths of the tubes have a tendency to agglomerate and form bundles and ropes [23,26]. To separate CNTs without the addition of surfactants or treatment of the CNTs one simple technique used for temporary dispersion of CNTs in aqueous suspensions is the use of high power sonication tips (1/8 in., 6 W, 22.5 kHz). However,

this technique is reported to have minimal success due to poor CNT dispersion percentages and poor shelf life [27,28,32]. Also the sonication of CNTs has been known to shorten their lengths, change the CNT diameters, and introduce defects due to the high power sonification required to break the Van der Waals forces and disperse the CNT bundles [27,29,30]. To mitigate the amount of sonication time and to significantly improve the shelf life, concentrations, and individual tube separations in aqueous suspensions the use of sonication alone is not common. Instead researchers are combining mild sonication with the addition of surfactants, polymer wrapping, or chemical modification techniques to achieve much better CNT suspensions.

2.1.2 Surfactant and Polymer Based Suspensions

Dispersion of CNT bundles and ropes into aqueous suspensions has improved with the use of surfactants and polymers to isolate individual CNTs from bundles and ropes and to produce stable suspensions [27,28]. Essentially the surfactants and polymers used in CNT suspensions work in a similar method by adsorbing onto the CNT surface and shielding the hydrophobic CNTs from the H₂O molecules and other CNTs. Three of the most common surfactants used are sodium dodecylbenzene sulfonate (NaDDBS), sodium dodecyl sulphate (SDS), and Triton X-100. Some theories as to how the surfactants adsorb onto the CNTs suggest random arrangement of the surfactant molecules, with the heads and tails of the surfactant molecules wrapping the CNTs [31]. Below is a schematic representation of another hypothesis for how three common surfactants could adsorb onto the CNT walls as hemimicelles and shield the CNTs (Figure 2.1) [27].

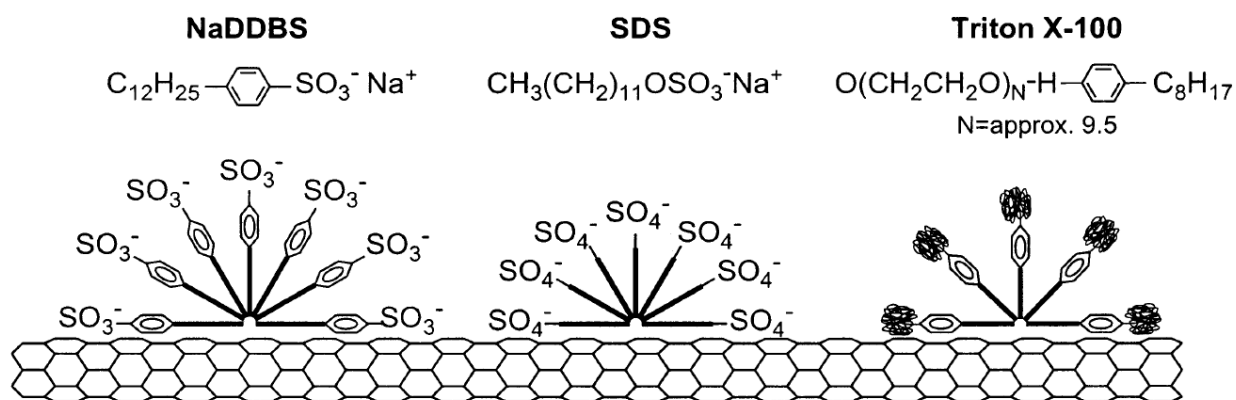


Figure 2.1 - Schematic representation of surfactant adsorption on CNT walls [27]

However, one of the issues described with the use of surfactants in the preparation of SWCNT suspension for use in the creation of SWCNT networks is the trapping of surfactants in the SWCNT network [32]. As the SWCNT network is formed the surfactant molecules can become trapped and affect the thermal and electrical properties of the network by impeding the formation of tube to tube junctions. In an attempt to remove the surfactant post formation, additional process steps can be required but due to the integration of the surfactant in the network it can be difficult to remove all surfactant or could disturb the processed SWCNT layers [32,33].

2.1.3 Functionalized Suspensions

The addition of molecular groups to, or functionalization of, SWCNTs can be an effective method for dispersing SWCNT bundles in polar suspensions such as H₂O or Ethanol without the use of surfactants [34,35]. Strong acids such as concentrated Nitric or Sulfuric acids can be used to add charged molecular groups, mainly carbonyl (CO) and carboxylic (COOH) groups, to the defect sites along the CNT walls. The bonding of these charged molecules give the CNTs a surface charge which helps to repel them from one another and disperse the individual tubes in the polar suspensions [36]. Figure 2.2 shows a representation of a SWCNT which has been functionalized with carboxylic acid groups.

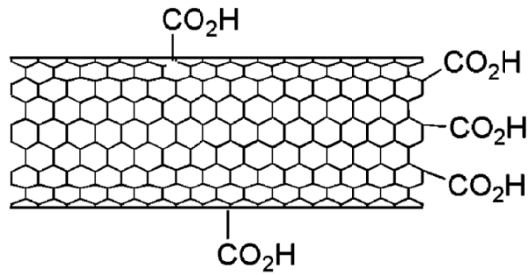


Figure 2.2 - Acid-cut nanotubes with carboxyl groups on ends and sidewalls [36]

The acid functionalized SWCNTs can become shorter in length due to cutting of the tubes by acid treatment which can affect the electrical properties of the nanotubes [37]. However, research has shown that post fabrication acid treatment of surfactant based CNT networks improves the electrical conductivity significantly, 95% increase, compared to the networks prior to surfactant removal [33]. Since the use of functionalized CNTs avoids the use of surfactants all together the effects of the acid treatment alone are less detrimental to the bulk CNT network than the use of surfactants followed by acid treatment purification. To emphasize the effectiveness of acid functionalization on the removal of CNT hydrophobicity, below is a figure showing the contact angle of water droplets on SWCNT networks that have been acid functionalized for various durations. This image shows a significant reduction in the hydrophobic properties of the SWCNT networks after functionalization.

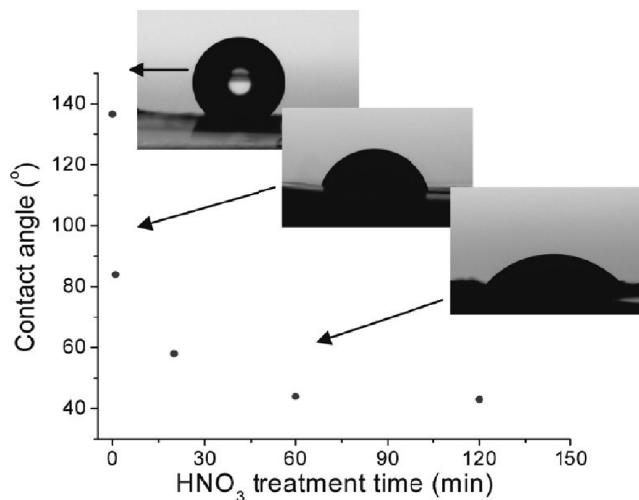


Figure 2.3 - Optical images of water droplet contact angle vs acid functionalization duration [38]

2.2 Single-Walled Carbon Nanotube Suspension Deposition Methods

For the creation of devices using nanomaterial suspensions such as SWCNTs in H₂O various techniques are considered for the uniform coating or deposition of suspensions onto substrates. Each method has advantages and disadvantages and their use depends on the properties of the final product including its size, intended use, and contact materials. Four common deposition methods for SWCNTs are described here.

2.2.1 Vacuum Filtration Method

The vacuum filtration method is used for SWCNTs where no current collector or other substrate is desired, as in the formation of a self supporting SWCNT film, also known as “Bucky paper”. In this method the SWCNT suspension is drawn through a cellulose, ceramic, or other filter of pore size in the micrometer range, 0.45 μm for example [39,40]. A vacuum or other pressure differential is created to force the suspension through the filter. As the SWCNT suspension moves through the filter the liquid suspension passes through the filter pores and the SWCNTs are trapped on the surface forming a random oriented network (Figure 2.4). The filters coated with the SWCNT network are then removed from the system and dried in an oven or room temperature to remove moisture. In some cases the SWCNT networks are used in conjunction with the filters while in other cases the filters are removed through wetting or chemical treatment such as immersing a cellulose filter in acetone [41,43].

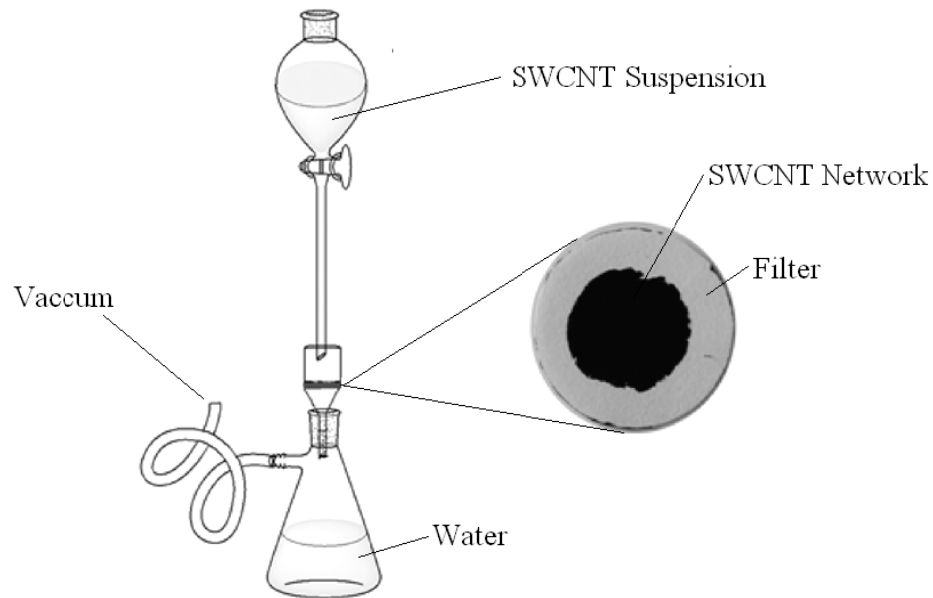


Figure 2.4 - Vacuum filtration setup for production of SWCNT films [40]

For this method the final thickness is dependent on the volume of suspension flowing through the filter and the concentration of the SWCNT suspension. This method is good for low volume fabrication of SWCNT films where no current collector or substrate is desired. Limitations for this method are thickness variation control, difficulty of SWCNT network separation from filters, slow process, limited size, and difficulty handling the processed films [39,40,41].

2.2.2 Spin Coating

For applications that require very thin even coatings spin coating is a useful process. For spin coating a substrate is required to receive the suspensions, but can be any material of sufficient smoothness to allow spreading of the coating material. The substrate is mounted to a horizontal rotating disk and the coating liquid is dropped onto the center of the rotating surface (Figure 2.5). Centrifugal forces cause the liquid suspension to spread radially from the center towards the edge of the substrate creating a uniform thickness layer of suspension.



Figure 2.5 - Schematic image of spin coating process [42]

The viscosity of the suspension, surface treatment of the substrate and the speed of rotation determine the overall surface coating thickness [42,43]. The spin coating process has been demonstrated effective in producing uniformly distributed CNT based thin films but is not ideally suited for large scale production due to the size limitations of the rotating equipment, the limitations on maximum surface thickness (related to viscosity and rotational speed), and the waste material that is lost due to surface run off [42,43,44].

2.2.3 Wire Wound Rod Coating

To address the size limitations and waste product issues observed in the filtration and spin coating methods the wire wound rod or bar coating method are also used to produce CNT coatings [45]. The wire wound rod coating process is used to produce uniform CNT thin films for use in high volume manufacturing such as the production of solar cells [46]. The wire wound rod technique utilizes the known space gaps between wound wire diameters to control the volume of fluid applied to a surface. Figure 2.6 below shows how larger diameters of wound wire will result in thicker films and smaller diameters will result in thinner films. The surface tension of the deposited fluid then flattens the film to create a uniform thin film of known thickness [47].

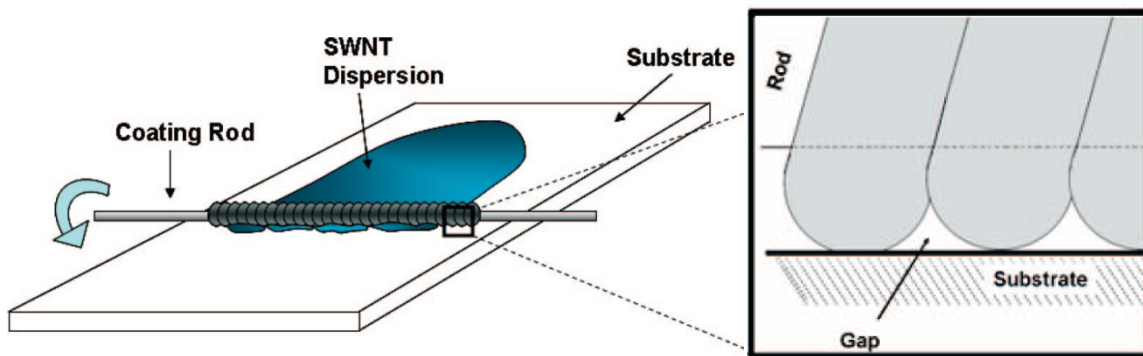


Figure 2.6 – Illustration of wire wound rod coating technique [48]

Advantages of the wire wound rod method are low equipment costs, scalability for large volume production, and ease of implementation. The disadvantages with this process are the waste material on the rod and sides of the substrate, the specific viscosity requirements, and the difficulty in obtaining undamaged or defective free films during handling and curing [45,48].

2.2.4 Electrophoretic Deposition

To address the surface imperfections and waste associated with rod coating electrophoresis or electrophoretic deposition (EPD) has also been investigated. EPD is similar to electroplating and uses voltage potential between two electrodes to move charged particles of desired coating material from a suspension and onto the surface of one of the electrodes [49]. For EPD to be effective both the electrode pair or substrate and the deposition particles in suspension need to be electrically conductive [50]. In the case of functionalized CNTs they are electrically conductive and have surface charges due to the functionalization making them a good candidate for the EPD process. An example EPD setup for processing of CNT suspensions is shown below in Figure 2.7.

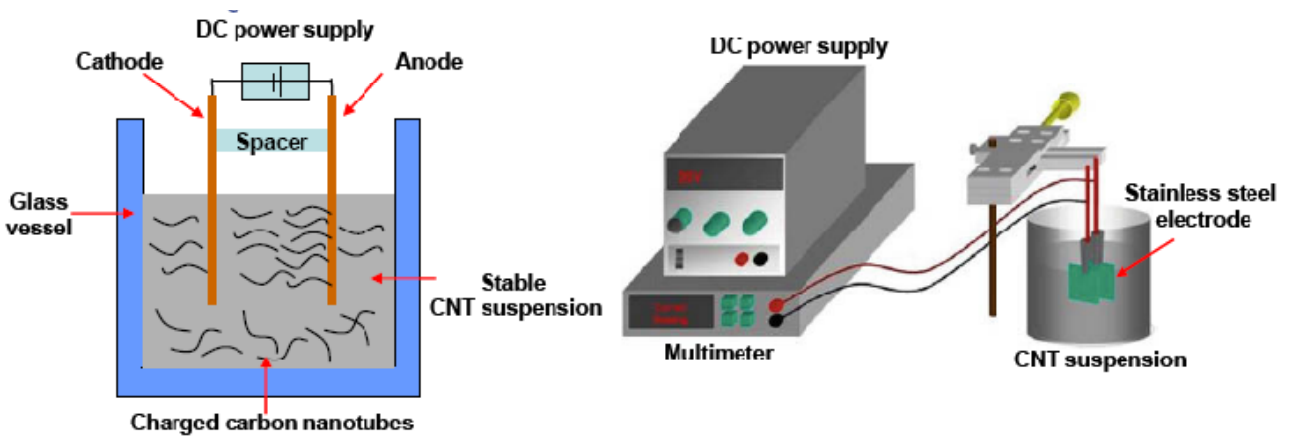


Figure 2.7 – Schematic of electrophoretic deposition cell used to create CNT thin films [51]

This process has been found to yield homogeneous surfaces covered by random networks of CNTs with low surface roughness. The surface roughness of the EPD CNT films has also shown to be comparable to ITO films and less than the surface roughness of other CNT deposition methods such as filtering. This low surface roughness makes the EPD process better suited for stacked thin films such as those in ultracapacitors where small surface defects could short circuit the devices. Figure 2.8 shows empirical data of average surface roughness for CNT films using additional fabrication techniques: Dip Coating, Filter Method, Spray Coating, and Electrophoretic Deposition versus indium tin oxide (ITO).

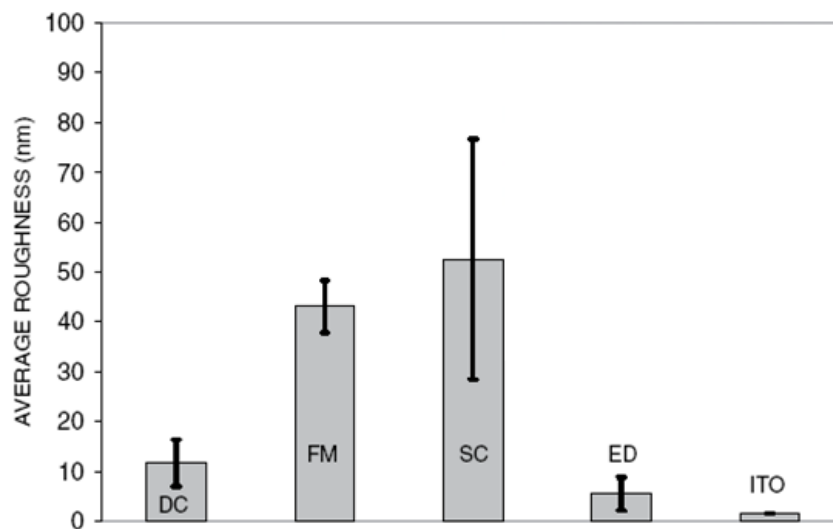


Figure 2.8 – Surface roughness for CNT films produced by various methods compared to ITO [52]

The films produced using EPD are reported to show limited voids in the network of less than 100nm and macroscopic homogenous structures with uniform thickness between 5-10 μ m depending on the applied voltage and deposition time [51,52]. EPD has also been used to produce thin transparent uniform CNT films for optoelectronic devices with thicknesses of approximately 54nm with only 40 seconds of deposition time [53]. A hot transfer process was needed to bond polyethylene terephthalate (PET) films to the very thin CNT films to create composite flexible transparent PET + CNT thin electrodes that could then withstand over 10,000 bending cycles [53]. These durable CNT composite sheets are well suited for mass produced fabrication. The benefits of EPD include short fabrication times and uniform surface properties with low surface resistance, minimal roughness, and excellent material utilization, while the issues with EPD are limited to the specific requirements for substrates and the complexity of the EPD cell [51,52,53]. These excellent properties make EPD ideally suited for mass produced electronic and energy storage devices and thus the primary focus of this work will be on the development and further characterization of the EPD process for producing SWCNT ultracapacitor electrodes.

2.3 Published Results and Commercial Benchmarks

As a basis for all research it is important to understand the current best known results or benchmarks for which a researcher is striving to surpass. A literature review of current published research capacitance values and list of commercially available ultracapacitors are included here.

2.3.1 Carbon Nanotube Ultracapacitor Properties

Table 2.1 below shows a summary of specific capacitance, differential capacitance, specific power, and specific energy values for ultracapacitor electrodes fabricated using different carbon types. Carbon types include MWCNT, SWCNT, activated carbon (AC), and graphene sheets. Whether the electrodes were treated or untreated to use pseudocapacitance and the scan rates at which the capacitance values were calculated are also included in this list [54-62].

Table 2.1 - Summary of published capacitance values for various carbon ultracapacitor electrodes

CNT Type	Pseudo-capacitance	Specific Capacitance (F/g)	Differential Capacitance ($\mu\text{F}/\text{cm}^2$)	Specific Power (kW/kg)	Specific Energy (Wh/kg)	Scan Rate	Ref.
MWCNT	Y - MnOx	378-469	-	120.1*	-	100mV/s	[55]
MWCNT	N	113	24	-	3.9	-	[56]
MMCNT	Y - NH3 Treated	207	240	-	5.8	0-1000mV/s	[57]
SWCNT	N	180	50	-	6.5	-	[58]
SWCNT	N	60	6	-	13.0	-	[59]
SWCNT	N	20	-	-	-	-	[60]
SWCNT	N	35	-	197.3	43.7	20mV/s	[61]
SWCNT + AC	N	142	-	22.0	50.0	5-200mV/s	[60]
AC	N	90	-	6.3	19.6	5-200mV/s	[60]
Graphene	N	245	-	-	-	10-100mV/s	[62]
Graphene	Y - MnO ₂	328	-	25.8	11.4	10-100mV/s	[62]

Calculated values indicated by “” all other data is as reported.

From the above summary it is clear that pseudocapacitance, which uses the partial chemical reaction of added species such as MnO₂ to increase the overall capacitance of ultracapacitors, has an additive effect to the electrochemical double layers capacitance [55,62]. However, for the purposes of this work the focus is on the creation of a SWCNT network which has good capacitance values without the use of pseudocapacitance. In future work it can be appreciated that the addition of MnO₂ or other additives to the optimized SWCNT network discussed here will yield further capacitance improvements. By focusing solely on the optimization of the core SWCNT network a solid foundation for the addition of pseudocapacitance in a later work has been laid.

2.3.2 Commercially Available Ultracapacitor Properties

In addition to looking at research values it can also be useful to have an understanding of the best in class commercial devices that are available on the market today. Commercial devices by necessity have typically undergone extensive durability, reliability and characterization testing to ensure that the product

has a useful life and will meet or exceed the expectations of customers. Although lower than research values, the values of commercial ultracapacitors as shown in Table 2.2 below are also a good benchmark for what is achievable in a repeatable large scale production environment.

Table 2.2 - Commercially available carbon EDLCs [1]

Company name	Device name	Capacitance (F)	Cell/module voltage (V)	Type
Asahi Glass	EDLC	500–2000	3, 14/42	Carbon/non-aqueous
AVX	Bestcap	0.022–0.56	3.5–12	Carbon/polymer/aqueous
Cap-XX	Supercapacitor	0.09–2.8	2.25–4.5	Carbon/non-aqueous
Cooper	PowerStor	0.47–50	2.3–5	Aerogel/non-aqueous
ELNA	Dynacap	0.333–100	2.5–6.3	Carbon/non-aqueous
Epcos	Ultracapacitor	5–5000	2.3,2.5	Carbon/non-aqueous
Evans	Capattery	0.01–1.5	5.5,11	Carbon/aqueous
Maxwell	Boostcap/PowerCache	1.8–2600	2.5	Carbon/non-aqueous
NEC	Supercapacitor	0.01–6.5	3.5–12	Carbon/aqueous Carbon/organic
Nippon	Chemi-Con DLCAP	300–3000	2.3,2.5	Carbon/non-aqueous
Ness	NessCap	3–5000	2.3,2.7	Carbon/organic
Matsushita/Panasonic	Gold capacitor	0.1–2500	2.3–5.5	Carbon/organic
Tavrima/ECOND	Supercapacitor	0.13–160	14–300	Carbon/aqueous

Chapter 3

Experimental Procedures

One of the key issues with the use of SWCNTs is the creation of bulk materials which demonstrate the excellent individual properties that SWCNTs possess. If the SWCNTs are not well distributed on a bulk surface and only cover a small percentage of the substrate then the bulk material may show little or no increase in the desired properties. Similarly, if the SWCNTs become agglomerated and group together then their individual properties such as high surface area and nanoporosity become reduced and the agglomerated properties again dominate the bulk material. Current research with powder based SWCNTs as discussed here is focused on the dispersion of SWCNTs into liquid suspensions and then the coating of the SWCNT suspensions onto large substrates for use in ultracapacitor electrodes. The experimental procedures discussed below describe the various dispersion and coating methods tested within this work and ultimately describes a procedure for successfully creating uniform nanoporous SWCNT coated electrodes efficiently and reproducibly.

3.1 Single-Walled Carbon Nanotube Suspensions

As produced powder CNTs are hydrophobic and do not disperse well into aqueous suspensions as discussed previously in section 2.1 and as shown in Figure 2.3 in section 2.1.3. For this work purified SWCNTs (97%) were obtained from Nano-C Inc. When mixed with H₂O the SWCNTs agglomerated together in clumps and floated to the surface. Even with the use of a sonication bath the SWCNTs did not disperse and thus a uniform suspension could not be created without further treatment.

3.1.1 Single-Walled Carbon Nanotubes in H₂O Using Surfactants

Surfactants such as sodium dodecyl sulfate (SDS) (CH₃(CH₂)₁₁OSO₃Na) have been shown to be effective in dispersing the CNTs into water suspensions [46]. By adsorbing SDS onto the surface of the CNT it has been reported possible to evenly disperse CNTs in water suspensions. To further understand the effect of

SDS on dispersion quality in this work various concentrations of SDS (Sigma-Aldrich) aqueous solution were prepared and mixed with equal masses of SWCNTs and sonicated in a Branson 5210 Ultrasonic cleaner for 1hr at 22°C. After sonication the suspensions were centrifuged for 30min at 4000RPM and decanted to remove agglomerated SWCNT bundles and particulate from the suspension. Figure 3.1 shows the optical density of various samples and shows that the surfactant concentration is found to be proportional to SWCNT dispersion quality. Here each tube contains 0.25mg/ml SWCNT in SDS concentrations varying from left to right: 0.1M, 0.01M, 0.001M, and 0M (no SDS, SWCNT in pure H₂O). Although each sample contains the same concentration of SWCNTs (0.25mg/ml) the samples on the left with higher concentrations of SDS show much better dispersion and thus much lower optical transparency.



Figure 3.1 – SWCNTs dispersed in H₂O using decreasing concentrations of SDS

For the use of surfactant based SWCNT suspensions it is important to minimize the surfactant concentration since the surfactant will adversely affect the electrical and capacitive properties of the SWCNTs networks [32]. After the CNT + SDS thin film has been created it is possible to remove some of the surfactant through further washing or treatment of the thin films, but this adds additional processing steps and in multilayer films some surfactant becomes trapped and not all surfactant can be removed.

From the SDS concentration experiments it was determined that an SDS concentration of 0.1M was optimal for the fabrication of SWCNT aqueous suspensions having good SWCNT dispersion and resistance to agglomeration while using a low mass of added surfactant.

3.1.2 Acid Functionalized Single-Walled Carbon Nanotubes in H₂O

As an alternative to surfactant based SWCNT suspensions and to eliminate the need for additional washing steps acid functionalized SWCNT aqueous suspensions were also prepared in this work. Purified SWCNTs (97%) obtained from Nano-C Inc. were first acid functionalized using a mixture of concentrated nitric (HNO₃) and sulfuric (H₂SO₄) acid in a ratio of 1:3 respectfully (Sigma-Aldrich). 10mL of the acid mixture was added to 250mg of SWCNT powder for 30min to complete the carboxyl functionalization [63-64]. During this process the acid mixture adds –COOH functional groups to defect and end sites on the SWCNTs [29,65]. This negatively polarizes the SWCNTs and allows them to disperse well in pure H₂O without the use of additional surfactants [66]. Since the addition of surfactants has been shown to negatively affect the performance of CNTs and it is difficult to remove the surfactant from the CNT network after processing the functionalization method for creating SWCNT suspensions is better suited for the fabrication of SWCNT ultracapacitor electrodes [32 ,67]. After acid functionalizing, the SWCNT acid mixture was diluted with de-ionized water and washed through paper filters (Whatman #4) to remove the acidity from the SWCNTs as shown in Figure 3.2. The process was repeated until the filtered SWCNT slurry reached a pH of 7, then the functionalized SWCNTs were washed from the filter into 500ml of di-water to produce a SWCNT aqueous suspension with a SWCNT concentration of approximately 0.5mg/mL H₂O. The suspension was then placed in a Branson 5210 ultrasonic cleaner for 30min at 22°C and centrifuged for 30min at 4000RPM to remove agglomerated SWCNT bundles from the suspension.

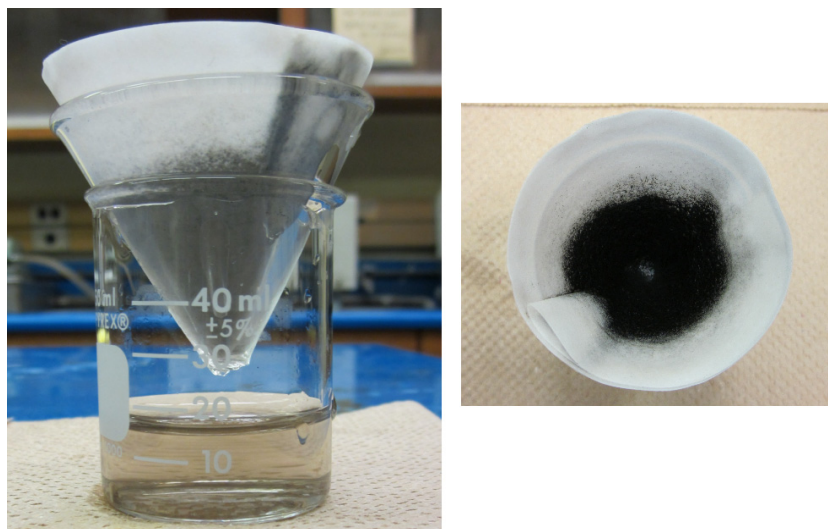


Figure 3.2 - Images showing acid removal and filtering of SWCNTs

The functionalized SWCNT aqueous suspension was found to have excellent dispersion of SWCNTs and strong resistance to agglomeration or precipitation of SWCNT bundles over time. A functionalized SWCNT suspension prepared 2 months prior to the photograph date is shown below (Figure 3.3).



Figure 3.3 - Optical image of functionalized SWCNT suspension two months after preparation

3.2 Single-Walled Carbon Nanotube Suspension Processing

Initial testing of the SWCNT suspensions was done using a simple drop coating technique to evaluate the dispersion quality of the surfactant based SWCNT aqueous suspensions. From the drop coating samples it was determined that the surfactant based suspension had issues with surfactant in the network and that the drop coating method itself had issues with uniform surface density. To address these issues later experiments used the functionalized SWCNT aqueous suspensions as an alternative to surfactant based suspensions and other experimental methods such as high voltage electro spraying (HVES) and inkjet printing were attempted in an effort to resolve the uniformity issues. Ultimately electrophoretic deposition (EPD) was used to as the primary processing method for functionalized SWCNTs. Detailed descriptions and figures are shown below of the experimental procedures for each SWCNT suspension processing method used in this work.

3.2.1 Drop Coating

Initially drop coated samples were prepared on various substrates including aluminum (Al), nickel (Ni) and stainless steel (SST) foils using SDS surfactant based SWCNT aqueous suspension prepared as described above in section 3.1.1. For drop coating, approximately 3-4 drop (0.1-0.2ml) of 0.5mg/ml SWCNT suspension was applied to horizontal substrates using a micropipette as shown in Figure 3.4 and allowed to dry in air for 24hrs before oven drying for 30min at 80°C.

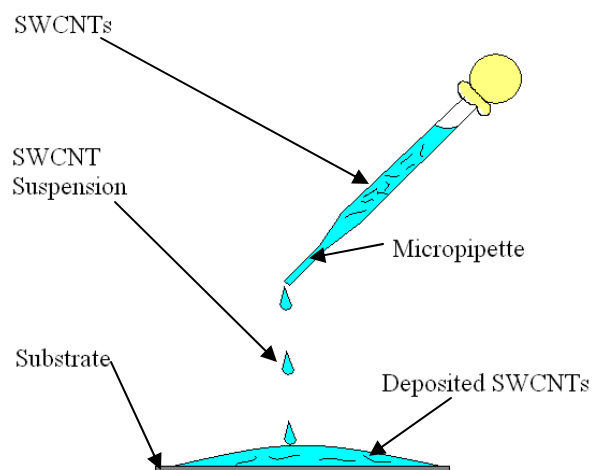


Figure 3.4 - Schematic diagram of SWCNT drop coating process

3.2.2 High Voltage Electro Spraying

High voltage electro-spraying (HVES) is a well known method for producing well mixed micro fibrous networks, typically using polymer materials [68,69]. For this work HVES was adapted in an attempt to use the method to disperse the acid functionalized SWCNT aqueous suspension as prepared previously in section 3.1.2. In high voltage electro-spraying of SWCNTs, Ni electrodes acted as substrates. The Ni electrodes were attached to the positive lead and placed approximately 25cm below a grounded dispensing needle containing 30mL of SWCNT suspension. An 8kV potential was introduced between the dispensing needle and the electrodes and the suspension was slowly ejected from the needle. For HVES both aqueous functionalized SWCNT suspensions as described in section 3.1.2 and ethanol based functionalized SWCNT suspensions as prepared using the same method but with ethanol replacing H₂O in the final rinsing step from were used. Figure 3.5 shows a schematic diagram of the HVES SWCNT coating process.

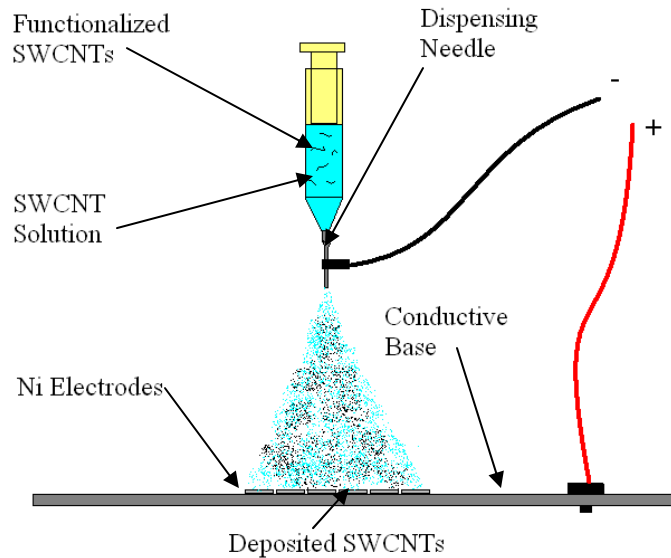


Figure 3.5 - Schematic diagram of HVES SWCNT coating process

3.2.3 Inkjet Printing

In addition to drop and HVES techniques for the coating of SWCNTs onto conductive substrates or electrodes, ink jet printing of SWCNTs was also investigated as an experimental technique for the fabrication of SWCNT ultracapacitor electrodes. Here the acid functionalized SWCNT suspension as prepared in section 3.1.2 was used to replace traditional black inks in consumer ink jet printers and used to coat copy paper and electrically conductive ITO coated PET (Sigma-Aldrich). Two printer types were used for this process (Figure 3.6):

- 1) Piezoelectric Epson Stylus NX510, 5760 x 1440 dpi, 2.0 picoliter droplet size [70]
- 2) Thermal HP Deskjet F4480, 600 x 600 dpi, 13.8 picoliter droplet size [71,72]



Figure 3.6 - 1) Epson Stylus NX510 and 2) HP Deskjet F4480 printers [70,71]

In each case the original inkjet cartridges (Epson T069 and HP 60) were removed from the printers and the black ink was extracted from the top of the cartridges using a syringe via their filling holes located under the top side label. Once all the original ink was removed, 5-10ml of de-ionized water was injected into the filling holes to rinse and remove all colored dyes from the ink cartridges. The de-ionized water was then removed and the process repeated until the injected water ran clear after extraction.

Once all of the black ink and di-ionized water was removed from the cartridges, the functionalized SWCNT suspension was sonicated in a Branson 5210 ultrasonic cleaner for 30min at 22°C and 5-10ml of SWCNT suspension was injected into the empty cartridges. The SWCNT inkjet cartridges were then sonicated for an additional 5min in a Branson 5210 ultrasonic cleaner at 22°C before being placed back into their respective printers. Various electrode shapes 3x1cm, 3x3cm, 3x5cm, etc were created in word and used to print the SWCNTs onto standard white copy paper or ITO coated PET. These non-electrically and electrically conductive substrates were then fed back into the printer repeatedly to increase the density of the SWCNT on the substrates by printing multiple layers onto the same location. In each case the cartridges were removed and re-sonicated for 5-10 minutes after every 5 prints. This helps to avoid nozzle clogging in the cartridges due to agglomerated SWCNT bundles and also allows the substrates to dry. The same shape was printed on the same substrate between 5 and 150 times for each electrode produced.

3.2.4 Electrophoretic Deposition

Experimentation with various SWCNT dispersion techniques also included the use electrophoretic deposition (EPD). Although research in the area of carbon nanotube (CNT) EPD has already been investigated by others as reported in section 2.2.4, it appears to be a promising technique for the fabrication of CNT electrodes for use in ultracapacitors and potential exists for improvement of the process. A summary of existing EPD parameter configurations and CNT suspensions and as reported by Boccaccini for use with CNT EPD processes is shown below in Table 3.1 and Table 3.2 below [50]. From these tables a need is identified for further CNT EPD characterization research. Specifically a need exists to look at the effect of extended EPD processing times beyond 10min and the effect of EPD processing temperature on the capacitance of thin SWCNT films for use in ultracapacitors.

Table 3.1 - Summary of EPD parameters used in EPD of CNTs [50]

Electrode properties	EPD parameters		
	Constant voltage	Deposition time	Distance between electrodes
Stainless steel ($1 \times 1 \times 0.2 \text{ cm}^3$)	5–50 V	0.5–10 min	20 mm
Aminopropoxysilane (APS) pretreated Optically Transparent Electrodes (OTEs)	500 V & 50 V	1 min & 2 min	~6 mm
Carbon Fibre paper Electrodes (CFE) ($2.25 \times 2.25 \times 0.6 \text{ cm}^3$)	~40 V	–	~5 mm
Aluminium electrodes	45 V	–	50 mm
Metal electrodes	45 V	–	50 mm
Titanium ($1 \times 1 \text{ cm}^2$) electrodes	–	–	–
Cathode: Glass plate ($1 \text{ cm} \times 0.5 \text{ cm}$) with ITO coating Anode: Glass plate ($1 \text{ cm} \times 0.5 \text{ cm}$) with aluminium coating	100–200 V	–	18, 11, 3 & 1 mm
Silicon wafer (cathode) and stainless steel mesh as an anode	30–600 V	–	20 mm
Stainless steel mesh (cathode) and a gated triode structure formed on a glass substrate (anode)	30–200 V	–	–
Indium tin oxide (ITO) coated glass	–	–	–
Conducting glass electrodes, optically transparent electrode (OTE)	100 V	–	5 mm
Conducting glass electrodes, optically transparent electrode (OTE)	<100 V & >100 V	2–3 min	5 mm
Polyimide film coated with titanium (cathode) and stainless steel (anode)	100 V	1–2 min	–
Stainless steel	20 V	–	10 mm
Patterned metal substrates	10–50 V	–	–
Patterned dielectric substrate with $1 \mu\text{m}$ thick polysilane film coating	2000 V/cm	A few min	–
Nickel and stainless steel substrates or metal-plated glass plate	200–300 V	2 min	20 mm
Nickel substrates ($10 \times 10 \text{ mm}^2$) etched with 20% HNO_3 for 10 min	20 V	5 min	–

Table 3.2 - Summary of CNT type and suspension preparation for CNT EPD [50]

CNT type	Suspension properties
MWNTs	Aqueous solutions of 0.25 and 0.55 mg/mL (CNT/H ₂ O)
SWNTs	10 mg of SWNTs mixed with 0.13 g of tetraoctylammonium bromide (TOAB) were dried and resuspended in 25 mL of Tetrahydrofuran (THF) + quaternary ammonium salt
SWNTs	10 mg of SWNTs with 100 mg of tetraoctylammonium bromide (TOAB) or Nafion in 25 ml of Tetrahydrofuran (THF)
MWNTs	Ethanol with EPI-Rez resin and EPI-CURE curing agent (aliphatic amine)
MWNTs	Mixtures of acetone and ethanol in different volume ratios
MWNTs	0.125 mg/ml (CNT/isopropyl alcohol) and small amount of bezalkonium chloride
SWNTs	Isopropyl alcohol with NiCl ₂
MWNTs	Isopropyl alcohol solution containing Mg(NO ₃) ₂ ; ethyl cellulose was also added to improve dispersion
SWNTs	De-ionised water mixed with pyrrole and lithium perchlorate
SWNTs	Ethyl alcohol with MgCl ₂
SWNTs	Tetraoctylammonium broamide (TOAB) in tetrahydrofuran (THF)
SWNTs	Tetraoctylammonium broamide (TOAB) in tetrahydrofuran (THF)
Not Specified	Isopropyl alcohol (IPA) with Mg(NO ₃) ₂ · 6H ₂ O
SWNTs	Methanol or dimethylformamide (DMF) with <1 wt% concentrated sodium hydroxide
SWNTs	Distilled water with Mg(NO ₂) ₂ · 6H ₂ O
MWNTs	Isopropyl alcohol (IPA)
MWNTs	2g of CNTs mixed with 500 ml <i>n</i> -pentanol with a small amount of anhydrous Mg(NO ₃) ₂ .
Not Specified	0.5 mg CNT/1 mL dimethylformamide (DMF) solution

In this work two electrophoretic deposition cells were created. The first cell uses a single power supply, a beaker, nylon spacer, and a hand clamp. This simple device was designed to allow initial experimentation of the EPD process for the coating of functionalized SWCNTs onto Ni and SST substrates. This first cell was a proof of concept device and was used to perform the first extended processing time fabrication of SWCNT electrodes processed at room temperature for 0 to 60 minutes. Approximately 90 SWCNT electrodes were produced using the first EPD cell. Using the initial cell as a template a second more advanced EPD cell was designed and fabricated to specifically evaluate the effect of EPD processing temperatures on the processing time vs capacitance curves. This second cell uses three power supplies, a fan, a thermoelectric cooler, a heat sink, a beaker, and a machined polycarbonate spacer with two integrated spring clamps. The second cell was used to perform extended processing time fabrication of SWCNT electrodes for 0 to 60 minutes at a range of EPD processing temperatures from 5 to 60°C.

3.2.4.1 Electrophoretic Deposition Cell 1

The initial EPD cell was fabricated with a working distance of 1cm between electrodes. Upon fabrication the positive electrodes from the EPD cell also acted as the current collectors for the characterization of the SWCNT ultracapacitors. Stainless steel (SST) 304 (70%Fe, 19%Cr, 11%Ni: wt%) sheets 0.100mm thick from Alfa Aesar were used as the current collectors and substrates for the SWCNT electrodes. The SST electrodes were cut, numbered, and weighed prior to deposition then installed into the EPD cell and lowered into the functionalized SWCNT aqueous suspension to a depth of 1cm. A DC power supply was used to apply 10-50V to the EPD cell for duration of 1-60 minutes. During EPD processing the negatively charged functionalized SWCNTs move towards the positive electrode and uniformly coated the surface. The SWCNT coated positive electrode is then removed from the suspension under applied voltage and disconnected from the voltage supply in air. The SWCNT coated electrodes were then dried in an oven at 80°C for 30min to remove moisture and solidify the SWCNT network. Figure 3.7 shows a schematic diagram of the first EPD cell showing SWCNTs coating the positive electrode.

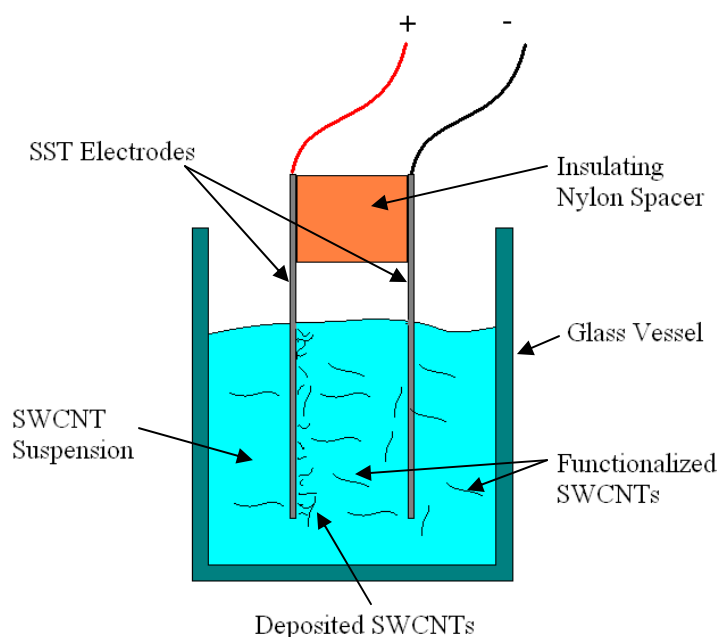


Figure 3.7 - Schematic diagram of EPD cell 1 SWCNT coating process

Through literature reviews and experimental procedures using EPD cell 1 it was determined that an EPD working voltage of 40V was optimal for the fabrication of SWCNT electrodes. Voltages less than 30V produced non-uniform coatings and were slow to process. Voltages above 50V started to produce hydrogen bubbles on the electrodes from the hydrolysis of H₂O and disrupted the SWCNT coating.

3.2.4.2 Temperature Controllable Electrophoretic Deposition Cell 2

A second EPD cell was designed and fabricated specifically to look at the effect of EPD suspension processing temperatures on the capacitance vs EPD processing time. This cell was designed to use a peltier device or thermoelectric cooler (TEC) to allow heating and cooling of the SWCNT suspensions in the new EPD cell. Applying current to the TEC causes one side to get hot and the other side get to get cool such that the TEC acts as a heat pump moving heat from one side to another. By swapping the current polarity on the TEC the temperature gradient can be reversed [73]. This enables the hot side to become the cool side and vice versa to allow the device to act as both a heater and a cooler by changing the polarity of the current to the device. As with the previous EPD cell 1, the new EPD cell 2 is fabricated with a working distance of 1cm between electrodes. Stainless steel (SST) 304 (70%Fe, 19%Cr, 11%Ni: wt%) sheets 0.100mm thick from Alfa Aesar were used as the current collectors and substrates for the SWCNT electrodes in EPD cell 2 as well. The SST electrodes were cut, numbered, and weighed prior to deposition then installed into the EPD cell 2 and lowered into the functionalized SWCNT aqueous suspension to a depth of 1cm. A DC power supply was used to apply 40V to the EPD cell for duration of 1-60 minutes. The TEC (Marlow Industries DT6-4L) was also powered by a separate DC power supply and was voltage limited between 3-6V to control the suspension temperature between 5-60°C. Under operation in an environment of approximately 22°C the TEC polarity needs to be positive to positive to cool the EPD SWCNT suspension below room temperature and reversed to be positive to negative for heating of the suspension. A Fluke 17B digital thermocouple was immersed in the EPD suspension and used to monitor the suspension temperature during processing. A third power supply was used to power a

cooling fan which was attached to a heat sink designed to remove the extracted heat from the TEC for the cooling mode or supply heat from the room for the heating mode. As in the previous cell, regardless of the EPD suspension temperature, the negatively charged functionalized SWCNTs move towards the positive electrode and uniformly coated the surface under the applied 40V voltage. The SWCNT coated positive electrode is then removed from the suspension under voltage and disconnected from the voltage supply in air. The SWCNT coated electrodes were then dried in an oven at 80°C for 30min to remove moisture and solidify the SWCNT network. Figure 3.8 shows a schematic diagram of the second EPD cell showing the TEC, thermocouple, heat sink, and other items similar to EPD cell 1 such as the SWCNT coated positive electrode.

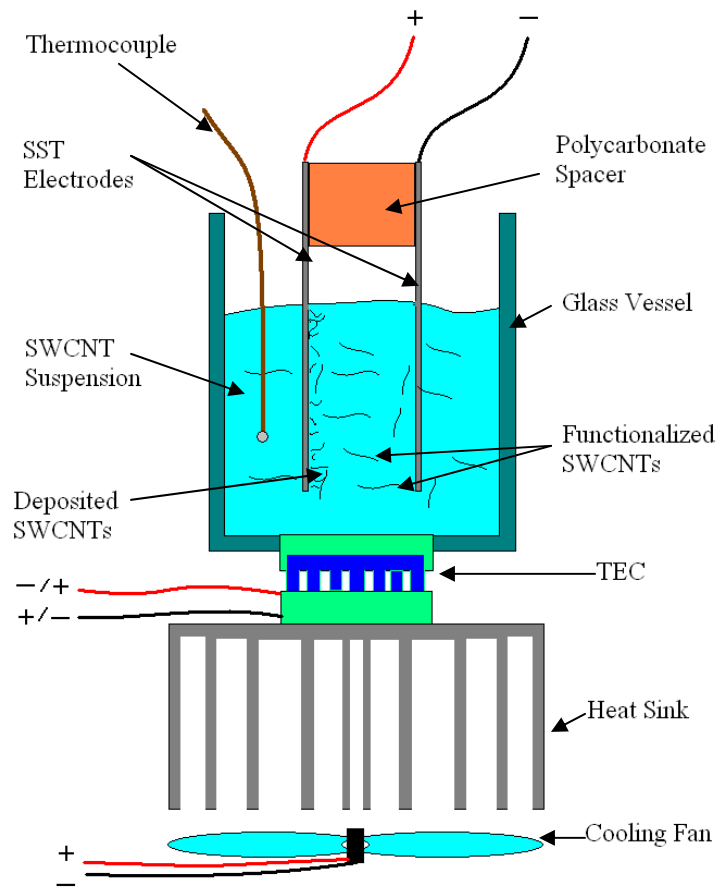


Figure 3.8 - Schematic diagram of EPD cell 2 with temperature controlled process

It is also interesting to note that EPD cell 2 had to be built twice. The first version of the temperature controlled EPD cell was created using cut polycarbonate sheets and an aluminum base as opposed to a glass vessel. A plastic adhesive was used to bond the polycarbonate sheets and aluminum base together to form a waterproof cell. The intention was to use the aluminum base for better heat transfer between the SWCNT suspension and the TEC thus allowing for a larger EPD temperature range. However, initial results with the polycarbonate EPD cell yielded strange and inconsistent results for SWCNT electrode fabrication. It was later determined from the residue on the walls and base of the EPD cell that the functionalized SWCNTs were being contaminated by either the polycarbonate or adhesive in the cell. To resolve the contamination issue a second temperature controlled EPD cell was built using a glass vessel as the fluid container. This simplified the cell and eliminated the contamination issue by removing the use of the polycarbonate walls, the adhesives, and the aluminum base, and ensured that only glass was in contact with the SWCNT suspension. Figure 3.9 below shows photographs of the temperature controlled EPD cell 2 with the initial polycarbonate vessel (left) and updated glass vessel (right).

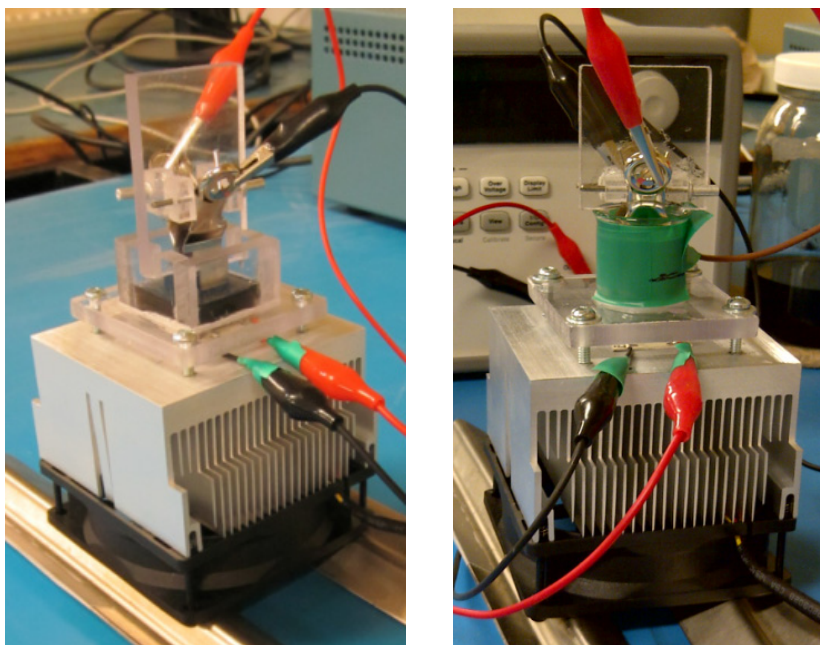


Figure 3.9 - Photos of temperature controlled EPD cell 2 with plastic (left) and glass (right) vessels

Chapter 4

Results

Scanning electron microscope (SEM) images were gathered on a LEO 1530 FE-SEM and were used to evaluate the uniformity, visualize the porosity, and measure the cross sectioned thickness of the coated SWCNT networks on the SST current collectors. The surface area and average pore size of an EPD sample was also measured on a SWCNT coated electrode using a NOVA 2200e BET tester to validate the SEM approximation of average pore size. A Raman spectroscopy device using a 633nm HeNe laser was used to verify the presence of SWCNTs in the inkjet printed samples. Cyclic voltammetry (CV) measurements were performed on all EPD samples to determine the capacitance of each electrode. A Princeton Applied Research Potentiostat / Galvanostat Model 273A, within a potential range of 0.0 to 1.0V at scan rates of 20, 50, and 100mV/s was used for initial characterization of SWCNT EPD electrodes with processing times of 0 to 8min. An eDAQ EA163 Potentiostat, within a potential range of -0.2 to 0.8V at a scan rate of 20mV/s was used for a follow up study of SWCNT EPD electrodes with longer processing times of 0 to 60min. A Gamry Reference 3000 Potentiostat within a potential range or -0.2 to 0.8V at scan rates of 20, 100, and 500mV/s was used for characterization of the final study for EPD processing temperatures of 5 to 60°C and processing times of 0 to 60min. Each potentiostat was used as access to equipment permitted and all produced similar results.

4.1 Structural and Morphological Characterization

Comparison of the nanoporous SWCNT networks under optical and scanning electron microscopes to evaluate the porosity, uniformity, and overall quality of the SWCNT networks as produced using the various methods was used to qualitatively evaluate the different materials and processes. Initial optical images of drop coated surfactant based SWCNT suspensions showed evidence of surfactant crystallization and streaking. Based on the poor uniformity and surfactant aggregates observed optically,

surfactant dispersion was abandoned and functionalization became the preferred method for dispersing SWCNTs into H₂O. From the optical and SEM images it was also clear that the HVES and inkjet printed electrodes had poor uniformity and poor network formation. Although the drop coating samples had good network formation in specific regions of the coating, the coating itself was not uniform across the entire coated area. The EPD samples showed good uniformity and network formation across the entire region. From the initial optical and SEM results the EPD process was determined to be the most repeatable and effective method of coating SWCNTs onto electrode current collectors. The qualitative results of all samples are shown below in sections 4.1.1-4.1.4. Based on the poor qualitative results the drop, HVES, and inkjet coating processes were not further characterized and capacitance data was gathered for the EPD process only.

4.1.1 Drop Coating Optical and Scanning Electron Microscope Results

The first SWCNT samples were created using surfactant based SWCNT suspensions prepared as described in section 3.1.1 using the drop coating method from section 3.2.1. Figure 4.1 shows optical images of drop coated SWCNT samples made using 0.1M SDS suspensions.

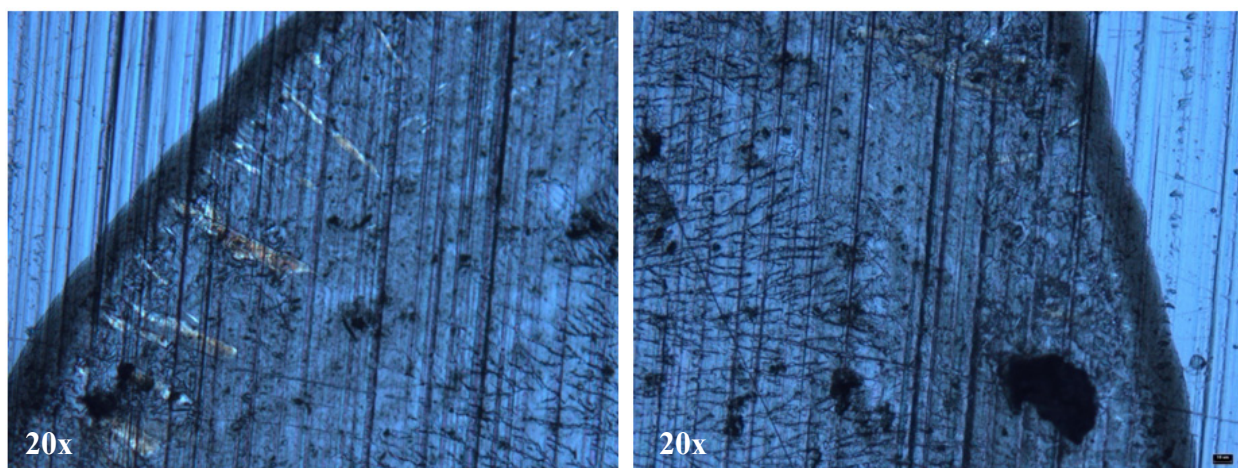


Figure 4.1 - Optical image of SWCNT SDS drop coated sample

From these optical images it is obvious that the dispersion uniformity is poor. A coffee ring effect is observed near the perimeter of the drop where a higher concentration of SWCNTs is indicated by the dark ring. Within the droplet there are varying densities of SWCNTs as indicated by the dark streaks. Surfactant aggregates can also be observed in the left image near the coffee ring edge as is indicated by the light colored streaks. In addition the right image shows significant SWCNT agglomeration or large particles of SWCNTs on the substrate. Further qualitative analysis of the surfactant based drop coated samples by SEM confirmed that the poor uniformity was also present at the nanoscale. Figure 4.2 shows medium (1000X) and high (50000X) magnification images of the SWCNT SDS drop coated samples. Striking can be observed in the medium magnification image and indicates poor uniformity across the 0.20mm image view. In the high magnification image SWCNT bundles can be observed stretching perpendicular to the streak directions. From this high magnification image it is hypothesized that as the drop samples dry in air the SWCNTs are drawn perpendicular to the streaks by surface tension of the fluid as it dries forming the observed streaks. From the SEM images the observed streaks appear to contain higher concentrations of SWCNT bundles and surfactant which helps support the hypothesis that the streaks are the last areas on the substrate to dry out.

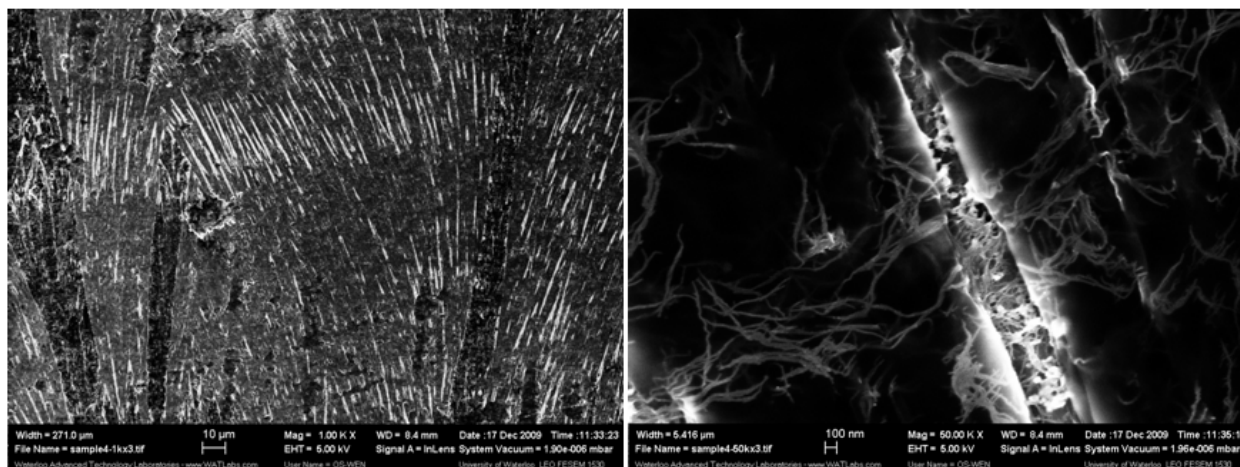


Figure 4.2 - SEM images of SWCNT 0.1M SDS drop coating samples (Left: 1000X, Right 50000X)

Further investigation on improving the uniformity of the SWCNT coatings by varying the concentration of SDS used in the suspensions was also investigated. Pure SWCNT H₂O suspensions without the use of SDS as well as 0.1M and 0.01M SDS suspensions all with of 0.5mg/ml SWCNTs were evaluated. Again each sample showed poor uniformity and varying SWCNTs densities across the substrate regardless of the SDS concentration. For the SWCNTs and pure H₂O samples the poor uniformity as seen in Figure 4.3 can be attributed to the inadequate dispersion quality of the base suspension resulting from the hydrophobic properties of the SWCNTs. For the 0.1M and 0.01M SDS samples both had poor uniformity and significant cracking was observed in the SWCNT coating. The effect of reduced surfactant seemed to reduce the width of the cracks but also increased their quantity (Figure 4.4).

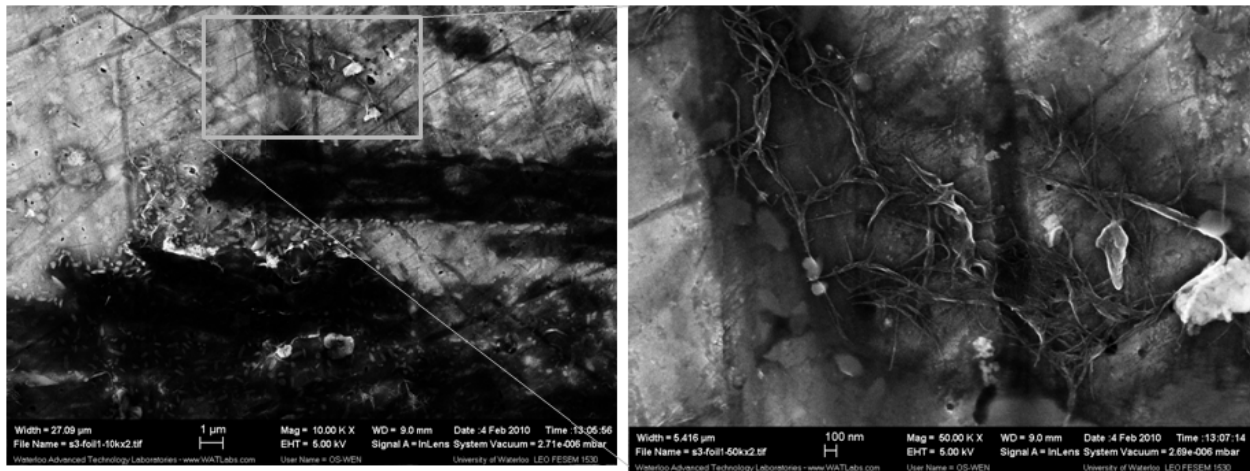


Figure 4.3 - SWCNT and pure H₂O drop coating samples (Left: 10000X, Right 50000X)

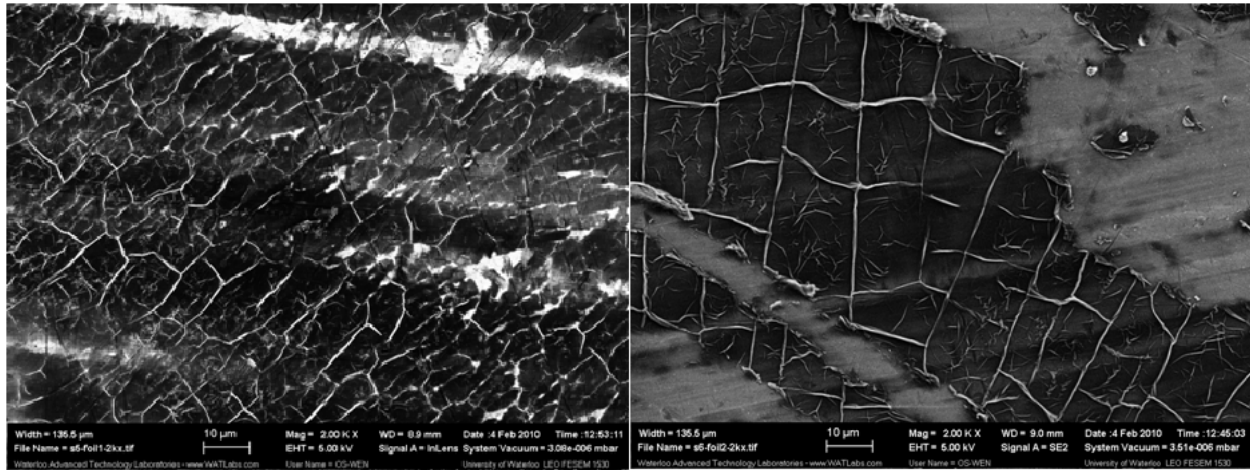


Figure 4.4 - SWCNT SDS drop coating samples 2000X (Left: 0.01M SDS, Right: 0.1M SDS)

To address the coffee ring effect produced by the drop coating method the aluminum substrate was treated with 0.4M phosphoric acid (H_3PO_4) to make it less hydrophobic to the SWCNT SDS suspensions. This treatment successfully prevented the formation of round droplets on the surface. After the treatment the SWCNT suspension wicked across the surface of the substrate and thus eliminated the coffee ring effect. However, instead of a coffee ring effect, areas of higher SWCNT concentration were still observed in lines and leaf patterns on the substrate as shown in Figure 4.5 and still contributed to poor uniformity.

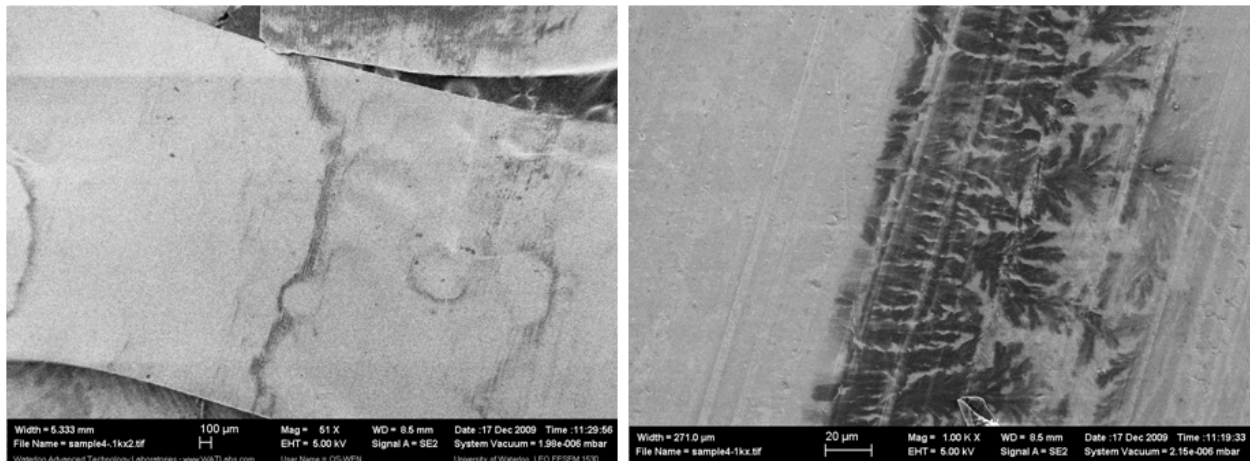


Figure 4.5 - Substrate treated 0.1M SDS drop coated sample (Left: 51X, Right: 1000X)

Based the observed qualitative results it was determined that surfactant based suspensions, due to surfactant trapping and SWCNT film cracking and streaking, are not well suited for the creation of a uniform nanoporous SWCNT networks. A new SWCNT suspension was prepared using acid functionalization as discussed in section 3.1.2 to address the observed issues with SDS based suspensions. The acid functionalization produced good dispersion of the SWCNTs in H₂O and the removal of surfactants from the suspension eliminated the previously observed SWCNT film cracking and streaking. Figure 4.6 shows the elimination of streaking and a good nanoporous SWCNT network formed by drop coating using the functionalized SWCNT suspension in specific regions of the sample.

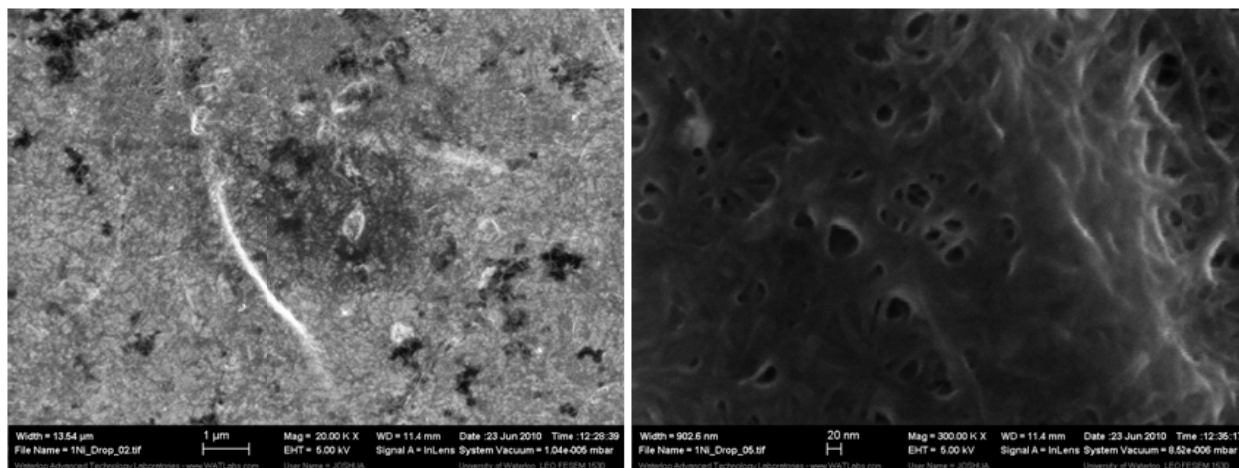


Figure 4.6 - Acid functionalized SWCNT drop coated sample (Left: 20000X, Right: 300000X)

From the overall suspension qualities and the SEM images of the drop coated samples the acid functionalized SWCNT suspension was determined to be much better suited for the creation of uniform SWCNT networks than the SDS SWCNT suspensions. Even with the acid functionalized suspension the use of drop coating still produced non-uniform surface coatings. The coffee ring and or leaf patterns as well as significant variations of SWCNT density across the larger coated regions were still observed. From the SDS and functionalized SWCNT suspension evaluations it was determined that, due to the poor uniformity and SWCNT densities across the coated areas, the limited electrode size, and inconsistencies

between samples, drop coating is not an appropriate method for the creation of SWCNT ultracapacitor electrodes.

4.1.2 High Voltage Electro Spraying Scanning Electron Microscope Results

In an effort to improve on the dispersion quality and create a more uniform SWCNT coating an experimental HVES process was evaluated using acid functionalized SWCNTs as described in section 3.2.2. For this experiment the acid functionalized SWCNT H₂O based suspensions were used as well as an acid functionalized ethanol based SWCNT suspension due to the higher evaporation rate of ethanol compared to H₂O. Although both suspensions had good SWCNT dispersion quality to start with, in both cases the processed electrodes had non-uniform coatings of SWCNTs. At low magnification small regions of the substrate could be observed to be coated while adjacent areas were left bare (Figure 4.7: left). Within the coated regions there was evidence of the start of a good nanoporous network, but significant variation in SWCNT density could also be observed (Figure 4.7: right).

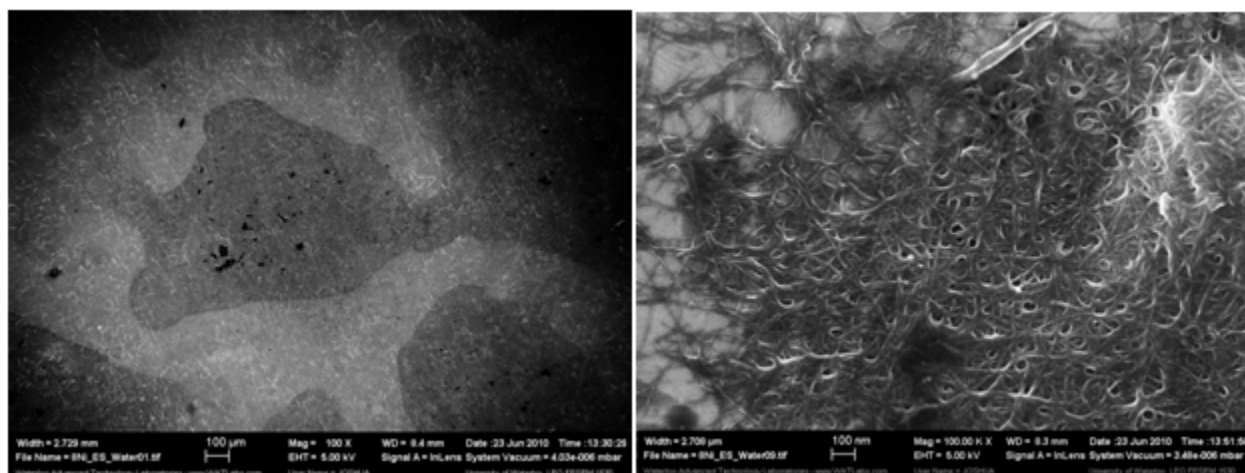


Figure 4.7 - H₂O based SWCNT HVES coating method (Left: 100X, Right: 100000X)

Even the use of ethanol based SWCNT suspensions did not improve the uniformity or SWCNT density. For the ethanol based samples regions of non uniformity could be easily identified and significant agglomeration of SWCNT bundles could be observed in the medium magnification images (Figure 4.8:

left). In the high resolution images, such as Figure 4.8: right, the SWCNTs bundles could be observed but they appeared isolated from one another and did not form a blended nanoporous network with good nanotube to nanotube junctions as seen with the H₂O based suspensions.

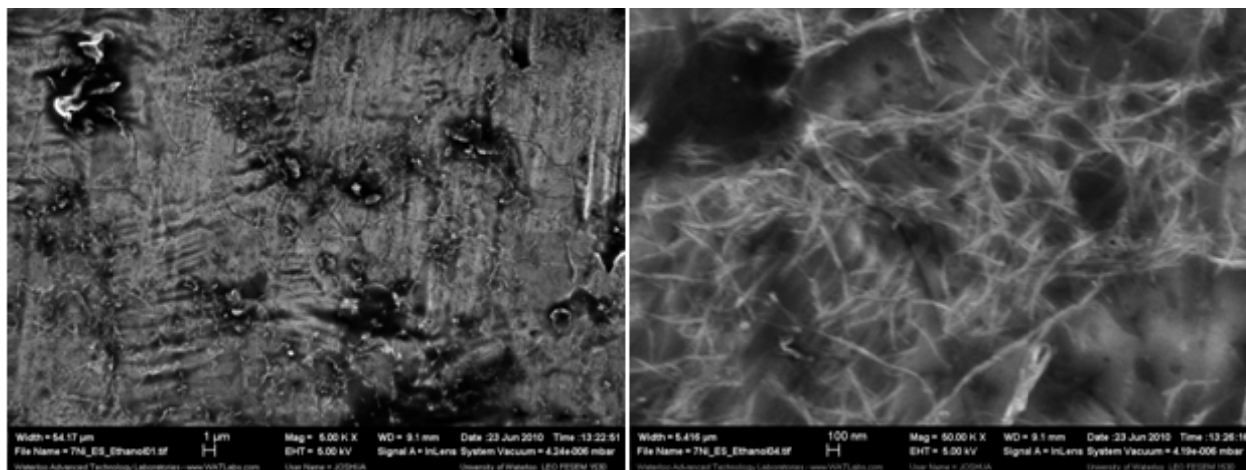


Figure 4.8 - Ethanol based SWCNT HVES coating method (Left: 5000X, Right: 50000X)

As a result of the qualitative analysis it was determined that the ethanol based suspensions did not perform as well as the H₂O based suspensions for the formation of SWCNT nanoporous networks. The use of HVES, although interesting and yielding some very small areas of good nanoporosity using H₂O based suspensions, was also determined to provide insufficient coverage of the substrate and poor uniformity of SWCNT density within the coated regions. Thus, it was determined that HVES is not a suitable method for SWCNT coated electrodes for ultracapacitors.

4.1.3 Inkjet Printing Scanning Electron Microscope and Raman Results

Another experimental method that was undertaken as part of this work was the use of consumer inkjet printers as a deposition method for SWCNT suspensions as described in section 3.2.3. For this method the traditional metallic substrates were not used and instead replaced by standard white copy paper and ITO coated PET. Although copy paper is not electrically conductive the goal of the inkjet printing process was

to coat the copy paper with a sufficient quantity of SWCNT layers such that an electrically conductive SWCNT network was formed on the copy paper by the SWCNTs themselves. Figure 4.9 shows an example of an electrically conductive network on standard copy paper which was created entirely from the functionalized SWCNT aqueous suspension using the drop coating method. This demonstrated that if the concentration of SWCNTs could be dense enough through the ink jet printing method that an electrically conductive SWCNT network could be printed onto standard copy paper.

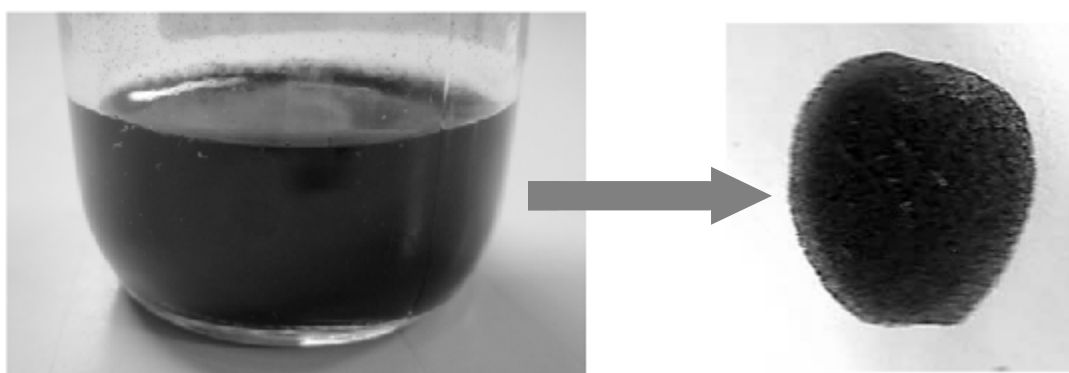


Figure 4.9 - Electrically conductive SWCNT network on copy paper using drop coating method

To validate the presence of SWCNTs on paper as transferred through the printing process, Raman spectroscopy was performed on the SWCNT coated paper samples. The Raman plots confirmed the presence of SWCNTs, however, do to the poor uniformity and low density of SWCNT material only specific locations of the sample showed the presence of SWCNTs. Below Figure 4.10 shows a reference Raman spectroscopy plot for SWCNTs identifying key peaks. An example Raman plot of a SWCNT inkjet printed sample from the HP Deskjet F4480 is shown in Figure 4.11 for comparison.

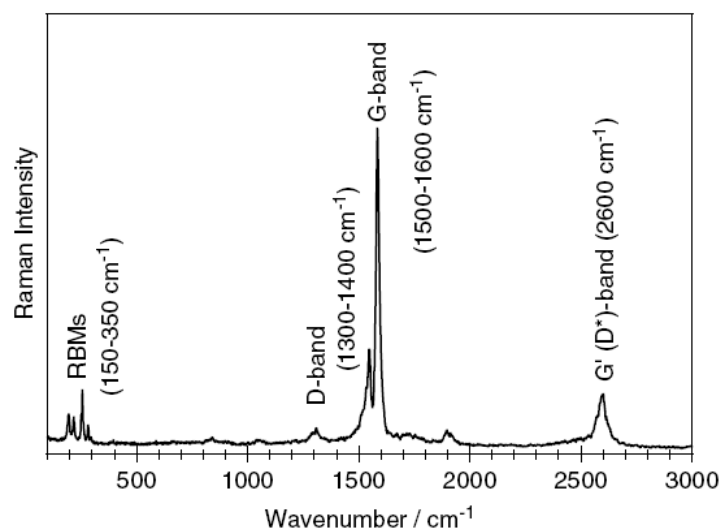


Figure 4.10 - Reference Raman plot for SWCNTs [74]

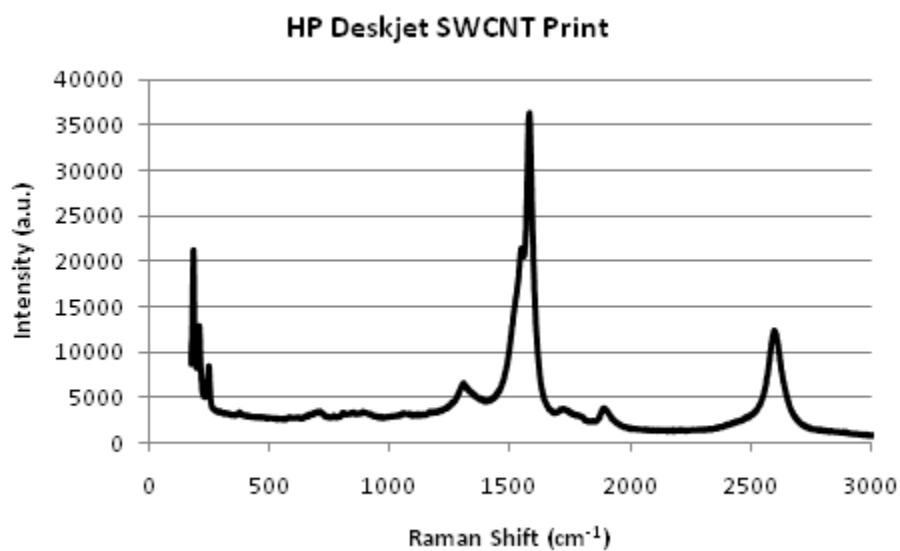


Figure 4.11 - Raman plot of SWCNTs printed using HP inkjet printer

From the reference plot important peaks such as the radial breathing mode (RBM) at 150-350 cm⁻¹ and the G band at 1500-1600 cm⁻¹ can be used to identify the presence of SWCNTs [74]. These peaks can be clearly seen on the HP Deskjet SWCNT Raman plot which indicates that, although found only in certain areas of the HP print and in low densities, SWCNTs were successfully printed through the HP Deskjet F4480 printer onto standard copy paper.

However, even with 150 printed SWCNT layers neither of the two inkjet printers evaluated could produce an electrically conductive SWCNT network due to inadequate SWCNT density. Figure 4.12 shows photographs of the inkjet printed SWCNTs for prints between 45-150 layers using different print patterns. From the images it is clear that increasing the number of printed SWCNT layers increases the SWCNT density but even after 150 prints the contrast, which is a representation of the SWCNT density, is not nearly as high as the drop coated sample shown in Figure 4.9.

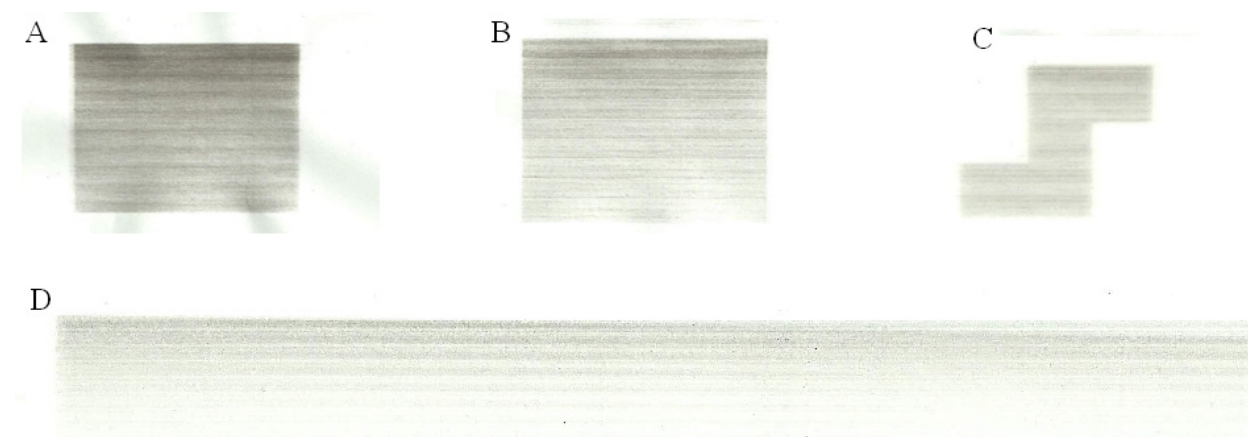


Figure 4.12 - Inkjet printed SWCNTs on copy paper A) 150 prints using HP printer, B) 50 prints using HP printer, C) 45 prints using HP printer, D) 80 prints using Epson printer

Further to the point of inadequate SWCNT density in the printed samples, SEM images of the electrically conductive drop coating sample on copy paper are shown in Figure 4.13. It is clear from the SEM images that the electrically conductive SWCNTs have sufficiently coated the long cellulose fibers of the copy paper to produce an electrically conductive network. By contrast Figure 4.14 shows the SEM images of SWCNTs coated onto copy paper using the HP inkjet printer with approximately 50 print layers. In these images the SWCNT density is insufficient to create an electrically conductive network and SEM charging causes very poor image quality.

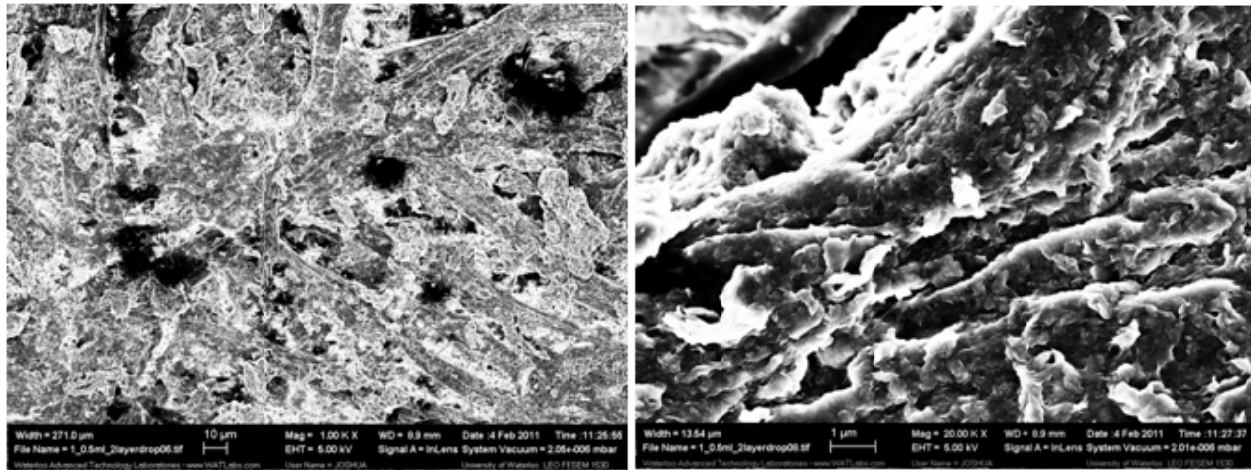


Figure 4.13 – SEM images of electrically conductive SWCNT network on copy paper using drop coating method (Left: 1000X, Right: 20000X)

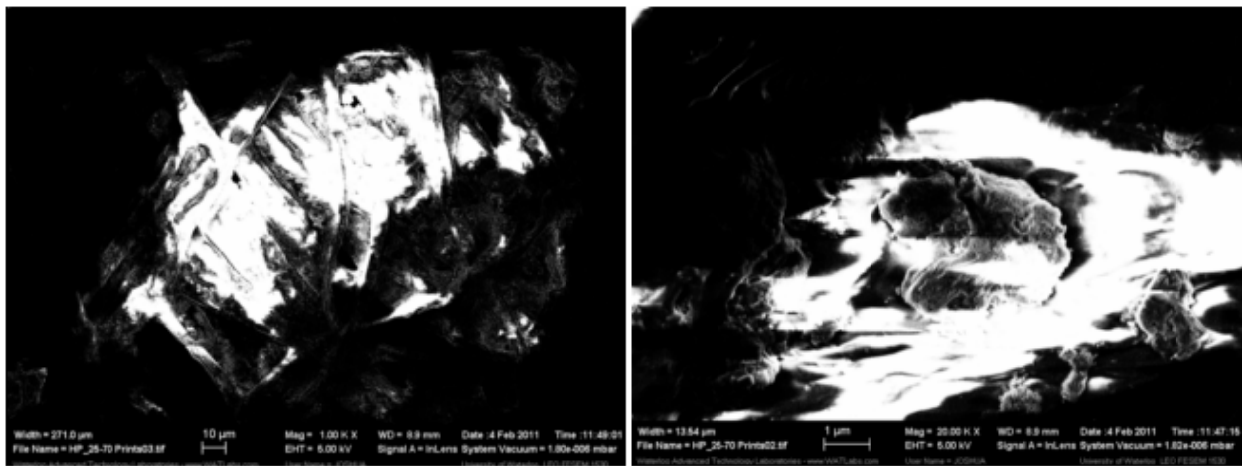


Figure 4.14 - SEM images of insufficient SWCNT coverage on copy paper using inkjet printing method (Left: 1000X, Right: 20000X)

Due to the insufficient SWCNT densities it is determined that the inkjet printing method used here is unable to produce an electrically conductive network of SWCNTs. Therefore, in order to use the inkjet printing method for the production of SWCNT ultracapacitor electrodes an additional electrically conductive current collector is needed. ITO coated PET was selected as an ideal current collector for the SWCNT inkjet printed electrodes due to its low thickness, its flexibility, and its use in solar cells and other electronic devices. By adding SWCNTs to the surface of the electrically conductive ITO the total

surface area of the electrode could be significantly increased. Even though the SWCNT densities were low and electrically conductive pathways between SWCNTs were not established, it was hypothesized that the ITO would provide adequate current flow to the SWCNT branches.

A sample of SWCNT coated ITO as prepared through the HP inkjet printer after 30 printed layers was created, however, issues existed with the adhesion and drying times for the SWCNT suspension on the ITO coated PET. Since the ITO and PET are not porous or absorb liquids like the cellulose paper, the individual picoliter droplets from the inkjet nozzles tended to pool together and remain on the surface requiring extended drying times between prints. Below right is an optical image of the ITO coated PET with 30 printed layers of SWCNTs and the intended pattern shown to the left (Figure 4.15)

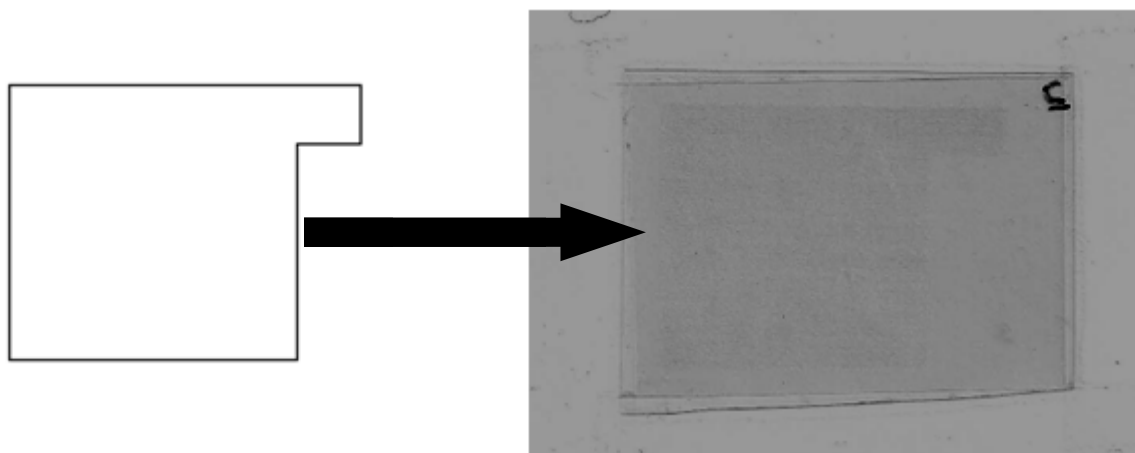


Figure 4.15 - Printed pattern (left) and actual SWCNTs printed pattern on ITO PET (right)

Although promising the printing process on ITO PET is very labor intensive requiring sonication of the SWCNT inkjet cartridge between every print to avoid SWCNT agglomeration during the 5 minutes required between prints for each print to dry. The density of SWCNTs appeared to be very low as indicated by the very light shading effect and further attempts at characterizing the printed electrode in aqueous electrolytes such as NaCl or KCl resulting in total loss of the printed pattern. It was later determined that either the visible pattern on the ITO PET may have been micro droplet water marks and that due to contamination or agglomeration within the cartridges contained little or no SWCNTs, or the

adhesion of the SWCNTs to the ITO was very poor due to the hydrophobic properties of the substrate. In either case the attempt to print a SWCNT network onto ITO PET was deemed unsuccessfully.

From the experimentation with the two printer types it was determined that contrary to expectations a larger nozzle droplet size is preferred for deposition of SWCNTs. With a droplet size of 13.8 picoliters the HP printer had fewer issues related to nozzle clogging than the Epson printer with its 2.0 picoliter droplet size. In addition to larger droplet size the HP inkjet nozzles are easier to unclog and clean since they are part of the ink cartridges and can be removed from the printer frequently and easily. This is in contrast to the Epson printer which has its nozzles built into the printer and uses the cartridges as ink reservoirs only. This made the Epson printer nozzles difficult to clean and prevented the possibility of routine sonication between prints. In the end the Epson printer succumbed to irreparable nozzle clogging. As a result of the labor intensive processes, difficulty in obtaining adequate SWCNT densities, and the issues obtaining robust SWCNT networks on ITO PET it was determined that the current inkjet printing processes are not suitable for the production of SWCNT electrodes for ultracapacitors.

4.1.4 Electrophoretic Deposition Scanning Electron Results

After looking at surfactant and functionalized SWCNT suspensions in drop coating, and water and ethanol based suspensions in HVES, it was determined that water based functionalized SWCNT suspensions produced the best nanoporous networks. To improve on the uniformity and SWCNT densities from previous coating methods the electrophoretic deposition method (EPD) was used. After initial fabrication of the EPD cell and experimentation of EPD processing parameters, such as electrode voltage, EPD showed promising results and became the primary process for electrode fabrication and characterization in this work. SEM images of electrodes coated with SWCNTs at various applied voltages between 10V and 50V and for various processing times confirmed the presence of SWCNT nanoporous networks. Figure 4.16 shows a nanoporous network of an EPD SWCNT coated electrode processed at 30V for 3min. The image shows a uniform coating and an average pore radius of approximately 20nm.

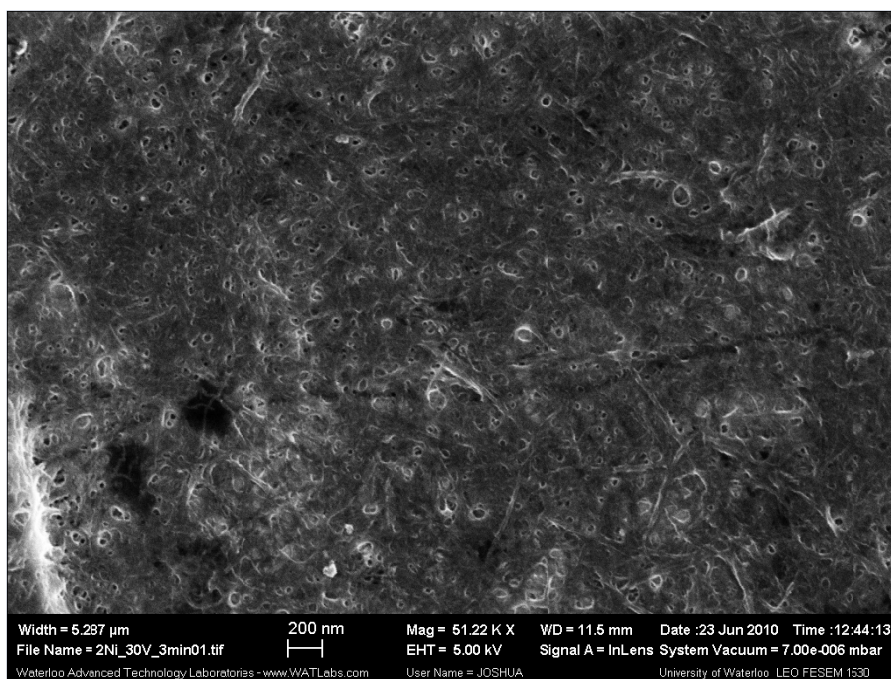


Figure 4.16 - SEM image of SWCNT network created using EPD at 30V for 3 minutes 51000X

SEM images of poor networks were observed for EPD samples processed at low voltages 10 to 20V or electrodes produced with short processing times of 1 to 2min as observed from Figure 4.17.

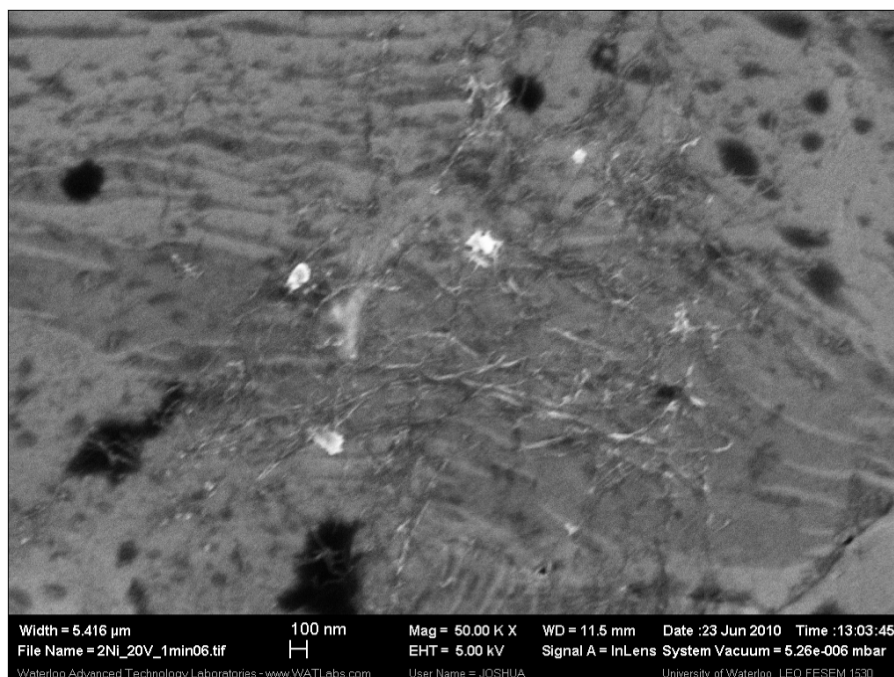


Figure 4.17 - SEM image of SWCNTs coated on substrate using EPD at 20V for 1min 50000X

For these low voltages and short processing times the formation of the SWCNT networks was sparse and the overall coverage of the electrode was not uniform. Although bundles of SWCNTs were visible, areas of bare SST could be readily observed, and the formation of a SWCNT nanoporous network was not complete. As expected, there appears to be a direct correlation between the EPD voltage, the processing time, and the SWCNT network formation. The creation of a SWCNT network can be observed visually from SEM images of a 30V 3min processed electrode which show the formation of a SWCNT network occurring over a hole in the SWCNT coating (Figure 4.18). SWCNT bundles can be observed spanning the hole and completing the SWCNT network. It is hypothesized that given a longer processing time or a higher processing voltage the hole on this sample would have completely filled in with SWCNTs to form a uniform nanoporous network such as the areas surrounding the hole.

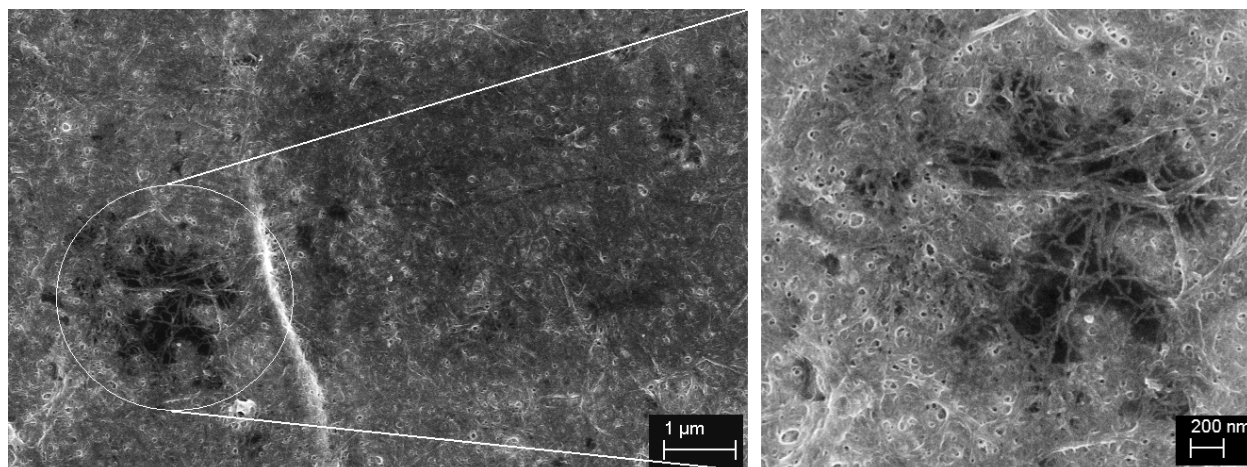


Figure 4.18 - Formation of SWCNT network across a hole using EPD at 30V for 3min

Further experimentation of EPD processing parameters determined that the optimal EPD processing voltage for SWCNTs was 40V as discussed previously in section 3.2.4. In addition to the working voltage EPD processing time and temperature using EPD cells 1 and 2 were also evaluated. Varying the processing parameters allowed for better and more uniform SWCNT coatings to be created. Figure 4.19 shows the excellent uniformity that is achieved using the EPD process. Figure 4.19-A is a low magnification image showing excellent bulk uniformity of the SWCNT network for an EPD sample

processed 40V for 30min at room temperature of 22°C. The image is approximately 0.5mm x 0.5mm and is an excellent representation of the 1cm x 1cm total electrode area. Figure 4.19-B shows a region of the same substrate or SST current collector which was not processed by EPD and is not coated with SWCNTs. Figure 4.19-C shows an EPD sample processed for only 8min but at an elevated EPD processing temperature of 45°C. Specifically this image highlights the strong edge separating the SWCNT coated and uncoated areas where the portion of the SST substrate immersed into the SWCNT EPD suspension meets the portion of the SST substrate which is left in air during the EPD process.

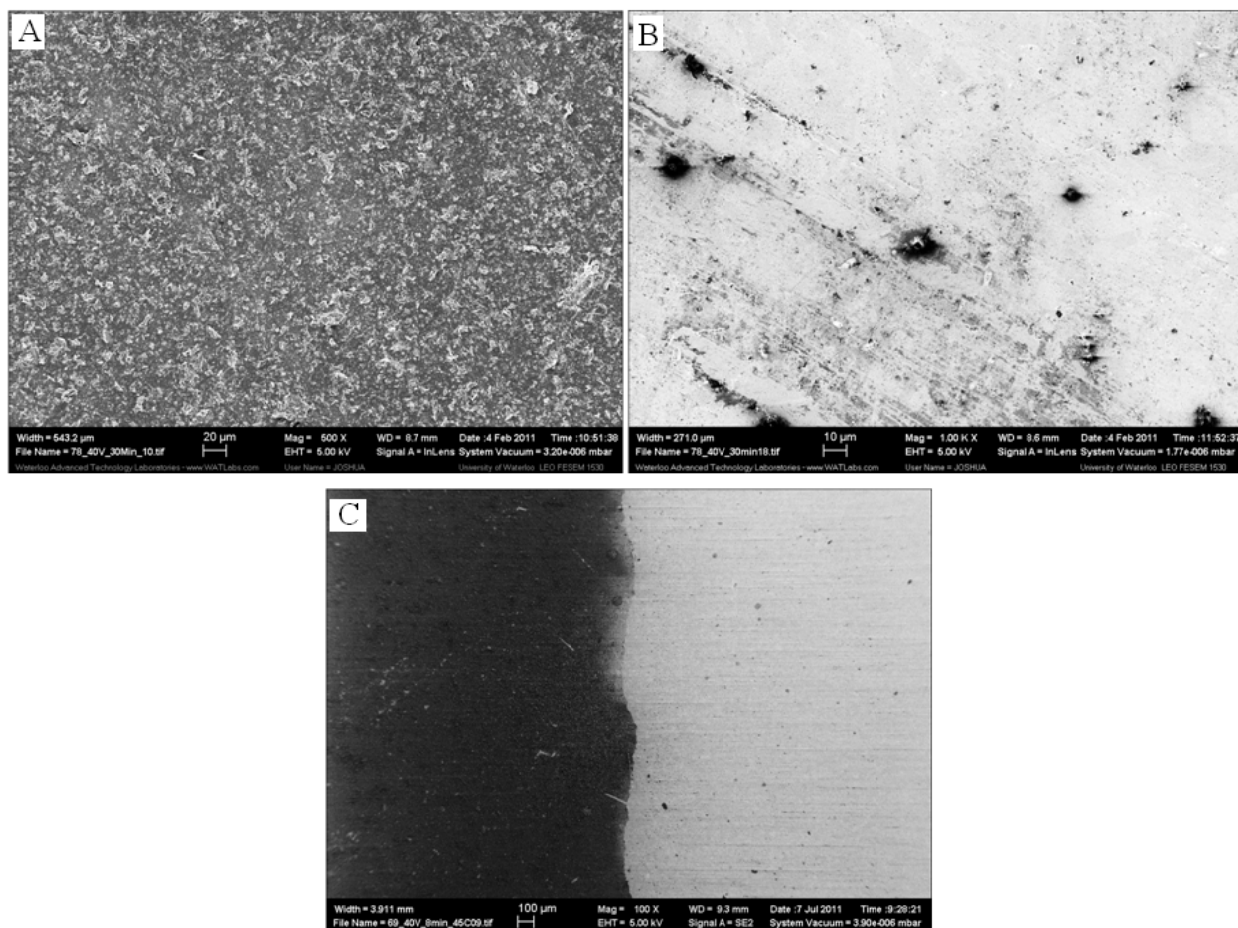


Figure 4.19 - Large area SEM images of A) Uniform 0.5mm EPD SWCNT network (500X), B) Bare SST substrate in uncoated region (1000X), C) Boundary between EPD SWCNT coated and uncoated areas (100X)

Structural characterization of the EPD networks using the SEM revealed that increasing processing time and processing voltage increased the density of SWCNT networks as shown in previous Figure 4.16- Figure 4.18. Similarly it was found from optical and SEM images that an increase in EPD processing temperature increased both the nanoscale SWCNT network densities as well as the bulk coating density. The increase in bulk coating density for different processing temperatures is especially noticeable for shorter EPD processing durations less than 15 minutes, as can be seen in Figure 4.20 below when comparing the optical density of the 3 and 8 minute samples prepared at 5°C versus 60°C.

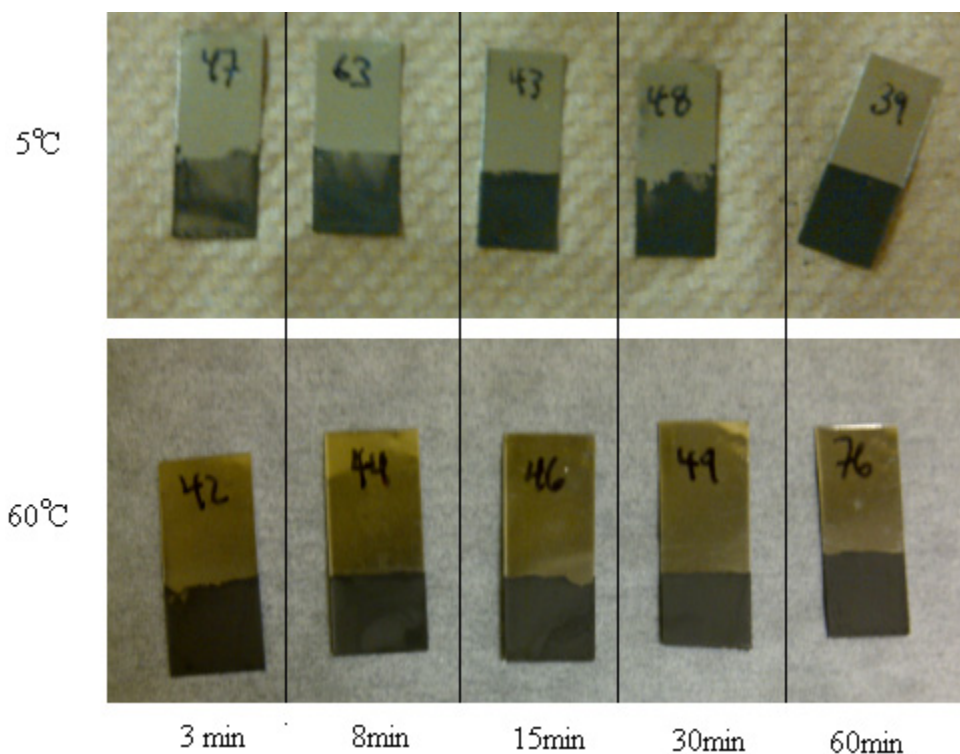


Figure 4.20 - Optical images of SWCNT electrodes coated using EPD at various processing times 3, 8, 15, 30, and 60 minutes at 5°C and 60°C

Figure 4.21 to Figure 4.24 below show medium (5000X) and high magnification (200000X) SEM images of SWCNT networks created each using 8 minute EPD durations at different processing temperatures of 5°C, 22°C, 45°C and 60°C. All processing parameters were the same for each sample,

including the processing time, except for the EPD processing temperature. It can be seen from the SEM images that the three dimensional structures of the samples becomes more pronounced as the processing temperature increases. This increases the amount of SWCNTs added to the network, increasing the surface area and potentially increasing access to pores in the network for increased ion storage and increased capacitance.

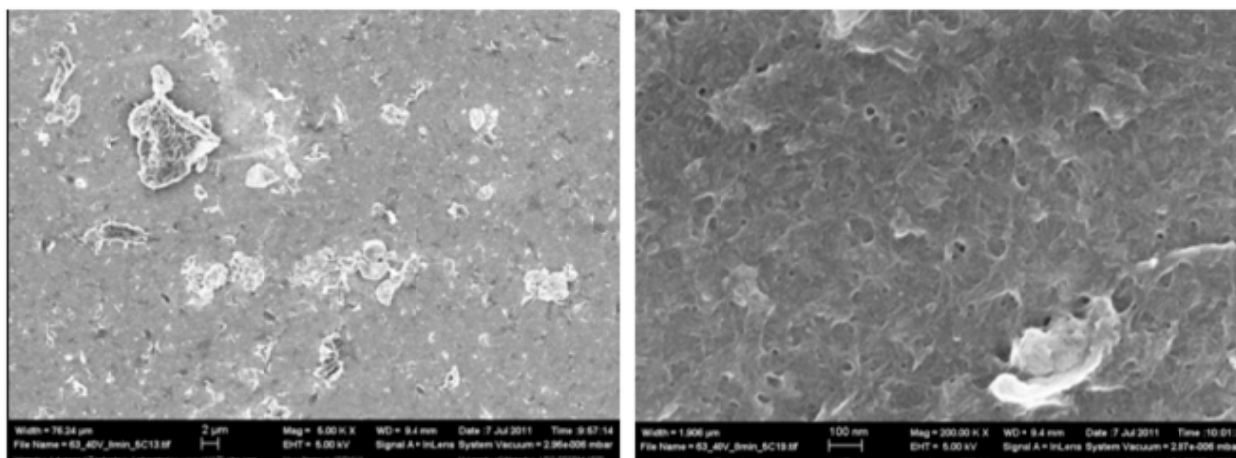


Figure 4.21- SWCNT network using EPD at 40V for 8 minutes at 5°C (Left: 5000X, Right: 200000X)

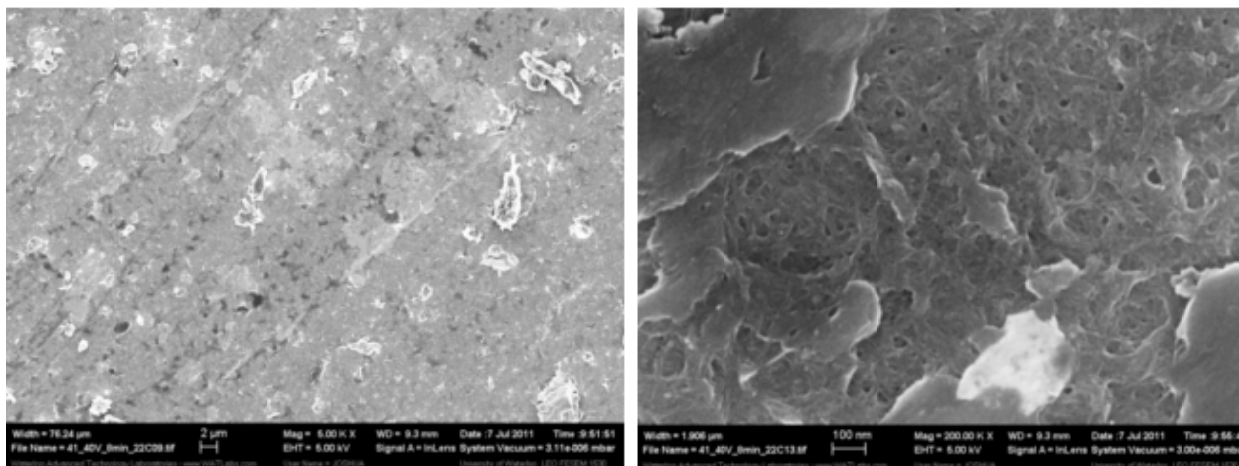


Figure 4.22- SWCNT network using EPD at 40V for 8 minutes at 22°C (Left: 5000X, Right: 200000X)

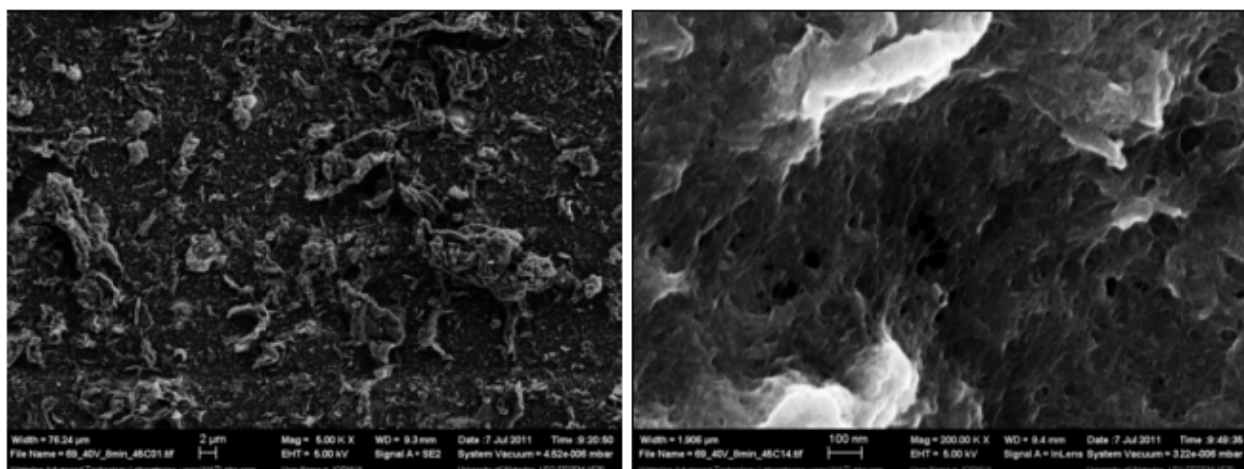


Figure 4.23- SWCNT network using EPD at 40V for 8 minutes at 45°C (Left: 5000X, Right; 20000X)

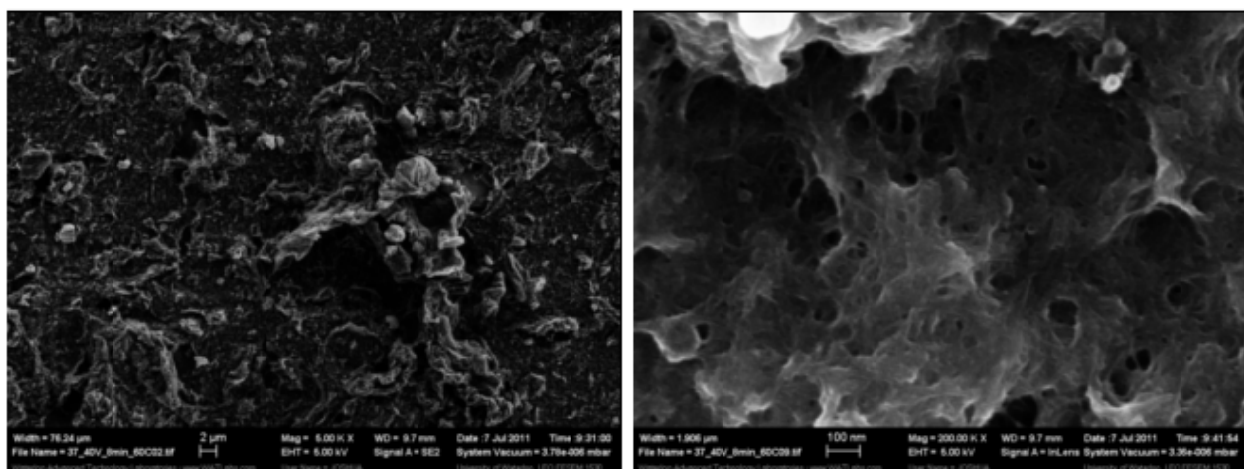


Figure 4.24- SWCNT network using EPD at 40V for 8 minutes at 60°C (Left: 5000X, Right; 20000X)

Although mass characterization would be preferred to further evaluate the effect of EPD processing temperatures on the formation of SWCNT networks and to correlate the amount of SWCNT material added to the substrates there were significant difficulties in obtaining accurate mass measurements of the added SWCNT material. The mass of the SST current collectors for the EPD process were quite heavy 180-220mg in relation to the amount of SWCNT material added to the processed electrode. Based on EPD cell volume of 5ml and a SWCNT suspension concentration of 0.5mg/ml the SWCNT mass will be

somewhere between 0 and 2.5mg depending on the processing time and processing temperature.

Unfortunately even at the max mass of 2.5mg the mass of the SWCNT material is at most about 1% of the total electrode mass and thus the error range of the day to day mass measurements were not accurate to provide useful data on the added SWCNT mass. From the data that was gathered variations in the mass of the same sample varied by as much as 0.5mg for multiple measurements which represented at least 20% , and potentially 100%, of the total SWCNT mass on the electrodes. Hence mass measurements could not be used as a characterization parameter for the SWCNT networks. As an alternative to SWCNT mass, the thickness of the EPD SWCNT networks was obtained by mounting the processed electrodes in resin, cross sectioning and polishing the samples, and measuring the SWCNT network thicknesses from SEM images. The thicknesses can then be used to provide quantitative values for the amount of SWCNT material added to the current collectors under the different processing temperatures and later to correlate those values to the capacitance data collected in the following section. Figure 4.25, Figure 4.26, Figure 4.27, and Figure 4.28 show SEM images of the various samples processed at 5°C, 22°C, 45°C and 60°C each for an 8 minute EPD processing time. From these images the 100µm SST substrate can be clearly identified and used a dimensional reference. The boundary of the SWCNT networks can be clearly identified by a sharp contrast line. Due to sample polishing some SWCNTs have been smeared into the softer epoxy resin darkening the surface, however the solid boundary line shows through and indicates where the full thickness SWCNT network lies. Based on the SEM images of the 8 minute processed samples the thicknesses for the various processing temperatures were found to be: 4.5-5.3µm for 5°C, 2.9-6.6µm for 22°C, 7.5-18.8µm for 45°C, and 9.9-20.1µm for 60°C.

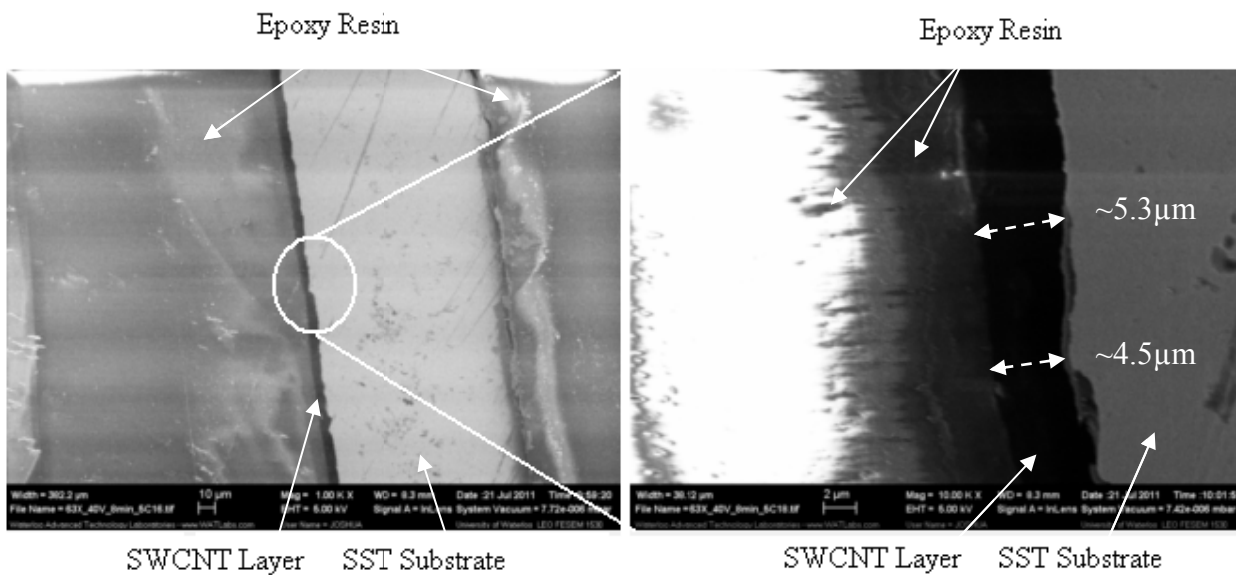


Figure 4.25 - Cross sections of SWCNT coated SST electrode using 40V EPD for 8min at 5°C

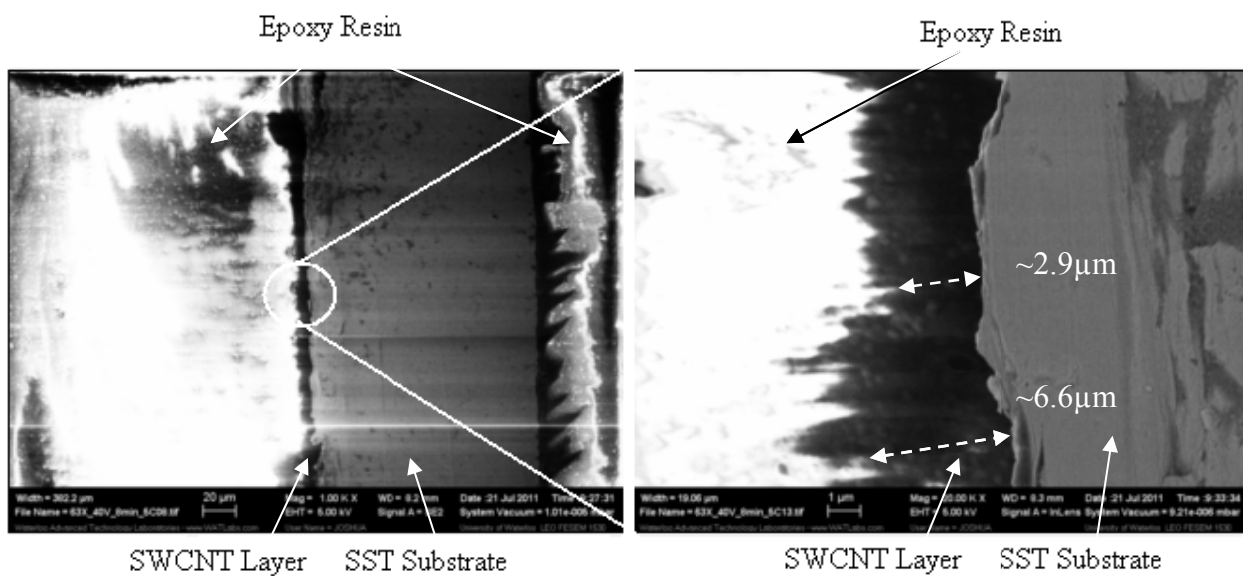


Figure 4.26 - Cross sections of SWCNT coated SST electrode using 40V EPD for 8min at 22°C

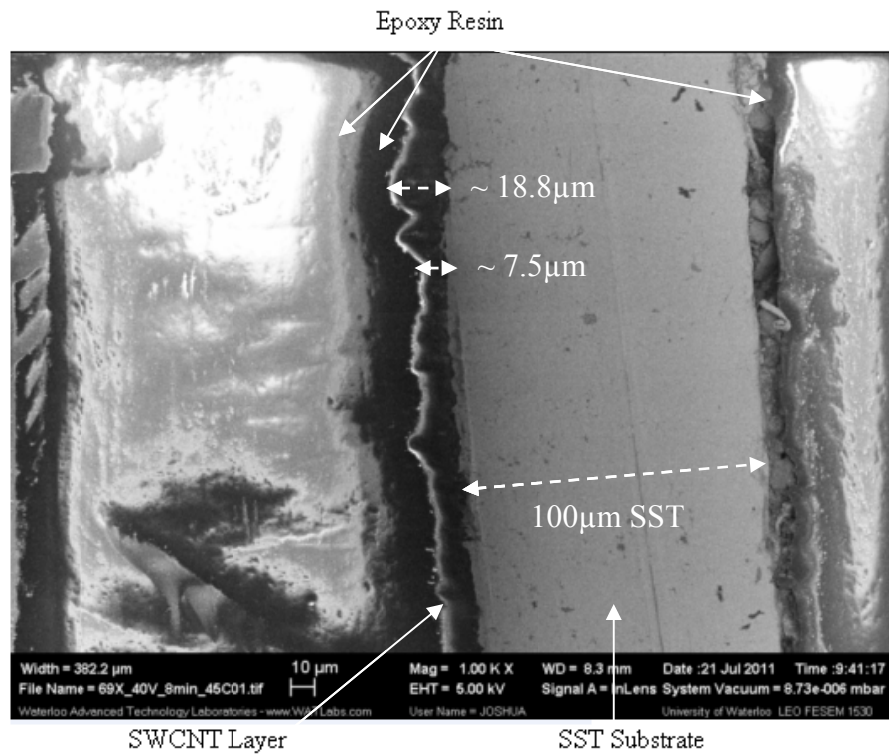


Figure 4.27 - Cross section of SWCNT coated SST electrode using 40V EPD for 8min at 45°C

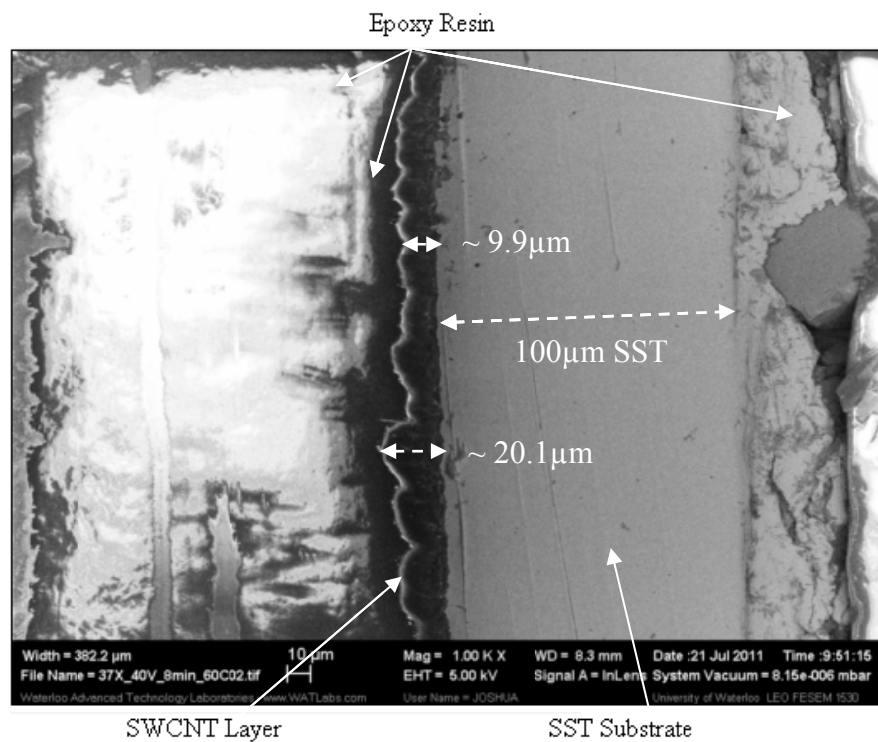


Figure 4.28 - Cross section of SWCNT coated SST electrode using 40V EPD for 8min at 60°C

The thickness variations within the same samples were found to be larger for the higher temperature EPD processed samples. For example the 5°C samples had a narrow range of less than 1µm or about 20% of the average 5µm thickness where the 60°C sample had a much larger range greater than 10µm or about 65% of the average 15µm thickness. This result agrees with the previous SEM images showing that the higher processing temperatures also appeared to have larger three dimensional networks or surface height variation.

Based on the SEM and optical analysis of the SWCNT structures it is clear that longer processing times yield better coverage and higher SWCNT densities. It is now also understood that elevated EPD processing temperatures produce thicker SWCNT films and deposit more SWCNT material onto substrates than SWCNT electrodes produced at room or reduced EPD processing temperatures given the same processing times as shown in Figure 4.29.

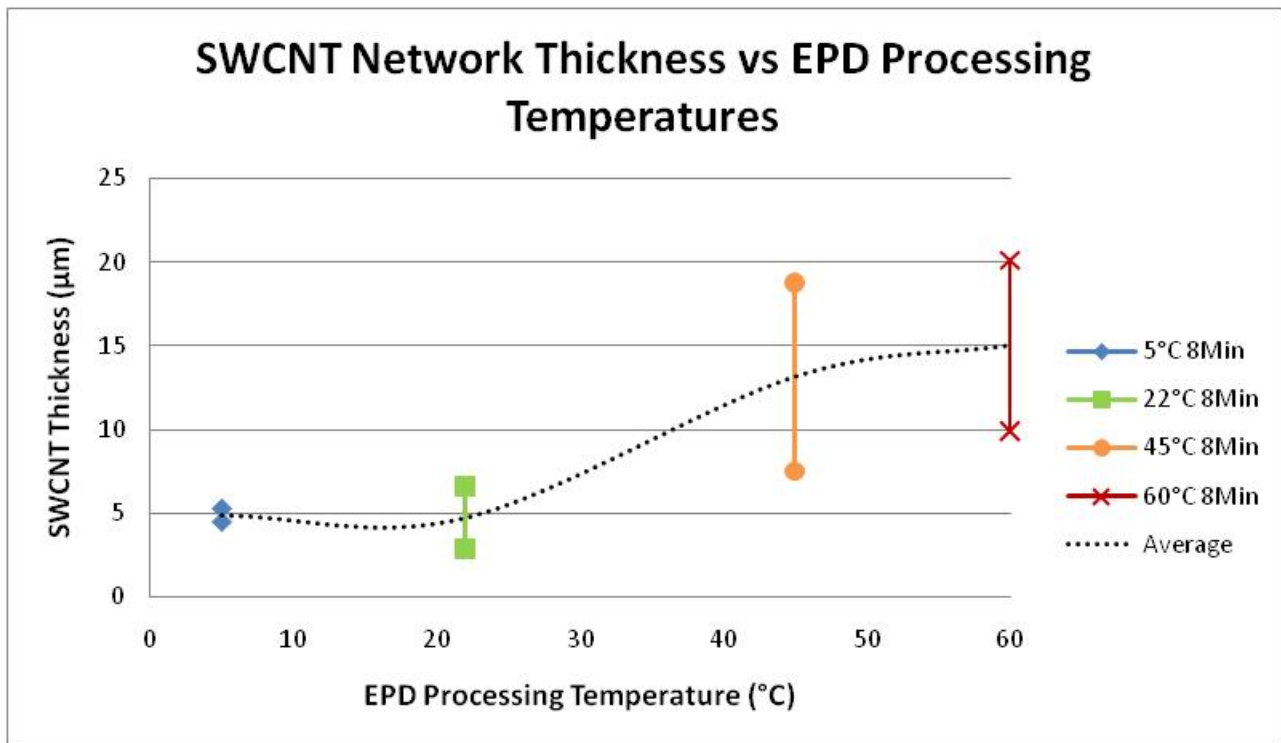


Figure 4.29 - Plot of SWCNT network thickness against EPD processing temperature

It is hypothesized that the increase in temperature of the SWCNT suspension in the EPD cell allows for higher mobility of SWCNTs within the suspension and that the elevated suspension temperature increases the electrical conductivity of the suspension thus reducing the overall EPD cell resistance and promoting thicker SWCNT films.

The structural results of the SWCNT coated electrodes produced using EPD show excellent promise for the use of SWCNT EPD produced electrodes in ultracapacitors. By varying process parameters a controllable process was identified which could deposit uniform SWCNT coatings on metallic current collectors. Although it is assumed that increases in the SWCNT densities and coating thicknesses will increase the capacitance of the SWCNT electrodes further characterization is needed to determine exactly how the EPD processing times and processing temperatures affect the capacitance. Specifically it is important to determine: 1) if a capacitance limit exists for extended EPD processing times, 2) if the relationship between processing time and capacitance is linear for extended EPD processing times, and 3) what is the effect of EPD processing temperature on the capacitance of SWCNT coated electrodes.

4.2 Brunauer-Emmett-Teller (BET) Pore Size Analysis

A BET surface analyzer was used to validate the pore sizes of the nanoporous SWCNT network as observed on in the SEM images of the EPD samples. Based on the SEM images of a 30V 3min EPD sample as shown previously in Figure 4.16 an average pore radius of approximately 20nm is observed. The BET surface analyzer confirmed that the visual approximations of pore radius from SEM images are accurate by yielding an average pore radius of 22.36nm for all pores less than 124.2nm in the same sample. Appendix A includes the raw BET data for the EPD sample.

Due to the difficulty in obtaining the specific mass of the SWCNTs added to the current collectors in the EPD process the total mass of the electrode (183.6mg), which includes both the SWCNTs and the current collector, was used for the BET measurement. Hence, the specific surface area of the SWCNT

network cannot be determined accurately. The specific surface area including the weight of the current collector was $0.1243\text{m}^2/\text{g}$. From the concentration ($0.5\text{mg}/\text{ml}$) and volume (5ml) of the SWCNT suspension used in the EPD process it can be estimated that the SWCNT mass deposited onto the current collectors is between $0.1\text{-}2.5\text{mg}$. Discounting the mass of the current collector the specific surface area of the SWCNT network can be approximated between $10\text{-}228\text{m}^2/\text{g}$ depending on the actual SWCNT mass deposited. This range aligns well with published data where CNT based electrodes report specific surface areas between $82\text{-}430\text{m}^2/\text{g}$ [54,60].

4.3 Electrical Resistance

Before testing the capacitance of the EPD samples the electrical resistance of the SWCNT networks was validated to ensure that electrical conductivity is maintained throughout the SWCNT networks and the current collectors. Internal resistance tests were performed on a few early generation Ni EPD samples to confirm that the SWCNT coated electrodes were suitable for capacitance characterization. For this test the SWCNT coated electrodes were clamped between flat conductive probes having a surface area of 0.785cm^2 using the mass of the upper electrode to provide uniform pressure. The electrical resistance was then measured through the SWCNT network and metallic current collector using an Agilent E4980A Precision LCR meter. To evaluate the effect of the SWCNTs on the current collector a bare Ni current collector, a poorly coated 20V 3min EPD SWCNT sample, a well coated 30V 3min EPD SWCNT sample, and a well coated drop method SWCNT sample were tested and their values were compared as shown in Table 4.1.

Table 4.1 - Internal resistance of SWCNT electrodes

Sample #	Description	Internal Resistance (R) Ohms
1	Bare Ni	42.00
2	SWCNT EPD Coated 20V - 3min	45.00
3	SWCNT EPD Coated 30V - 3min	6.50
4	Drop Coated	1.22

From the electrical resistance results it was observed that the SWCNTs had a net positive effect on lowering the internal resistance of the electrodes. For the poorly coated 20V EPD sample the internal resistance was essentially the same as the uncoated current collector. However, the 30V EPD sample, which had a thick coating of SWCNTs on the current collector, and the drop coated sample, which also had a well coated SWCNT network on the current collector, both had lower internal resistance values than the uncoated current collector. It is hypothesized that the electrically conductive SWCNT networks may have penetrated the thin oxide layer on the Ni surface and thus the internal resistance was lower in the samples with thick well formed SWCNT networks. The poorly formed SWCNT network may have had insufficient SWCNT density to penetrate the oxide layer or too few SWCNT junctions to create an electrically conductive SWCNT network and hence did not reduce the internal resistance of the electrode. Based on these results the addition of SWCNTs to the uncoated current collectors does not increase the internal resistance of the electrodes and shows that excellent electrical conductivity exists between the current collectors and SWCNT networks.

4.4 Electrochemical Characterization – Cyclic Voltammetry

Cyclic voltammetry (CV) is a valuable characterization tool for evaluating ultracapacitor electrode performance and is the primary characterization tool used to evaluate the performance of the EPD processed SWCNT electrodes in this work. CV curves were obtained for each EPD electrode produced and from the CV curve a capacitance value could be generated. This allows for the comparison of various processing variables such as processing time and processing temperature to be plotted and analyzed versus their respective capacitance values.

4.4.1 Cyclic Voltammetry – Electrophoretic Deposition Time Dependence

At a constant EPD voltage of 40V SST electrodes were prepared using EPD processing times of 0, 3, 5, 8, 15, 30, and 60 minutes to investigate the SWCNT network formation over extended processing times.

Cyclic voltammetry curves were then gathered to determine the effect of the EPD processing time on the capacitance of the SWCNT coated SST samples.

CV curves were recorded for each processed electrodes using an Ag/AgCl reference electrode and a Pt counter electrode in a three electrode cell. The working electrolyte for the CV curves was 1M HSO₄.

Figure 4.30, Figure 4.31, and Figure 4.32 are the CV curves for the SWCNT coated electrodes processed between 0-8min at scan rates of 20, 50, and 100mV/s. These figures show that at each scan rate an increase in EPD processing time resulted in an increase in the area within the CV curves. This indicates increases in electrode capacitance with increasing EPD processing time regardless of the scan rate.

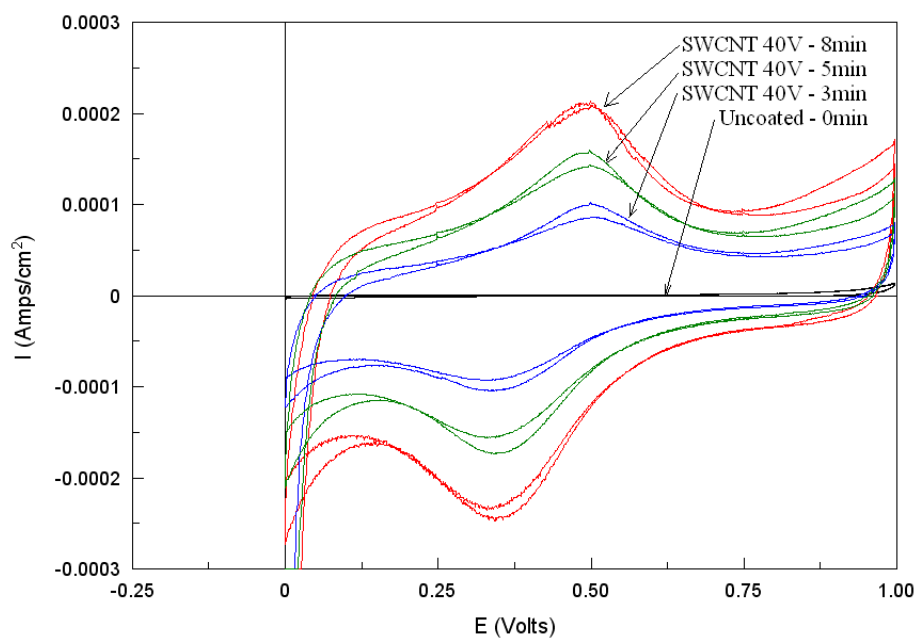


Figure 4.30 - CV curves of SWCNT coated SST electrodes at 20mV/s showing the effect of EPD processing time on capacitance for 0-8 minutes

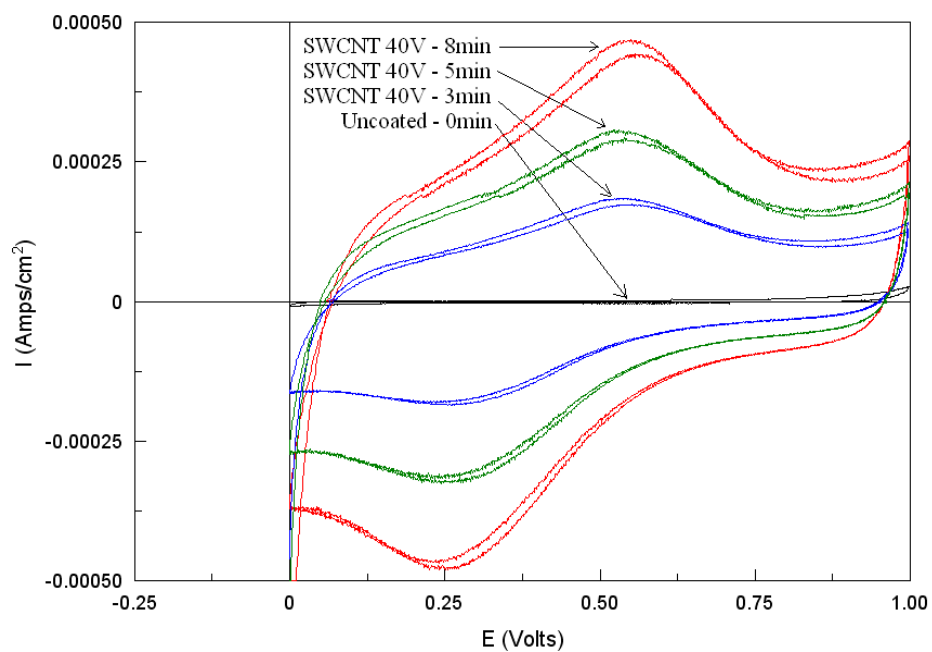


Figure 4.31 - CV curves of SWCNT coated SST electrodes at 50mV/s showing the effect of EPD processing time on capacitance for 0-8 minutes

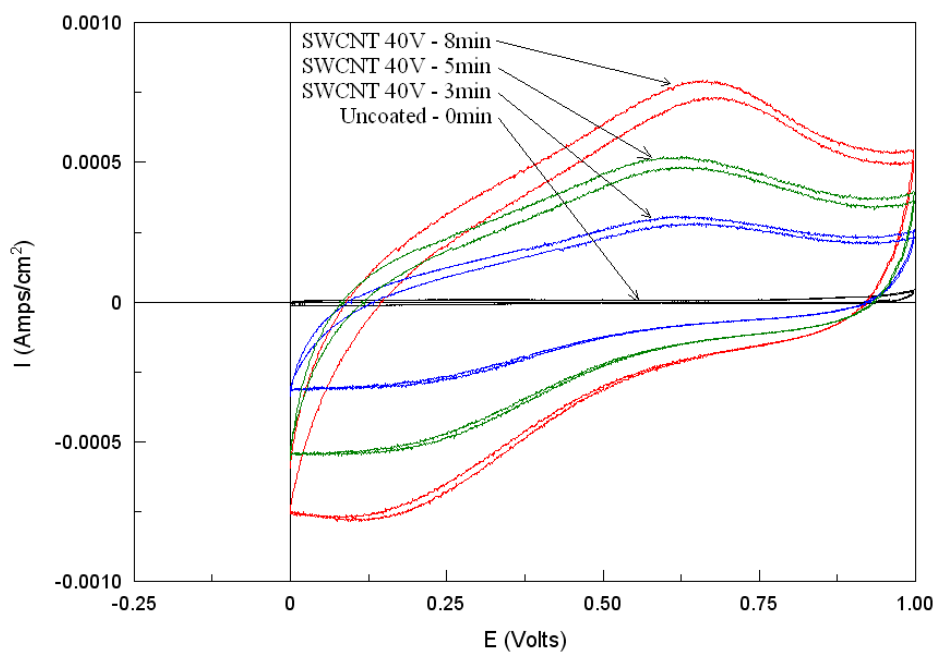


Figure 4.32 - CV curves of SWCNT coated SST electrodes at 100mV/s showing the effect of EPD processing time on capacitance for 0-8 minutes

From the CV plots the capacitance of the electrodes can be characterized by integrating the areas under the curves [75]. The previous CV curves indicate that the EPD processing time has a direct effect on the capacitance of the SWCNT coated SST electrodes as evidenced by the increasing size of the CV curves for EPD processing times from 0-8min. To quantify this effect further SWCNT coated electrodes were produced for EPD processing times of 0-60 minutes and characterized at a scan rate of 20mV/s. Figure 4.33 shows the CV curves for processing times of 0, 3, 5, 8, 15, 30, and 60 minutes. From this plot it is evident that further increases in EPD processing time yield larger areas within the CV curves and thus higher capacitance.

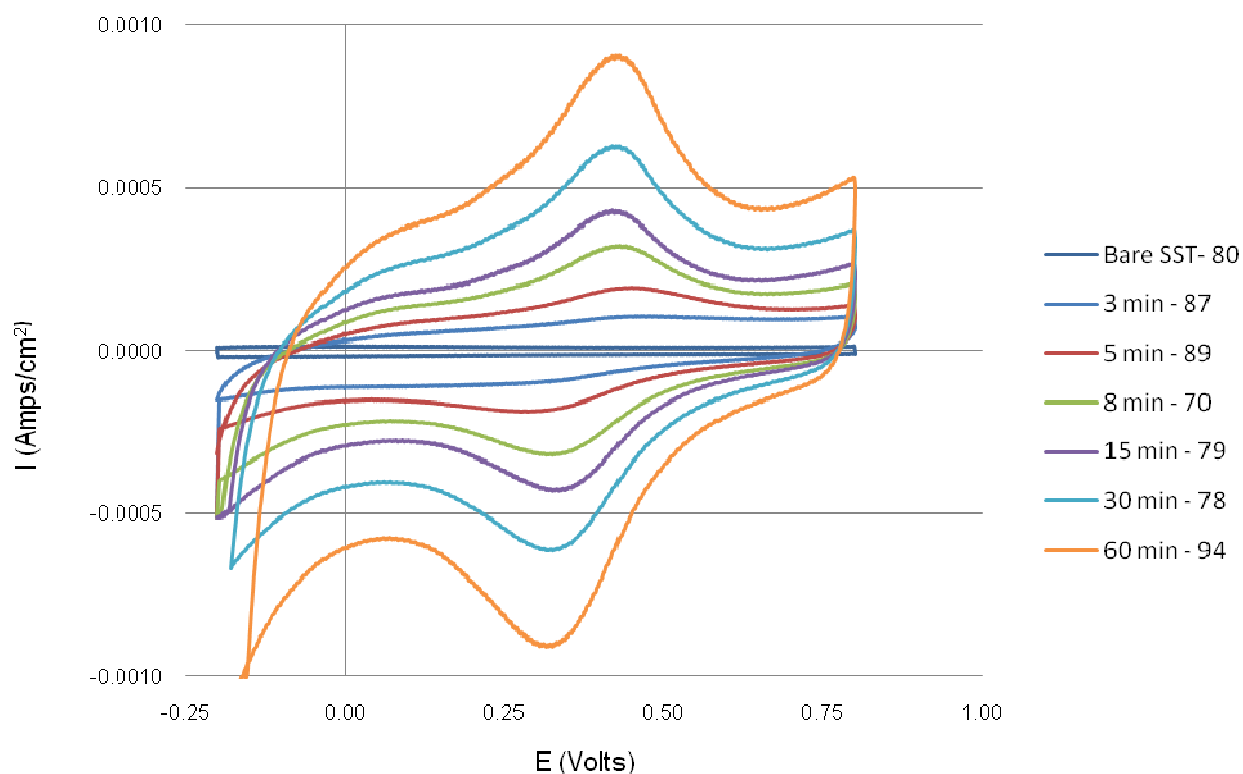


Figure 4.33 - CV curves of SWCNT coated SST electrodes at scan rate of 20mV/s for EPD processing times 0-60min

It is important to note that the mass of SWCNT material added to the SST electrode was very small. Approximately 0.1-2.5mg of SWCNTs material was added to the SST electrodes representing less than 0.05-1.0% wt of the total electrode mass. Thus the specific capacitance of the SWCNT material was

difficult to accurately determine and so the projected current collector area in cm^2 was used for capacitance reference. Capacitance values of approximately 0.16, 3.12, 5.16, 7.40, 12.53, 18.57, and 26.50 mF/cm^2 were calculated from the CV curves in Figure 4.33 for EPD processing times of 0, 3, 5, 8, 15, 30, and 60 minutes at 20mV/s respectively. Figure 4.34 shows a plot of the relationship observed between EPD processing time and the capacitance of the SWCNT coated SST electrodes for EPD processing times from 0-60 minutes.

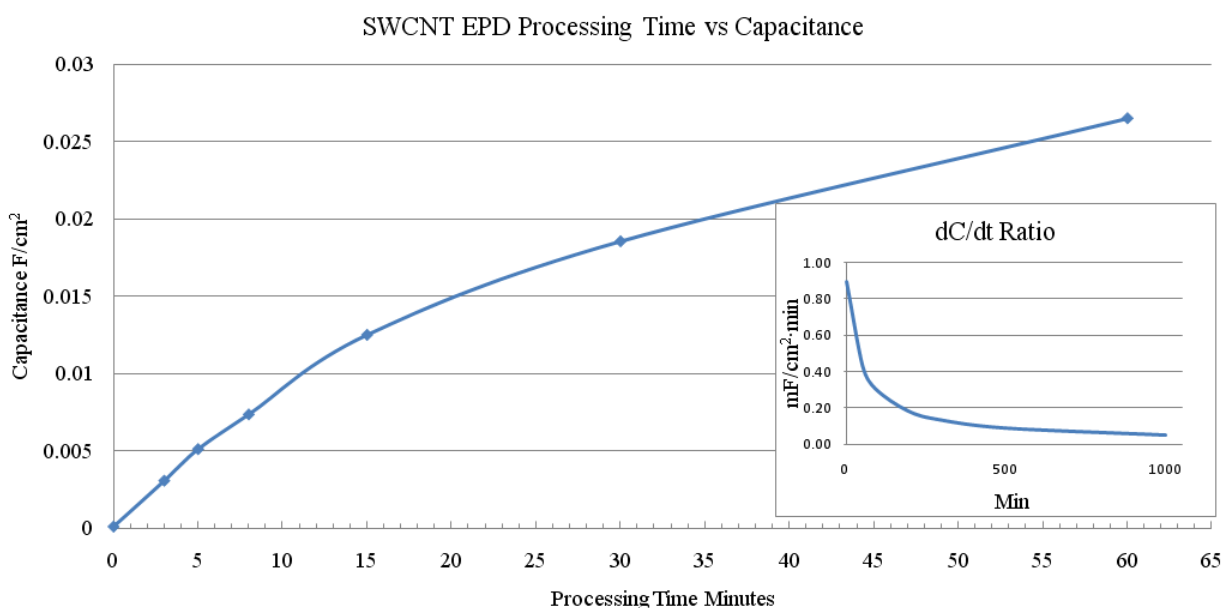


Figure 4.34 - Relationship between SWCNT EPD processing time and capacitance 0-60min, with inset extrapolated slope curve showing trail off of capacitance to processing time ratio

For processing times less than 10min a nearly linear relationship between the EPD processing time and the capacitance of the SWCNT electrodes is observed. A capacitance to processing time relationship of approximately $1.0\text{mF}/(\text{min}\cdot\text{cm}^2)$ was calculated from the slope of the capacitance vs time curve in this linear region. Beyond a processing time of 10 minutes the capacitance to processing time ratio trails off to less than $0.5\text{mF}/(\text{min}\cdot\text{cm}^2)$ at 60 minutes and the curve follows a logarithmic approximation of:

$$y = 0.0094\ln(x) - 0.0127 \text{ F/cm}^2 \quad (4.1)$$

Extrapolating the experimental data curve and plotting the slope (inset of Figure 4.34) indicates that the capacitance gains due to extended processing time significantly decreases beyond EPD processing times of 200 minutes to less than $0.05\text{mF}/(\text{min}\cdot\text{cm}^2)$. This information is useful for the determination of processing parameters for the fabrication of SWCNT coated electrodes for ultracapacitors in high volume manufacturing. Using this information an optimal processing time can be selected which balances the production costs and the gains in electrode capacitance associated with extended EPD processing times.

Comparing the capacitance of the 0 minute (bare SST) and the 60 minute EPD processed SWCNT electrodes from this first EPD cell shows that the addition of SWCNTs to the SST substrate by EPD significantly improved the capacitance of the uncoated SST electrode. The capacitance of the SWCNT coated SST electrode was 165 times larger than the uncoated SST electrode. From the plot it can be predicted that further processing time could yield additional increases in capacitance, but that the relationship between increased capacitance and processing time significantly decreases as processing time become large, specifically greater than 200 minutes. Shorter processing times less than 10 minutes yield the best return for the time to capacitance gain ratio.

4.4.2 Cyclic Voltammetry – Electrophoretic Deposition Temperature Dependence

In an effort to further increase the capacitance gains of SWCNT electrodes produced by EPD a second EPD cell was created which could change the processing temperature of the SWCNT suspension within the EPD cell. Similar to the original EPD time dependent experiments, a constant EPD voltage of 40V was used and SWCNT coated SST electrodes were prepared using EPD processing times of 0, 3, 8, 15, 30, and 60 minutes. In addition to the investigation of the SWCNT network formation with increasing processing times the processing temperature of the EPD suspension was maintained at 5°C, 22°C, 45°C, and 60°C for each series of processing times. CV curves were then gathered for each electrode to determine the effect of the EPD processing temperature on the capacitance of the SWCNT coated SST samples at specific processing times.

As in the previous section CV curves were recorded for each processed electrodes using an Ag/AgCl reference electrode and a Pt counter electrode in a three electrode cell. The working electrolyte for the CV curves was 1M HSO₄.

Figure 4.35 A-D are the CV curves for the SWCNT coated electrodes processed between 3-60 minutes at a scan rate of 20mV/s for EPD processing temperatures of 5°C, 22°C, 45°C, and 60°C. In each plot it can again be seen that an increase in EPD processing time results in an increase in the area within the CV curves and thus an increase in electrode capacitance. However, it is interesting to note that at the higher processing times of 60 minutes the CV curves for each figure are similar in size regardless of the processing temperature. In addition it is clear that the higher processing temperatures result in much larger CV curves for shorter processing times as indicated by the openness of the 45°C and 60°C figures. As the processing temperatures increase the CV curves become more open in the middle. This indicates that the effect of processing time is diminished when using elevated EPD processing temperatures and is an important finding for the manufacturing of SWCNT electrodes by EPD.

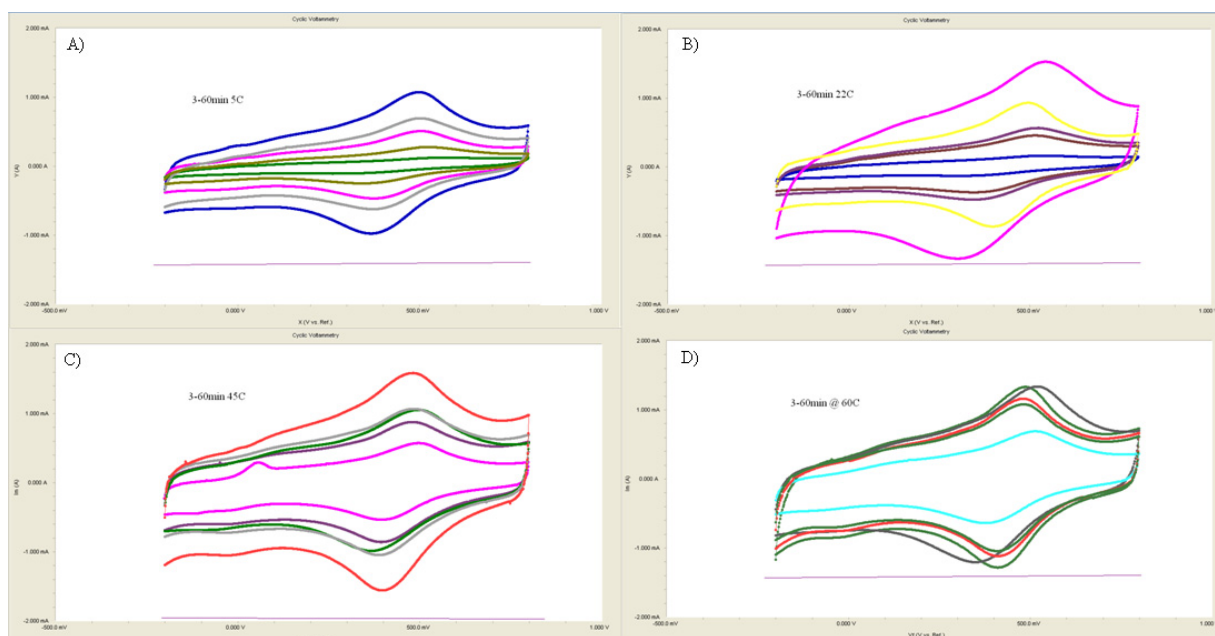


Figure 4.35 - CV curves for SWCNT EPD processed electrodes at a scan rate of 20mV/s for 3-60 minutes at various EPD processing temperatures: A) 5°C, B) 22°C, C) 45°C, D) 60°C

The 20mV/s scan rates were used to compare all sample processing temperatures and processing times, however, higher scan rates were also evaluated for some samples to determine the capability of the SWCNT electrodes to operate at higher charge and discharge rates which is an important characteristic of ultracapacitors. Figure 4.36 below shows the CV curves of the SWCNT electrodes EPD processed for 60 minutes at EPD temperatures of 5°C, 22°C, 45°C, and 60°C. Figure 4.36 A shows the electrodes at a scan rate of 100mV/s and Figure 4.36 B shows the electrodes as a scan rate of 500mV/s.

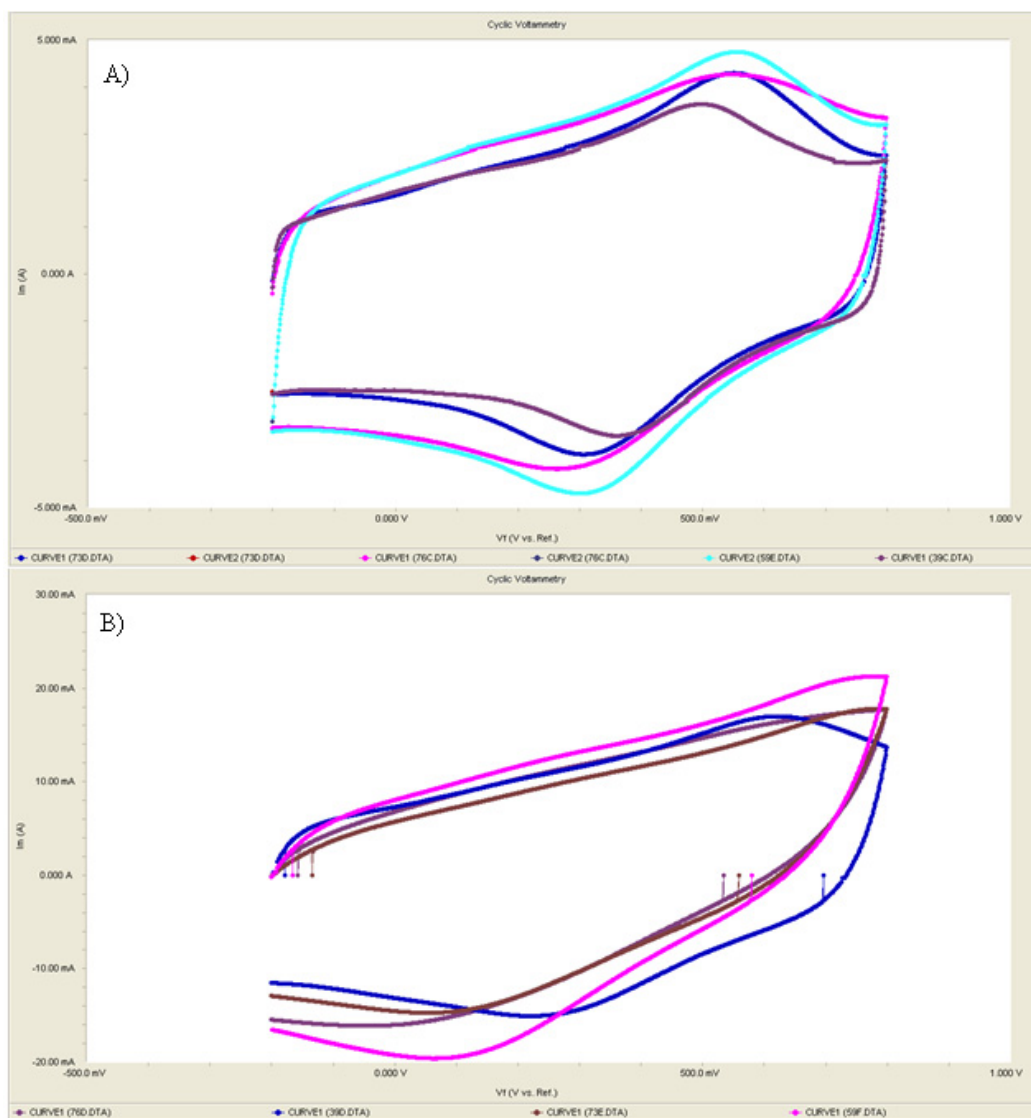


Figure 4.36 - CV curves of SWCNT coated electrodes using EPD for 60min at 5°C, 22°C, 45°C, 60°C: A) Scan rate of 100mV/s, B) Scan rate of 500mV/s

In each case the electrodes show excellent capacitance characteristics and maintain the desired rectangular CV curve shape. As the scan rate increases the internal resistance of the electrodes can limit the current flow and thus charge absorption of the electrodes. For electrodes with high internal resistance the CV curves at higher scan rates will tend to slop towards the upper right corner and the body of the CV curve will flatten. Although some flattening and sloping can be observed in Figure 4.36 B the scan rate is very high at 500mV/s and in general the curves shape is still partially rectangular. In electrodes with high internal resistance high scan rates can have significantly lower capacitance values due to the resistive behavior of the electrodes and at high enough scan rates the electrodes are choked off and exhibit highly resistive behavior with no little or no capacitance. The high scan rate CV curves of the SWCNT electrodes produced in this work show that good capacitance can still be achieved at scan rates as high as 500mV/s. Figure 4.37 shows the relationship between capacitance and scan rate for three of the electrodes in this work. From this plot it can be observed that approximately 70% of the original capacitance is still achieved at the faster 500mV/s scan rate which is 25 times faster than the original 20mV/s scan rate.

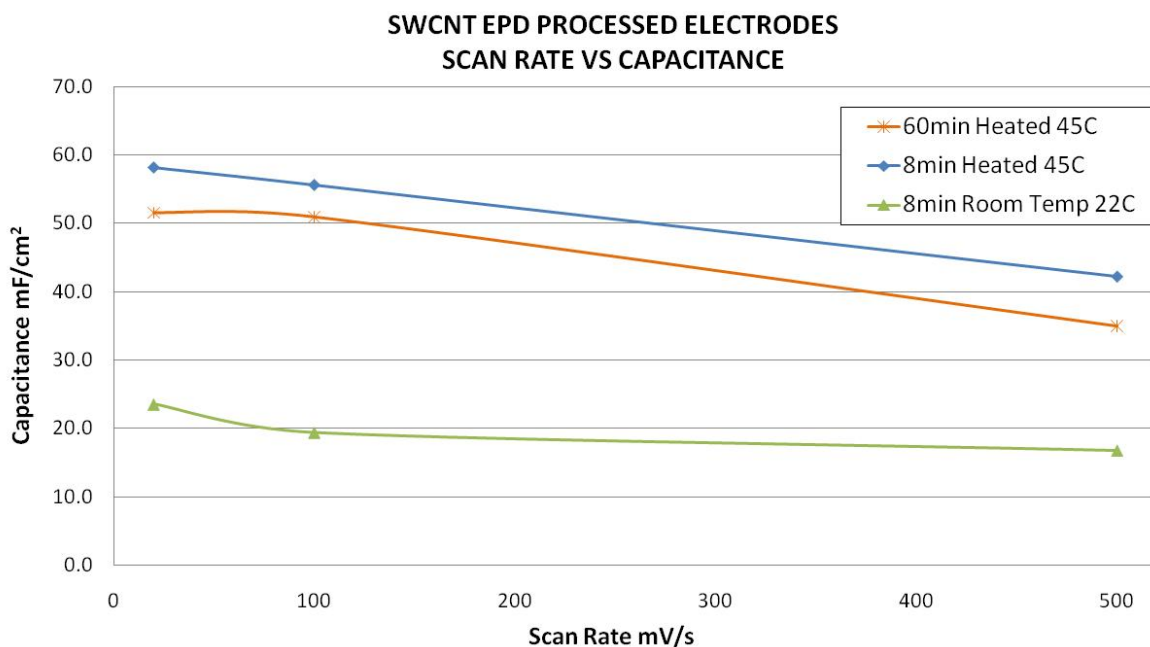


Figure 4.37 - Plot showing small decrease in capacitance with increasing scan rates 20-500mV/s for SWCNT electrodes

The capacitance values of the remaining temperature processed electrodes were obtained through integration of the CV curves shown in Figure 4.35 at a scan rate of 20mV/s. As with the time dependent SWCNT EPD samples only 0.1-2.5mg of SWCNTs material was added to the SST electrodes representing less than 0.05-1.0% wt of the total electrode mass. Hence the projected current collector area in cm^2 was used for capacitance reference. Capacitance values ranged between $0.23\text{mF}/\text{cm}^2$ for the uncoated SST electrode to $91.56\text{mF}/\text{cm}^2$ for the SWCNT coated electrodes and resulted in an increase in capacitance of 398 times the capacitance of the uncoated sample. Assuming a SWCNT mass of 2.0mg and projected current collector area of 1cm^2 a specific capacitance of $45.78\text{F}/\text{g}$ can be estimated which aligns well with the published data from section 2.3.1. Figure 4.38 shows the capacitance values and trend lines for all SWCNT EPD electrodes with processing times of 0, 3, 8, 15, 30, and 60 minutes and for EPD processing temperatures of 5°C , 22°C , 45°C , and 60°C . From this plot the observations from Figure 4.35 which indicated that effects of EPD processing times are diminished at higher EPD processing temperatures are validated. Here it can be seen that high capacitance values can be achieved with short 8 minute processing times when the EPD processing temperature of the SWCNT suspension is increased. In addition it is apparent that the effect of EPD processing time is limited to the first 10 minutes for increased EPD processing temperatures of 45°C and 60°C . At elevated temperatures the capacitance plateaus or dips after maxing out at approximately 10-15min of EPD processing time. It is hypothesized that for these higher temperature EPD suspensions the mobility of the SWCNT is increased and that due to the higher deposition rate the EPD cell could be consuming all of the functionalized SWCNT material after only 10-15 minutes.

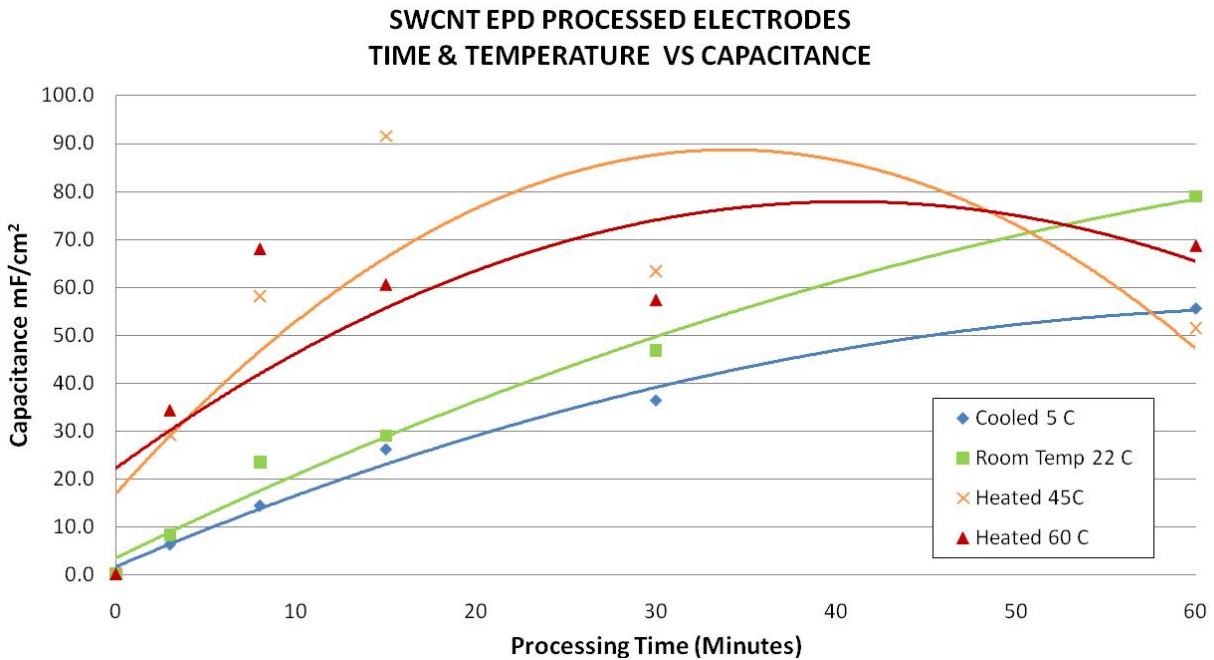


Figure 4.38 - Capacitance values and trend lines of SWCNT coated electrodes EPD processed for 0-60 minutes at 5°C, 22°C, 45°C, and 60°C

Figure 4.39 shows the capacitance values of the SWCNT electrodes created under EPD for the various processing temperatures but isolates the samples to those less than 10 minutes. Here the effect of EPD processing temperature on the capacitance of SWCNT electrodes can be clearly seen. In this shorter EPD processing range the slope of capacitance vs processing time for the 60°C samples is almost 4 times steeper than the slope for the 5°C samples. Likewise the capacitance of the electrode processed at 60°C for 8 minutes is 4.7 times larger than the electrode processed at 5°C for the same 8 minute processing time, 68.14mF/cm² vs 14.50mF/cm² respectively.

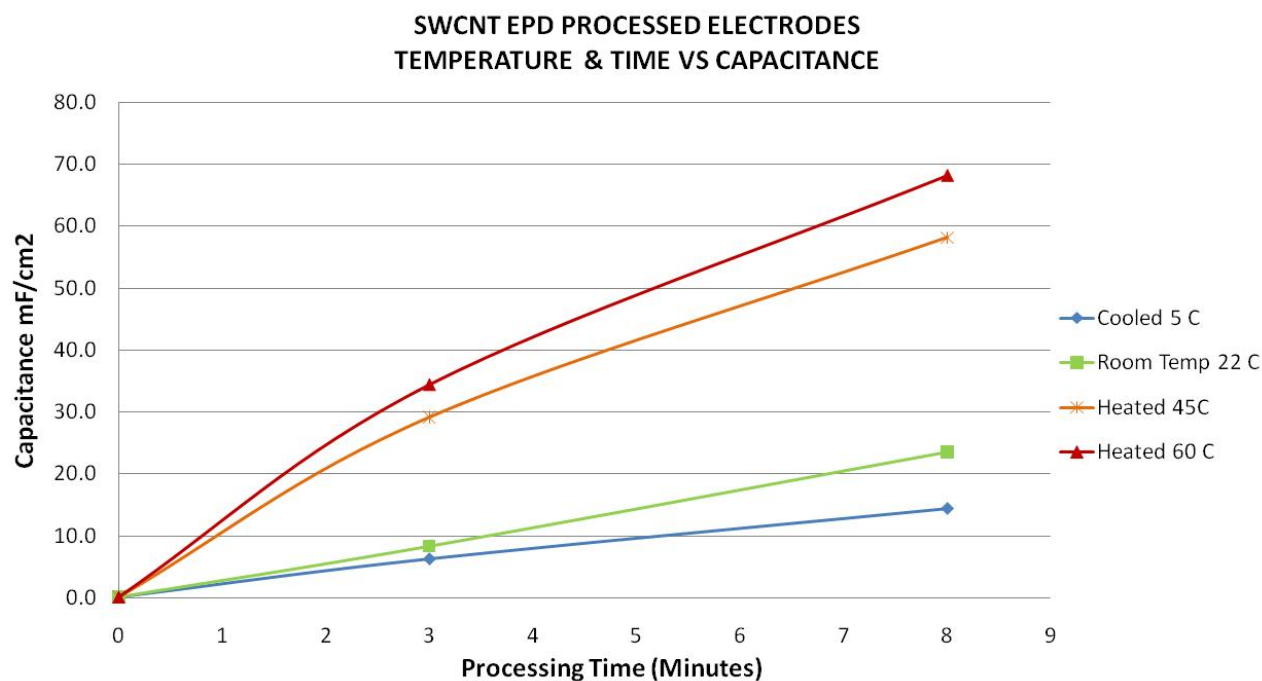


Figure 4.39 - Capacitance curves of SWCNT coated electrodes EPD processed for 0-8 minutes at 5°C, 22°C, 45°C, and 60°C

As mentioned previously the mass of the SWCNTs added to the current collector is difficult to measure since the contribution from the SWCNTs is so small relative to the total mass of the electrode, however the SWCNT network thickness data obtained through cross section and SEM analysis in section 4.1.4 allows a correlation between the SWCNT thickness and the capacitance to be made. Figure 4.40 shows the relationship between the deposited SWCNT networks and the capacitance of the electrodes for electrodes of varying different thicknesses as created using the different EPD processing temperatures. The result is a nearly linear correlation between SWCNT network thickness and measured electrode capacitance.

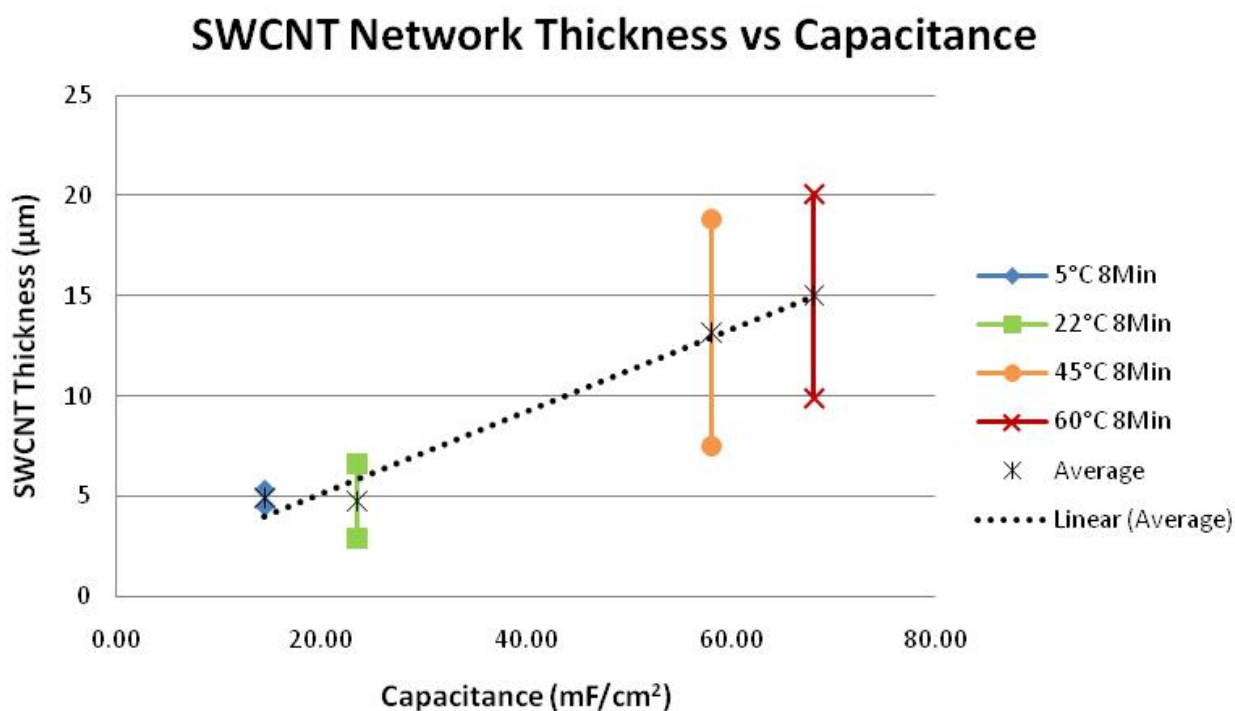


Figure 4.40 - Linear relationship between EPD SWCNT network thickness and electrode capacitance

The plot shows that the increases in capacitance observed under elevated processing times and increased processing temperatures can be attributed to an increase in SWCNT network thickness and thus the volume of SWCNT material. By increasing the EPD processing time and processing temperature the amount of SWCNT material added to the electrodes is increased and thus the capacitance is also increased. This is an important finding such that the capacitance gains are affected only by the amount of SWCNT material added to the electrode. By increasing the processing temperature the SWCNT deposition rate is increased shortening the deposition time required to achieve high capacitance values.

The investigation into the effect of EPD processing temperature on the capacitance of EPD produced SWCNT electrodes yielded excellent capacitive results and new insights into the effects of EPD processing temperatures on the fabrication of SWCNT coatings.

Chapter 5

Conclusions

Within this work various methods for the fabrication of SWCNT electrodes were investigated for the purpose of creating SWCNT electrodes for ultracapacitors. Ultimately a process has been illustrated which is suitable for large scale high volume production of SWCNT ultracapacitor electrodes from bulk SWCNT powders using acid functionalization and EPD. By maintaining the EPD processing voltage above 40V and using a processing time greater than 3min a repeatable process has been identified for coating SST electrodes with SWCNTs. The formation of uniform SWCNT networks on the surface of SST electrodes with nanopore radii of approximately 20nm has been demonstrated. Further investigation of the EPD process has also shown that increases in the processing time and the processing temperature result in increases in SWCNT network density, thickness, and coverage.

The EPD processing time parameter has been characterized at 40V and shows that at room temperature increases in EPD processing time directly correspond to increases in electrode capacitance. A relationship between EPD processing time and capacitance gain has been quantified showing optimal processing gains between 0-10min, diminishing capacitance gains from 10-60min, and predicts a saturation of the capacitance to EPD processing time ratio for processing times beyond 200min.

The EPD processing temperature parameter has also been characterized at 40V and shows that increases in EPD processing temperatures directly correspond to increases in electrode capacitance for EPD processing times less than 10min. Within this time range the capacitance gains are 4 times larger for SWCNT electrodes produced at EPD processing temperatures of 60°C compared to those produced at 5°C for the same duration. This is an important finding for high volume manufacturing where higher processing temperatures of the SWCNT suspension in the EPD cell will allow for the production of increased capacitance SWCNT electrodes with shorter manufacturing times and thus lower cost.

The thicknesses of SWCNT coatings produced at different EPD processing temperatures show that the SWCNT thicknesses and thickness variations increase with EPD processing temperature. SWCNT coatings processed for 8 minutes at a low processing temperature of 5°C had approximately a 1µm variation in thickness between 4.5-5.3µm and at a high processing temperature of 60°C had approximately a 10µm variation in thickness between 9.9-20.1µm.

A linear correlation was also identified between the SWCNT coating thickness and the capacitance values obtained from the SWCNT electrodes. From this correlation it was determined that the effective gains in capacitance from both extended EPD processing times and processing temperatures can be attributed to the additional SWCNT material added to the electrodes. The effect of EPD processing time and temperature on capacitance can then be related directly to their ability to increase the deposition of SWCNT material onto the SST current collectors. In this work, time dependence shows that the optimum SWCNT deposition rates are achieved during EPD processing times less than 10 minutes and temperature dependence shows that further increases in SWCNT deposition rates are achieved at elevated EPD processing temperatures of 60°C or higher.

The investigation into the effect of EPD processing times and temperatures on the capacitance of EPD produced SWCNT electrodes yielded electrodes with excellent capacitance and shed new light on the benefits of increased EPD processing temperatures for the creation of SWCNT coatings. In this work the addition of a SWCNT network to a SST electrode by EPD resulted in an increase in capacitance of 398 times the capacitance of the uncoated electrode. A capacitance value of 0.091F/cm² or approximately 45.78F/g of SWCNT material was achieved.

Chapter 6

Recommendations

In future work the effect of the SWCNT suspension concentration on the SWCNT electrode capacitance could be investigated. A hypothesis for this relationship is that above a certain SWCNT concentration the EPD process is limited by mobility of the SWCNTs through the fluid and not the proximity of SWCNTs to the deposition electrode. In this work it is shown that the capacitance does increase with shorter processing times when the EPD processing temperature is raised above room temperature. However, it would be interesting to see if the capacitance can increase further with shorter processing times using higher concentration SWCNT suspensions and elevated processing temperatures together. The current work uses a SWCNT suspension concentration of 0.5mg/ml but variations in concentration of 0.25, 0.50, 1.00, and 2.0mg/ml could be investigated in future work.

This work looked at the capacitive behavior of a SWCNT network fabricated by EPD without the use of pseudocapacitance. However, literature has shown that the addition of molecular groups such as MnO_2 to SWCNTs and MWCNTs can provide further increases in the capacitance of CNT electrodes. Now that a stable process has been identified and characterized the addition of pseudocapacitance to the SWCNT networks formed by EPD could be used as a method for obtaining additional increases in the capacitance of the EPD produced SWCNT electrodes.

The sensitivity of the functionalized SWCNT suspension to contamination is evident throughout the various processes. Specifically, strong evidence of contamination was observed in the first polycarbonate fabricated temperature controlled EPD cell and in the use of HP printer cartridges which included foam inserts. Future work could look at the interaction between the functionalized SWCNTs and contaminating elements such as cellulose, polymers, and other compounds which were observed to react with and cause the SWCNTs to drop out of suspension. In addition, future work with inkjet printers having custom

cartridges or modified cartridges with all foam inserts removed could have the potential to yield better printed results by avoiding the observed contamination.

The fabrication of an ultracapacitor device made from EPD processed SWCNTs could also be investigated in future work. Although this work focuses primarily on the development of single electrodes, future work could combine sets of single electrodes processed by the EPD method defined here to create functional ultracapacitor devices. These devices could then be evaluated for reliability, performance, and compared to commercially available devices.

A conceptual diagram of a reel to reel high volume production adaptation of the EPD temperature cell created in this work is shown below in Figure 6.1. In future work the fabrication of such a production EPD cell could enable the fabrication of very large continuous SWCNT coated electrodes for use in commercial applications. Such a device has the potential to revolutionize the use of powder SWCNTs in large scale fabrication of electronic components, such as ultracapacitors.

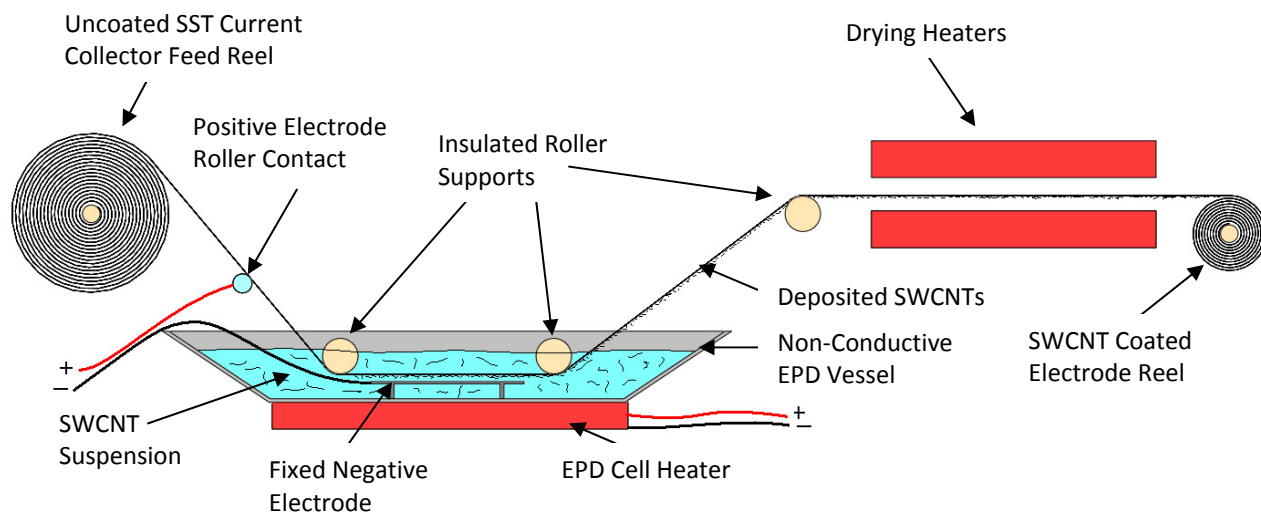


Figure 6.1 - Schematic diagram of reel to reel EPD cell for continuous SWCNT deposition

Appendix A
BET Surface Analyzer Data

Quantachrome Instruments
NOVA 2200, Version 9.01
High Speed Gas Sorption Analyzer
Summary Analysis Report

Page 1

Data File = N072902.dat Station = B
User ID = JM Sample ID = Ni SUCNT
Analysis Setup = Setup_63.dat Sample Cell Number = 3
Comments:
Sample Weight = 0.1836 g Sample Volume = 0.1918 mL
Sample Density = N/A Sample Volume = MEASURED
P0 Type = DEFAULT P0 = 739.57 mm Hg
Adsorbate Name = Nitrogen Bath Temperature = 77.40 K


ADSORPTION SETUP DESORPTION SETUP
Tolerance = 0.10 mm Hg Tolerance = 0.10 mm Hg
Equil Time = 60 secs Equil Time = 60 secs
Dwell Time = 180 secs Dwell Time = 180 secs

Analysis Started : Thu Jul 29 09:49:32 2010
Analysis Finished: Thu Jul 29 14:07:31 2010
Elapsed Time : 257.98 Minutes (2 Station Run)

* * * ANALYSIS RESULTS * * *

20 POINT BET

* Specific Surface Area = 0.1243 sq. m/g
Slope = 41489.5586
Intercept = -13461.8135
Correlation Coefficient = 0.4768
BET C = -2.0820

km
 1 cm x 2

SINGLE POINT BET (Point @ 0.3481 P/P0)

* Specific Surface Area = 2.0842 sq. m/g

PORE SIZE (For all pores less than 1242.1288 Angstrom)

* Total Pore Volume = 1.3892 e-3 mL/g
* Average Pore Radius = 223.6109 Angstrom

Quantachrome Instruments
NOVA 2200, Version 9.01
High Speed Gas Sorption Analyzer
Detailed Analysis Report

Page 1

```

Data File       = N072902.dat      Station         = B
User ID        = JM                Sample ID      = Ni5W CNT
Analysis Setup = Setup_63.dat     Sample Cell Number = 3
Comments:

Sample Weight   = 0.1836 g         Sample Volume   = 0.1918 mL
Sample Density  = N/A              Sample Volume   = MEASURED

P0 Type        = DEFAULT           P0              = 739.57 mm Hg
Adsorbate Name = Nitrogen          Bath Temperature = 77.40 K
  
```

```

          ADSORPTION SETUP                DESORPTION SETUP
Tolerance    = 0.10 mm Hg                Tolerance      = 0.10 mm Hg
Equil Time   = 60 secs                   Equil Time     = 60 secs
Dwell Time   = 180 secs                   Dwell Time    = 180 secs
  
```

```

Analysis Started : Thu Jul 29 09:49:32 2010
Analysis Finished: Thu Jul 29 14:07:31 2010
Elapsed Time     : 257.98 Minutes (2 Station Run)
  
```

* * * A N A L Y S I S R E S U L T S * * *

20 POINT BET

```

* Specific Surface Area = 0.1243 sq. m/g
  Surface Area         = 0.0228 sq. m

Slope                  = 41489.5586
Intercept              = -13461.8135
Correlation Coefficient = 0.4768
BET C                  = -2.0820
  
```

SINGLE POINT BET (Point @ 0.3481 P/P0)

```

* Specific Surface Area = 2.0842 sq. m/g
  Surface Area         = 0.3827 sq. m
  
```

* * * B E T D A T A * * *

Target Pressure [mm Hg]	Actual Pressure [P/P0]	Volume [STP] Adsorbed [mL/g]	BET Transform 1/(W[P0/P - 1])
36.79	0.0518	0.1902	229.8922
73.59	0.1019	0.3396	267.4680
110.38	0.1521	0.4311	333.0164
147.17	0.2021	0.4824	420.0505
183.97	0.2517	0.5876	458.0885
220.76	0.3020	0.5924	584.2740
257.55	0.3481	0.7346	581.7047

Quantachrome Instruments
NOVA 2200, Version 9.01
High Speed Gas Sorption Analyzer
Detailed Analysis Report

Page 2

Data File = N072902.dat Station = B
 User ID = JM Sample ID = Ni SWCNT
 Analysis Setup = Setup_63.dat Sample Cell Number = 3
 Comments:

* * * B E T D A T A * * *

Target Pressure [mm Hg]	Actual Pressure [P/P0]	Volume [STP] Adsorbed [mL/g]	BET Transform 1/(W(P0/P - 1))
257.55	0.3481	0.7346	581.7047
294.35	0.3948	0.7110	734.1006
331.14	0.4463	0.9889	652.1163
367.93	0.4993	0.7219	1105.2930
404.73	0.5472	0.9518	1015.9893
441.52	0.5989	0.9202	1298.3224
478.31	0.6504	0.8862	1679.3723
515.11	0.7000	0.7646	2441.9895
551.90	0.7471	1.0414	2269.3132
588.69	0.8014	0.6668	4842.8521
625.49	0.8442	1.1381	3808.7410
662.28	0.8932	0.7578	8828.0391
699.07	0.9440	0.7342	18365.4141
735.87	0.9923	0.8994	115198.3125

Quantachrome Instruments
NOVA 2200, Version 9.01
High Speed Gas Sorption Analyzer
Detailed Analysis Report

Page 3

Data File = N072902.dat Station = B
 User ID = JM Sample ID = Ni
 Analysis Setup = Setup_63.dat Sample Cell Number = 3
 Comments:

SWCNT

*** BJH PORE SIZE DISTRIBUTION DATA ***

Pore Radius [Angstrom]	Pore Volume [mL/g]	Pore Area [sq m/g]
727.1121	2.6653E-04	7.3312E-03
139.2682	4.1310E-05	5.9324E-03
82.2264	7.7889E-04	1.8945E-01
60.2626	1.0231E-03	3.3955E-01
47.5367	8.2498E-04	3.4709E-01
38.6137	6.3304E-04	3.2788E-01
32.7792	2.3982E-04	1.4632E-01
28.2163	5.1302E-06	3.6364E-03
24.6089	9.9293E-06	8.0697E-03
21.8041	6.7602E-04	6.2009E-01
19.4702	8.1531E-04	8.3750E-01
17.4156	8.8565E-04	1.0171E+00
14.3410	4.2540E-04	5.9327E-01
11.7583	2.8311E-04	4.8156E-01
9.3792	1.8406E-04	3.9250E-01
8.1129	4.6166E-04	1.1381E+00

Quantachrome Instruments
NOVA 2200, Version 9.01
High Speed Gas Sorption Analyzer
Detailed Analysis Report

Page 4

Data File = N072902.dat Station = B
User ID = JM Sample ID = NiSUCMT
Analysis Setup = Setup_63.dat Sample Cell Number = 3
Comments:

PORE SIZE (For all pores less than 1242.1288 Angstrom)

- * Total Pore Volume = 1.3892 e-3 mL/g
- * Average Pore Radius = 223.6109 Angstrom

*** TOTAL PORE VOLUME DATA ***

Target Pressure [mm Hg]	Actual Pressure [P/P0]	Volume [STP] Adsorbed [mL/g]
735.8672	0.9923	0.8994

Quantachrome Instruments
NOVA 2200, Version 9.01
High Speed Gas Sorption Analyzer
Detailed Analysis Report

Data File = N072902.dat Station = B
 User ID = JM Sample ID = Ni *SWCNT*
 Analysis Setup = Setup_63.dat Sample Cell Number = 3
 Comments:

* * * Isotherm Data * * *

Target Pressure [mm Hg]	Actual Pressure [P/P0]	Volume [STP] Adsorbed [mL/g]
36.79	0.0518	0.1902
73.59	0.1019	0.3396
110.38	0.1521	0.4311
147.17	0.2021	0.4824
183.97	0.2517	0.5876
220.76	0.3020	0.5924
257.55	0.3481	0.7346
294.35	0.3948	0.7110
331.14	0.4463	0.9889
367.93	0.4993	0.7219
404.73	0.5472	0.9518
441.52	0.5989	0.9202
478.31	0.6504	0.8862
515.11	0.7000	0.7646
551.90	0.7471	1.0414
588.69	0.8014	0.6668
625.49	0.8442	1.1381
662.28	0.8932	0.7578
699.07	0.9440	0.7342
735.87	0.9923	0.8994
699.17	0.9493	0.2886
662.47	0.8995	0.5819
625.76	0.8491	0.8788
589.06	0.7864	0.4034
552.36	0.7477	0.7194
515.66	0.7014	0.2926
478.96	0.6523	0.3433
442.26	0.5878	0.2522
405.56	0.5493	0.3400
368.86	0.5030	-0.0160
332.16	0.4521	0.2748
295.46	0.4044	0.1119
258.76	0.3547	0.1371
222.05	0.2911	0.0343
185.35	0.2523	0.0484
148.65	0.2059	-0.0222
111.95	0.1374	-0.0636
75.25	0.1031	-0.1578
38.55	0.0455	-0.2558
1.85	0.0058	-0.2629

References

- [1] A.G. Pandolfo; A.F. Hollenkamp, Carbon properties and their role in supercapacitors, *Journal of Power Sources*, 157, 11-27 (2006)
- [2] M.Winter; R. J. Brodd, What Are Batteries, Fuel Cells, and Supercapacitors?, *Chemical Reviews*, 104 (10), 4245-427 (2004)
- [3] S.M. Lukic; J. Cao; R.C. Bansal; F. Rodriguez; A. Emadi, Energy storage systems for automotive applications, *IEEE Transactions on Industrial Electronics*, 55 (6), 2258-2267 (2008)
- [4] Image courtesy US Defense and Logistics Agency, retrieved (2011) from: <http://www.mpoweruk.com/performance.htm>
- [5] A.S. Aricò; P. Bruce; B. Scrosat; J. Tarascon; W. van Schalkwijk, Nanostructured materials for advanced energy conversion and storage devices, *Nature Materials*, 4, 366-377 (2005)
- [6] A. Burke, Ultracapacitors: why, how, and where is the technology, *Journal of Power Sources*, 91, 37-50 (2000)
- [7] B.E. Conway, *Electrochemical Super-capacitors: Scientific, fundamentals, and technology applications*, Kluwer, New York, 1999
- [8] J. Chmiola; G. Yushin; Y. Gogotsi; C. Portet; P.Simon; P.L. Taberna; Anomalous increase in carbon capacitance at pore sizes less than 1 nanometer, *Science*, 313, 1760-3 (2006)
- [9] S. Patrice; A. Burke, Nanostructured carbons: double-layer capacitance and more, *Electrochemical Society Interface*, 17-1, 38-43 (2008)
- [10] J. Li; Q.M. Yang; I. Zhitomirsky, Nickel foam-based manganese dioxide-carbon nanotube composite electrodes for electrochemical supercapacitors, *Journal of Power Sources*, 185, 1569-1574 (2009)
- [11] D.V. Kosynkin; A.L. Higginbotham; A. Sinitskii; J.R. Lomeda; A. Dimiev; B.K. Price; J.M. Tour, Longitudinal unzipping of carbon nanotubes to form graphene nanoribbons, *Nature*, 458, 872-876 (2009)
- [12] B.P. Grady, Polymer and nanomaterials characterization group, Carbon Nanotube Composites, Retrieved (2011) from: <http://coecs.ou.edu/Brian.P.Grady/nanotube.html>
- [13] X. Wang; Q. Li; J. Xie; Z. Jin; J. Wang; Y. Li; K. Jiang; S. Fan, Fabrication of Ultralong and Electrically Uniform Single-Walled Carbon Nanotubes on Clean Substrates, *Nano Letters*, 9-9, 3137-3141 (2009)
- [14] G. Centi; S. Perathoner, Problems and perspectives in nanostructured carbon-based electrodes for clean and sustainable energy, *Catalysis Today*, 150 (1-2), 151-162 (2010)

-
- [15] Raymond M. Reilly, Carbon nanotubes: Potential benefits and risks of nanotechnology in nuclear medicine, *The Journal of Nuclear Medicine*, 48-7, 1039-1042, (2007)
- [16] M. Yu; O. Lourie; M. J. Dyer; K. Moloni; T. F. Kelly; R.S. Ruoff, Strength and breaking mechanism of multiwalled carbon nanotubes under tensile load, *Science*, 287 (5453), 637–640 (2000)
- [17] P.G. Collins; P. Avouris, Nanotubes for electronics, *Scientific American*, 67–69 (2000)
- [18] V.M. Dubin; C.D Thomas, et al, Engineering gap fill, microstructure and film composition of electroplated copper for on-chip metallization, *Proc of the IEEE 2001 International, Interconnect Technology Conf*, San Francisco, CA, 271-273 (2001)
- [19] S. Hong; S. Myung, Nanotube electronics: A flexible approach to mobility, *Nature Nanotechnology*, 2 (4), 207–208 (2007)
- [20] P. Avouris, Carbon nanotube electronics, *Chemical Physics*, 281, 429–45 (2002)
- [21] G.G. Wallave; J. Chen; D. Li; S.E. Moulton; J.M. Razal, Nanostructured carbon electrodes, *Journal of Materials Chemistry*, 20, 3553–3562 (2010)
- [22] J.M. Boyea; R.E. Camacho; S.P. Turano; W.J. Ready, Carbon nanotube-based supercapacitors: Technologies and markets, *Nanotechnology Law and Business*, 585-593 (2007)
- [23] P.K. Rai; A.N. Parra-Vasquez; J. Chattopadhyay; R.A. Pinnick; F. Liang; A.K. Sadana; R.H. Hauge; W.E. Billups; M. Pasquali; *Journal of Nanoscience and Nanotechnology*, 7 3378–3385 (2007)
- [24] A.R. Boccaccini; I. Zhitomirsky; Applications of electrophoretic and electrolytic deposition techniques in ceramics processing, *Solid State and Material Science*, 6, 251-260 (2002)
- [25] G. Girishkumar; M. Rettker; R. Underhile; D. Binz; K. Vinodgopal; P. McGinn; P. Kamat; Single-walled carbon nanotube-based proton exchange membrane assembly for hydrogen fuel cells, *Langmuir*, 21, 8487-8494 (2005)
- [26] L.A. Girifalco; M. Hodak; R.S. Lee, Carbon nanotubes, buckyballs, ropes, and a universal graphitic potential, *Physical Review B*, 62, 13104–13110 (2000)
- [27] M.S. Strano; V.C. Moore; M.K. Miller; et al., The role of surfactant adsorption during ultrasonication in the dispersion of single-walled carbon nanotubes, *Journal of Nanoscience and Nanotechnology*, 3 (1-2), 81-86 (2003)
- [28] M.F. Islam; E. Rojas; D. M. Bergey; A.T. Johnson; A.G. Yodh, High weight fraction surfactant solubilization of single-wall carbon nanotubes in water, *Nano Letters*, 3 (2), 269-273 (2003)
- [29] M.S.P. Shaffer; X. Fan; A.H. Windle, Dispersion and packing of carbon nanotubes, *Carbon*, 36 (11), 1603–1612 (1998)

-
- [30] T. Yamamoto; S. Noda; M. Kato, A simple and fast method to disperse long single-walled carbon nanotubes introducing few defects, *Carbon*, 49 (10), 3179-3183 (2011)
- [31] N.R. Tummala, SDS surfactants on carbon nanotubes: Aggregate morphology, *ACS Nano*, 3 (3), 595-602 (2009)
- [32] L. Ren; S. Wang, Tailoring optical and electrical properties of carbon nanotube networks for photovoltaic applications, *Carbon*, 48 (15), 4397-4402 (2010)
- [33] H.Z. Geng; K.K. Kim; K.P. So; Y.S. Lee; Y. Chang; Y.H. Lee, Effect of acid treatment on carbon nanotube-based flexible transparent conducting films, *Journal of the American Chemical Society*, 129, 7758-7759 (2007)
- [34] Y.P. Sun; K. Fu; Y. Lin; W. Huang, Functionalized carbon nanotubes: Properties and applications, *Accounts of Chemical Research*, 35 (12), 1096-1104 (2002),
- [35] W. Huang; Y. Lin; S. Taylor; J. Gaillard; A.M. Rao; Y.P. Sun, Sonication-assisted functionalization and solubilization of carbon nanotubes, *Nano Letters*, 2, 231-234 (2002)
- [36] D. Tasis; N. Tagmatarchis; A. Bianco; M. Prato, Chemistry of carbon nanotubes, *Chemical Reviews*, 106 (3), 1105-1136 (2006)
- [37] S. Niyogi; M. A. Hamon; H. Hu; B. Zhao; P. Bhowmik; R. Sen; M. E. Itkis; R. C. Haddon, Chemistry of single-walled carbon nanotubes, *Accounts of Chemical Research*, 35 (12), 1105-1113 (2002)
- [38] A.G. Nasibulin; A. Kaskela; K. Mustonen; et al., Multifunctional free-standing single-walled carbon nanotube films, *ACS Nano*, 5 (4), 3214-3221 (2011)
- [39] P. Aldeanueva-Potel; M.A. Correa-Duarte; R.A. Alvarez-Puebla; L.M. Liz-Marzán, Free-standing carbon nanotube films as optical accumulators for multiplex SERRS atomolar detection, *ACS Applied Materials & Interfaces*, 2 (1), 19-22 (2010)
- [40] H. Gu; T.M. Swager, Fabrication of free-standing, conductive, and transparent carbon nanotube films, *Advanced Materials*, 20, 4433-4437 (2008)
- [41] W. Zhuangchun; Z. Chen; X. Du; J.M. Logan; J. Sippel; M. Nikolou; K. Kamaras; J.R. Reynolds; D.B. Tanner; A.F. Hebard; A.G. Rinzler, Transparent, conductive carbon nanotube films, *Science*, 305, 1273-1276 (2004)
- [42] J.W. Jo; J.W. Jung; J.U. Lee; W.H. Jo, Fabrication of highly conductive and transparent thin films from single-walled carbon nanotubes using a new non-ionic surfactant via spin coating, *ACS Nano*, 4, 5382-5388 (2010)
- [43] G. Wu; B.Q. Xu, Carbon nanotube supported Pt electrodes for methanol oxidation: A comparison between multi- and single-walled carbon nanotubes, *Journal of Power Sources*, 174, 148-158 (2007)

-
- [44] J. H. Yim; Y.S. Kim; K.H. Koh; S. Lee, Fabrication of transparent single wall carbon nanotube films with low sheet resistance, *Journal of Vacuum Science & Technology B*, 26, 851–855 (2008)
- [45] T. Kitano; Y. Maeda; T. Akasaka, Preparation of transparent and conductive thin films of carbon nanotubes using a spreading/coating technique, *Carbon*, 47, 3559–3565 (2009)
- [46] X. Yu; R. Rajamani; K.A. Stelson; T. Cui, Fabrication of carbon nanotube based transparent conductive thin films using layer-by-layer technology, *Surface & Coatings Technology*, 202, 2002–2007 (2008).
- [47] Chemsultants International Inc., Mentor, OH, Sample preparation devices – Lab coaters – Wire wound rod coating, Retrieved (2010) from: <http://www.chemsultants.com/testing-equipment-products/sample-preparation-devices/wire-rod-coating-rods.aspx>.
- [48] B. Dan; G.C. Irvin; M. Pasquali, Continuous and scalable fabrication of transparent conducting carbon nanotube films, *ACS Nano*, 3, 835–843 (2009)
- [49] M.D. Lima; M.J. de Andrade; C.P. Bergmann; S. Roth, Thin, conductive, carbon nanotube networks over transparent substrates by electrophoretic deposition, *Journal of Materials Chemistry*, 18, 776–779 (2008)
- [50] A.R. Boccaccini; J. Cho; J.A. Roether; B.J.C. Thomas; E.J. Minay; M.S.P. Shaffer, Electrophoretic deposition of carbon nanotubes, *Carbon*, 44, 3149–3160 (2006)
- [51] J. Cho; K. Konopka; K. Roźniatowski; E. García-Lecinac; M.S.P. Shaffer; A.R. Boccaccini, Characterization of carbon nanotube films deposited by electrophoretic deposition, *Carbon*, 47, 58–67 (2009)
- [52] M. Jung de Andrade; M. Dias Lima; V. Skákalová; C.P. Bergmann; S. Roth, Electrical properties of transparent carbon nanotube networks prepared through different techniques, *Solid State Physics (RRL)* 1, 5, 178–180 (2007)
- [53] S. Pei; J. Du; Z. You; C. Liu; H.M. Cheng, The fabrication of a carbon nanotube transparent conductive film by electrophoretic deposition and hot-pressing transfer, *Nanotechnology*, 20, 235707-7 (2009)
- [54] R. Signorelli; D.C. Ku; J.G. Kassakian; J.E. Schindall, Electrochemical double-layer capacitors using carbon nanotube electrode structures, *Proceedings of the IEEE*, 97 (11), 1837-1847 (2009)
- [55] C.J. Hung; J.H. Hung; P. Lin; T.Y. Tseng, Electrophoretic fabrication and characterizations of manganese oxide/carbon nanotube nanocomposite pseudocapacitors, *Journal of The Electrochemical Society*, 158 (8), 942-947 (2011)
- [56] C. Niu; E. K. Sichel; R. Hoch; D. Moy; H. Tennent, High power electrochemical capacitors based on carbon nanotube electrodes, *Applied Physics Letters*, 70, 1480-1482 (1996)

-
- [57] B.J. Yoon; S.H. Jeong; K.H. Lee; H.S. Kim; C.G. Park; J.H. Han, Electrical properties of electrical double layer capacitors with integrated carbon nanotube electrodes, *Chemical Physics Letters*, 388, 170-174 (2004)
- [58] K.H. An; W.S. Kim; Y.S. Park; J.M. Moon; D.J. Bae; S.C. Lim; Y.S. Lee; Y.H. Lee, Electrochemical properties of high-power supercapacitors using single-walled carbon nanotube electrodes, *Advanced Functional Materials*, 11, 387-392 (2001)
- [59] D.N. Futaba; K. Hata; T. Yamada; T. Hiraoka; Y. Hayamizu; Y. Kakudate; O. Tanaike; H. Hatori; M. Yumura; S. Iijima, Shape-engineerable and highly densely packed single-walled carbon nanotubes and their application as super-capacitor electrodes, *Nature*, 5, 987-994 (2006)
- [60] W. Lu; R. Hartman; L. Qu; L. Dai, Nanocomposite electrodes for high-performance supercapacitors, *The Journal of Physical Chemistry Letters*, 2, 655-660 (2011)
- [61] Z. Niu; W. Zhou; J. Chen; G. Feng; H. Li; W. Ma; J. Li; H. Dong; Y. Ren; D. Zhao; S. Xie, Compact-designed supercapacitors using free-standing single-walled carbon nanotube films, *Energy & Environmental Science*, 4, 1440-1446 (2011)
- [62] Q.Cheng; J. Tang; J. Ma; H. Zhang; N. Shinya; L.C. Qin, Graphene and nanostructured MnO₂ composite electrodes for supercapacitors, *Carbon*, 49, 2917-2925 (2011)
- [63] M. Kaempgen; C. K. Chan; J. Ma; Y. Cui; G. Gruner, Printable thin film supercapacitors using single-walled carbon nanotubes, *Nano Letters*, 9 (5), 1872-1876 (2009)
- [64] T. Kitano; Y. Maeda; T. Akasaka, Preparation of transparent and conductive thin films of carbon nanotubes using a spreading/coating technique, *Carbon*, 47, 3559-3565 (2009)
- [65] B.A. Kakade; V. K. Pillai, An efficient route towards the covalent functionalization of single walled carbon nanotubes, *Applied Surface Science*, 254, 4936-4943 (2008)
- [66] J. Cho, K. Konopka, K. Rozniatowski, E. Garcia-Lecina, M. Shaffer, A.R. Boccaccini, *Carbon*, 47 (2009) 58-67.
- [67] A. Ma; K. Yearsley; M. MacKley; F. Chinesta, A review of the microstructure and rheology of carbon nanotube suspensions, *Journal of Nanoengineering and Nanosystems*, 222, 71-94 (2008)
- [68] M.B. Bazbouz; G.K. Stylios, Alignment and optimization of nylon 6 nanofibers by electrospinning, *Journal of Applied Polymer Science*, 107, 3023-3032 (2008)
- [69] C. Burger; B.S. Hsiao; B. Chu, Nanofibrous materials and their applications, *Annual Reviews*, 36, 333-68 (2006)
- [70] Epson Canada, Epson Stylus NX510 Printer Specifications, Retrieved (2011) from: http://www.epson.ca/cgi-bin/ceStore/jsp/Product.do?BV_UseBVCookie=yes&sku=C11CA48202

[71] HP USA, HP Deskjet F4480 Datasheet, Retrieved (2011) from:
http://h10010.www1.hp.com/wwpc/pscmisc/vac/us/product_pdfs/3742084.pdf

[72] HP USA, HP 60 Black Inkjet Cartridge Specifications, Retrieved (2011) from:
<http://h10010.www1.hp.com/wwpc/us/en/sm/WF06c/A10-12771-64199-69422-69422-3564563-3564600-3564609.html>

[73] J.P. Srivastava, Elements of solid state physics, Prentice-Hall of India Pvt. Ltd, 2nd Revised edition, (2006)

[74] R. Graupner, Raman spectroscopy of covalently functionalized single-wall carbon nanotubes, Journal of Raman Spectroscopy, 38, 673-683 (2007)

[75] C. Portet; J. Chmiola; Y. Gogotsi; S. Park; K. Lian, Electrochemical characterizations of carbon nanomaterials by the cavity microelectrode technique, Electrochimica Acta, 53, 7675-7680 (2008)